SCHOOL OF GRADUATE STUDIES

SCHOOL OF EARTH SCIENCES

CHARACTERIZATION OF SELEN WUHA MAFIC-ULTRAMAFIC MASSIF OF RAYA MARGINAL GRABEN, NORTHERN ETHIOPIA

BY SENAY REDAE ZINABU

A THESIS SUBMITTED TO THE SCHOOL OF GRADUATE STUDIES OF ADDIS ABABA UNIVERSITY IN PARTIAL FULFILLMENT OF THE REQUIREMENTS FOR THE DEGREE OF MASTER OF SCIENCE IN EARTH SCIENCES (PETROLOGY).

MAY, 2018
ADDIS ABABA, ETHIOPIA

ADDIS ABABA UNIVERSITY

SCHOOL OF GRADUATE STUDIES

SCHOOL OF EARTH SCIENCES

CHARACTERIZATION OF SELEN WUHA MAFIC-ULTRAMAFIC MASSIF OF RAYA MARGINAL GRABEN, NORTHERN ETHIOPIA

BY SENAY REDAE ZINABU

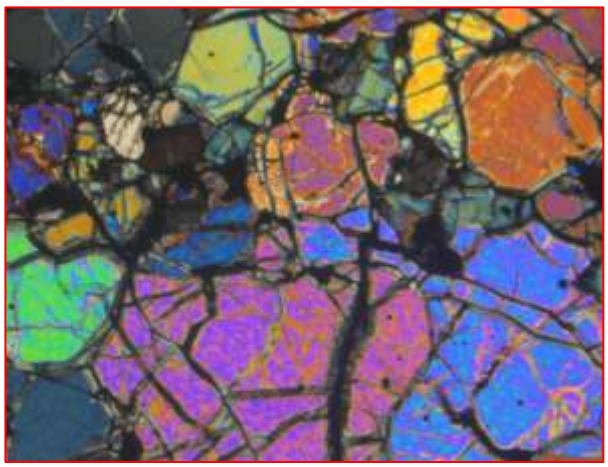

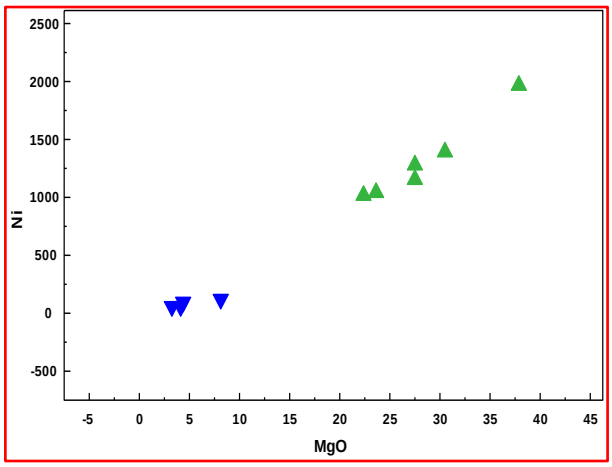

ADVISOR

PROF. GEZAHEGN YIRGU

CO-ADVISOR

PROF. ASFAWOSSEN ASRAT

A THESIS SUBMITTED TO THE SCHOOL OF GRADUATE STUDIES OF ADDIS ABABA UNIVERSITY IN PARTIAL FULFILLMENT OF THE REQUIREMENTS FOR THE DEGREE OF MASTER OF SCIENCE IN EARTH SCIENCES (PETROLOGY).

MAY, 2018
ADDIS ABABA, ETHIOPIA

ADDIS ABABA UNIVERSITY

SCHOOL OF GRADUATE STUDIES

SCHOOL OF EARTH SCIENCES

CHARACTERIZATION OF SELEN WUHA MAFIC-ULTRAMAFIC MASSIF OF RAYA MARGINAL GRABEN, NORTHERN ETHIOPIA

BY SENAY REDAE ZINABU

Approved by Examining Committee:

Name	Position	Signature	Date
Dr. Balemwal Atnafu	Head, SES	_____	_____
Prof. Gezahegn Yirgu	Advisor	_____	_____
Prof. Asfawossen Asrat	Co- Advisor	_____	_____
Prof. Dereje Ayalew	Examiner	_____	_____
Dr. Tarekegn Tadese	Examiner	_____	_____

MAY, 2018
ADDIS ABABA, ETHIOPIA

Declaration of Originality

I am declaring that this thesis is my original MSc study under the supervision of Prof. Gezahegn Yirgu and Prof. Asfawossen Asrat, School of Earth Sciences, Addis Ababa University in 2018. In addition, I am assuring that this work has not been presented or submitted to any other university or institution for the award of any degree or diploma. It has not published anywhere else. All sources and materials used in this thesis are well referenced and duly acknowledged.

Senay Redae Zinabu _____ _____

Signature Date

Prof. Gezahegn Yirgu _____ _____

Signature Date

Prof. Asfawossen Asrat _____ _____

Signature Date

Acknowledgement

I would like to thank the University of Gondar for sponsoring me to attend my MSc program in Addis Ababa University. I am also thankful to Addis Ababa University, Department of Earth Sciences, which helped me to conduct my MSc. thesis study in petrology stream.

I would like to give special sincere gratitude for my advisor Prof. Gezahegn Yirgu not only for his excellent guidance and endless encouragement throughout the study but also for his humanity and fatherhood approach to give valuable suggestion, daily constructive comment and directions, making technical discussion and his vigorous support. My heartfelt gratitude extends to my co-advisor Prof. Asfawossen Asrat for his volunteerism to advise me and his continuous valuable academic advice, constructive comment and supports to improve my potential and quality on the present thesis work.

Geochemical data has a great powerful to enhance the quality and reliability of the research work however it requires huge cost particularly for those researchers living in third world countries. Therefore, Special gratitude is awarded to Dr. Karen Fontijn for sponsoring me in preparing the major oxide and trace element geochemical analysis which was my headache when I thought about the quality of this thesis study.

I am also thankful to various institutions such as Geological Survey of Ethiopia, Federal Water Works Design and Supervision Enterprise (WWDSE) and Ethiopian map agency from where I got all kinds of necessary data that have helped me to accomplish all my works successfully.

I heartfelt acknowledge for the Society of Selen Wuha area for their kindness, respectfulness and dutifulness in giving information about the area and about anything that I have request.

Furthermore, an absolutely massive thank is given to all my friends for helping me in every aspect of my difficulties.

Eventually, my deep gratitude is awarded to my wife Fikirte Ayal not only for the determination and encouragement she shows to attend and concentrate only on my study but also taking care of our son Samual Senay and daughter Adyam Senay. Thanks a lot to all my families for their moral support and encouragement they offered me during my study.

Abstract

Ultramafic intrusion is found in Selen Wuha area of Raya marginal graben. Selen Wuha area is located 600km away from Addis Ababa to the northern Ethiopia. Some of the previous researchers were considered it as basement low grade metamorphic unit while others have not conformed to this idea and considered is as young aged un-metamorphosed igneous intrusion. Thus, the target of this study is to resolve this gap by characterizing the intrusion using field observation, petrography and geochemical data. The study area covers about 20km^2 and it has mapped with the scale of 1:25,000. Accordingly, ultramafic unit, plagioclase-olivine phyric basalt, pyroclastic material and alluvial sediment deposit are recognized major mappable units. Moreover, small intrusions (dykes), normal faults, lineaments, joints and veins are identified geologic structures of the area. Hence, the contact of ultramafic with adjacent units is controlled by tectonic contacts. Minerals in the ultramafic are coarse grained Cpx, Opx, Ol and Fe-Ti oxide. Similarly, minerals in gabbroic units are coarse grained plag, Cpx, Ol and Fe-Ti oxides. Texturally, both units are porphyritic-phaneritic in which the size of grains is range from medium pheneritic to coarse pheneritic. Plagioclase-olivine phyric basalt has porphyritic texture in which Ol and plag are the dominant phenocryst minerals. Based on the proportion of Ol, Pxn, and concentration of MgO, the studied ultramafic unit is classified into pyroxenite and peridotite. Since any sign of metamorphism is not found in the unit, it is an igneous intrusion which has intruded in early Cenozoic formations and Mesozoic sedimentary successions. Accordingly, the studied ultramafic unit is not Neoproterozoic in age however it is Cenozoic aged intrusion. From the geochemistry point of view, the ultramafic unit is derived from depleted mantle source since it shows high concentration of MgO (22.31 wt. % to 37.08 wt. %), Mg # (72.63 to 81.94), Cr (1690ppm to 3000ppm), Ni (1030ppm to 1980ppm) and Co (96ppm-143ppm). It shows also slight depleted in LREE and very low concentration of the highly incompatible trace elements. Furthermore, the samples are co-genetic, sourced from homogeneous source and related by fractional crystallization since they show good correlation in the selected major oxide and trace element variation diagrams.

Key words: Depleted mantle source, Porphyritic- Phaneritic texture, Pyroxenite, Peridotite, Co-genetic, Homogenous source, Related by fractional crystallization

List of Acronym and abbrvetions

<	Below Detection Limit
4X	Four times Magnification Power
Cpx	Clinopyroxene
DEM	Digital Elevation Model
Fig.	Figure
GPS	Geographical Positioning System
HCl	Hydrochloric Acid
HFSEs	High Field Strength Elements
HREEs	Heavy Rare Earth Elements
IUGS	International Union Geologcal Society
LA-ICP-MS	Laser ablation Inductively Coupled Plasma Mass Spectrometer
LOI	Loss On Ignition
LREEs	Light Rare Earth Elemements
Ma	Million years Ago
Mg#	Mg Number
MREEs	Middle rare earth elements
NNE	North North East
NWN	North West North
Ol	Olivine
Op	Opaque
Opx	Orthopyroxene
PPL	Plane polarized light
Pxn	Pyroxene
REST	Relief Society of Tigray
RVDP	Raya Valley Development tudy Project
SSW	South South west
Vs	Versus
Wt%	Weight in percent
WWDSE	Water Works Design and Suprvision Enterprise
XPL	Cross polarized light
XRF	X-ray fluorescence

Table of Contents

List of Figures

List Tables

CHAPTER ONE

INTRODUCTION

1.1. Background

Selen Wuha area is located in the northern part of Ethiopia. It is about 600 km away from Addis Ababa. Particularly, it is located at the southeast margin of Alamata sub-basin. This is in the eastern escarpment of Raya marginal graben. It is obvious that Raya marginal graben is situated at the western margin of Afar rift or Afar depression (fig.1.1).

A breakage of Afro-Arabian plateau and formation of Afar rift (Afar depression) are associated with the effect of Afar Palaeogene mantle plume. As the result of this mantle plume, intense magmatic and tectonic activity had happened in the region including the Red Sea, Gulf of Aden and the Ethiopian rifts. This was occurred during the lower Tertiary period (mainly between 31 and 26 Ma). Therefore, huge amount of flood basalts/trap series of volcanic rocks cover a large part of northern Ethiopia and today dominantly it makes the geology of that area (Pik et al., 1999; Ukstins et al., 2002 as cited in Tesfamichael Gebreyohannes et al., 2010). Flood basalt and associated rhyolites of the northern Ethiopian plateau were erupted between 31 and 29.

The active triangular-shaped Afar depression is bordered on the west by African plate (Ethiopian–Eritrean Plateau), on the southeast by Somali plate and on the northeast by the Danakil and Ali-Sabieh (Aisha) blocks (Danakil micro plate). This lowland plain of Afar rift, which covers about 200,000 km^2, is characterized by ribbed topography. The main land forms are grabens, horsts and linearly aligned high relief peaks representing the axial shield volcanoes (Mohr, 1983a as cited in Bosworth et al.,2005; Samson Tesfaye et al., 2003).

In Afar rift and its adjacent marginal area, six-fold divisions of the geologic history are recognized by different researchers such as Gass (1970); Varet (1978); Zanettin, (1993); as cited in Bosworth et al. (2005). These six-fold divisions of geologic history are made based on the integrated outcrop data acquired from the interior of Afar rift, its marginal areas and Danakil Alps. These are Neoproterozoic basement, Pre-rift Mesozoic strata and Early Tertiary volcanic rocks, Oligocene plume volcanism, Syn-rift Miocene volcanic rocks, Syn-drift Pliocene and Pleistocene volcanic rocks, and Quaternary volcanic rocks and lake sediments. The pre-rift stratigraphic sequence of the Afar region is best exposed in the Danakil Alps where the composite section reaches over 4000m. The oldest strata are generally early Jurassic

or possibly Triassic covering crystalline basement, with higher units extending into the early Cretaceous. This Mesozoic section represents a major transgressive and regressive cycle. The base of the section is comprised of fluvial, deltaic, and marginal marine sandstones and conglomerates of the Adigrat sandstone that attain a thickness of about 1600m. These siliciclastic rocks are overlain conformably by over 2400 m of the Bathonian to Tithonian Antalo limestone. A return to continental conditions occurred in the latest Jurassic to early Cretaceous, with deposition of the fluvial Amba-Aradom sandstone (Merla et al., 1979; Bunter et al., 1998 as cited in Bosworth et al., 2005). Neoproterozoic crystalline basement rocks of the Nubian shield are exposed along the margin of the Afar depression and within the Danakil and Ali-Sabieh blocks. These rocks were assembled and metamorphosed from 800 to 650 Ma (Vail, 1985; Kazmin et al., 1978; Stern, 1994; Kusky et al., 2003 as cited in Bosworth et al., 2005).

From the idea of Tenalem Ayenew et al. (2013) Raya marginal graben is bounded by the Northwestern Ethiopian Plateau in the west and the Afar Rift in the east. The valley is an elongated intermountain graben filled with Quaternary sediments. It is bordered to the east and west by rugged volcanic mountains. According to Melese Tadesse et al. (2011) Raya marginal graben is bounded on the east and west by Ashangi formation which is the oldest flood basalt volcanism on the north western Ethiopian plateau. There are also rare rhyolites from fissures and dissected by dikes and sills, small granitic intrusions and sandstones. In general wide variety of rock units are exposed in Raya valley and they range in age from Precambrian to Quaternary. Accordingly, Precambrian basement rocks have overlain by Mesozoic sedimentary rocks and the Tertiary volcanic and recent Quaternary alluvial and fluvial sediments are rested on top of Mesozoic sedimentary rocks (Merhawi GebreEgziabher, 2011; WWDSE, 2011; Tenalem Ayenew et al., 2013). These authors have also noted that exposure of Precambrian aged low grade metamorphosed rocks of pyroxenite, gabbro and anorthosite with other volcanic rocks around Selen village in the eastern scarp of Raya valley. These intrusions were also studied or documented by Gezahegn Yirgu (2010). According to this study, they are considered as un-metamorphosed probably Oligocene aged holocrystalline coarse grained and texturally inequigranular igneous intrusions. In general, these studies have proposed two different ideas concerning the age and origin of these intrusions (massif). Consequently, the massif required further geological, structural, geochemical and petrological investigations. Therefore, the purpose of this study is to resolve these gaps using previous work, direct field observation data, petrographic study and geochemical analysis.

1.2. General overview of the study area

1.2.1. Location and accessibility

The study area is located at the southeast margin of Alamata sub-basin in the Chercher Mountains belt of both Raya Alamata and Raya kobo woredas of northern Ethiopia (fig. 1.1). Geographically, it is situated between Easting: 576556 and 580372 and Northing: 1359831 and 1364954 and it covers about 20km^2. The study locality is about 21km southeast of Alamata town and about 20 km northeast of Kobo town. Both Alamata and Kobo towns are about 600 km and about 591km far away from Addis Ababa (capital city of Ethiopia) respectively. They are also about 180 km and 189 km south of Mekelle respectively. Mekelle is a capital city of Tigray regional state. Kobo town is located in northeast corner of Semien Wollo zone of Amhara regional state while Alamata is situated in the southern zone of Tigray regional state (Gidey Yirga, 2010; https://en.wikipedia.org/wiki/Alamata).

Both Alamata and Kobo towns are located on the Addis Ababa – Axum highway. Bedano-loko is another small town which is located in the axis of the valley (in the west direction of the study area). But there is no even gravel road connecting this small town with the main highway. However, there are foot paths in which the people of the study area and its vicinity are using for their day to day activities. Since the graben is bounded in west and east by relatively elevated Mountains, the drainages having dendritic pattern are drained toward the valley from both of the elevated mountains. Hence, during the rainy season the plain of the valley and its vicinity inhabits by flood and mud. Therefore, these footpaths, connecting the villages in the study area and its vicinity, are not giving service during this rainy season. However, during the dry season the valley and its vicinity are dried. Consequently, accessibility of the area is better during this season than of the wetly season.

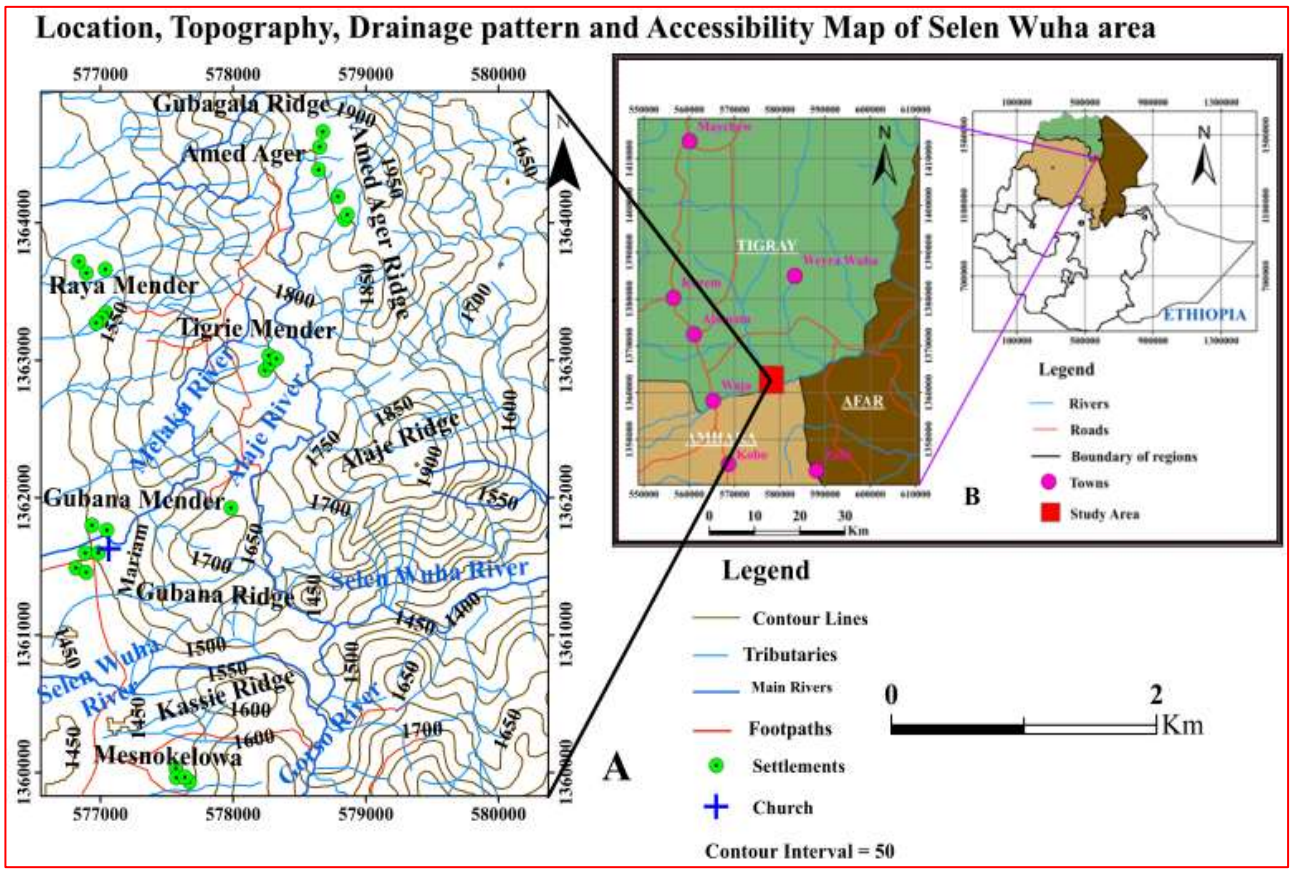

Figure 1. 1: Location, drainage pattern, settlement and accessibility map of the study area and its vicinity. *(A) Drainage pattern, settlement and accessibility of the study area. (B) Location of the study area in regional scale and accessibility near the study area.*

1.2.2. Physiography and drainage pattern

Alamata sub-basin of Raya marginal graben has different physiographic features. The dominated landforms in this basin are mountainous ridge, hills and rivers. However, the study area is located on the mountainous belt and therefore has rugged or undulating topography with altitude variation ranges from about 1400m above mean sea level (in the Selen Wuha river) to about1900m above mean sea level (near Alaje mountain ridge).

Sulula and Selen Wuha rivers are the two main interconnected rivers in the study area. They flow in different directions. Sulula river is found in the west of the study area at the axis of the valley and it flows from north to south. Hence, it feeds to Selen Wuha river. Selen Wuha river outlet, which crosses the study area, is flowing from west to east. This is from Tigray and Amhara regions to Afar region. It is the only river which serves as river outlet for the flood collected in the valley. The major tributaries for these two main rivers in the study area are Melaku, Alaje and Gorso rivers (Fig.1.2). From These three major tributaries of the main rivers, Alaje and Gorso rivers are drained to Selen Wuha river While Melaku river has drained

to Sulula river. All these major tributaries have also their own many small tributaries. Since the study area is located on the elevated topography, all the major and minor tributaries with the main rivers in the study area have together made dendritic drainage pattern. Selen Wuha river is annually river while the other rivers (tributaries) are seasonal rivers.

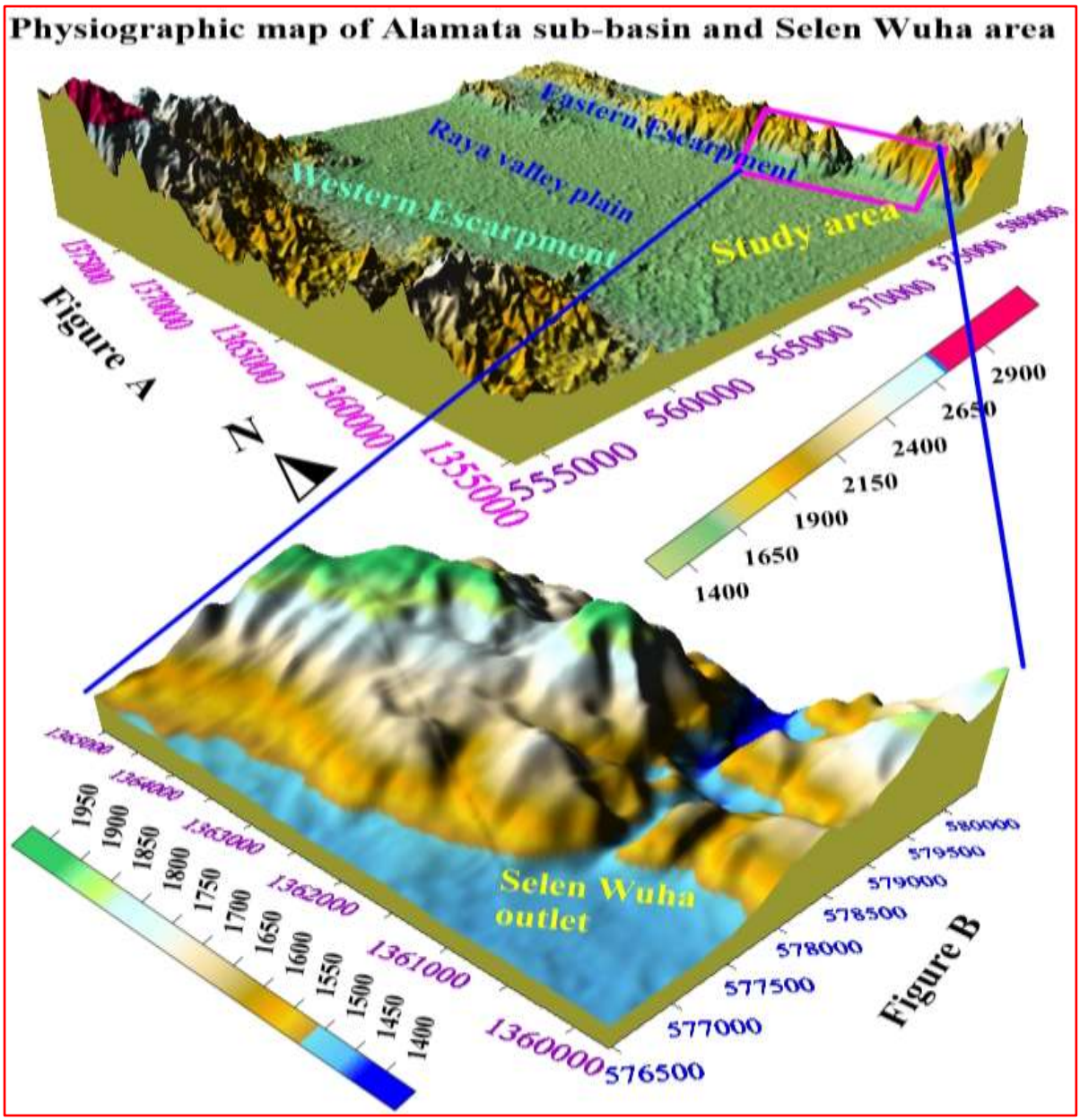

Figure 1. 2: Digital Elevation Model map showing physiographic feature of Selen Wuha area and Alamata sub basin. *(A) Physiographic map of Alamata sub-basin. (B) Physiographic map of the study area.*

1.2.3. Climate condition and vegetation

Raya valley has tropical climate condition. In the valley, the summers are much rainier than the winters. The average annual temperature of the valley ranges from 22°C to 22.6°C and its average annual precipitation is also range from 782mm to 815mm (https://en.climate-data.org/location/512432/). The driest and warmest month is June and its mean precipitation and temperature are reported about 10 mm and 25.3 °C respectively. On the other end, the greatest amount of precipitation occurs in August. In this month the average precipitation is about 180mm. The lowest average temperature in the year is recorded in January. This is around 19.2°C.

Raya valley has seasonal bimodal Rainfall. These are short and long rainy seasons. The short rainy season covers 80% of the area while the long rainy season covers the whole area of the valley. The short rainy season is between the end of February and the beginning of April. The highest amount of precipitation of this season is occurred in March which is greater than 180mm.This precipitation is almost similar with the amount of precipitation in August. The long rainy season extends from the end of June to the beginning of September. Generally, Rainfall in Raya valley is usually intense and short duration (Afework Desalegn, 2011; Nigus Gebremedhin, 2011; Gidey Yirga, 2010; https://en.climate-data.org/location/512432/).

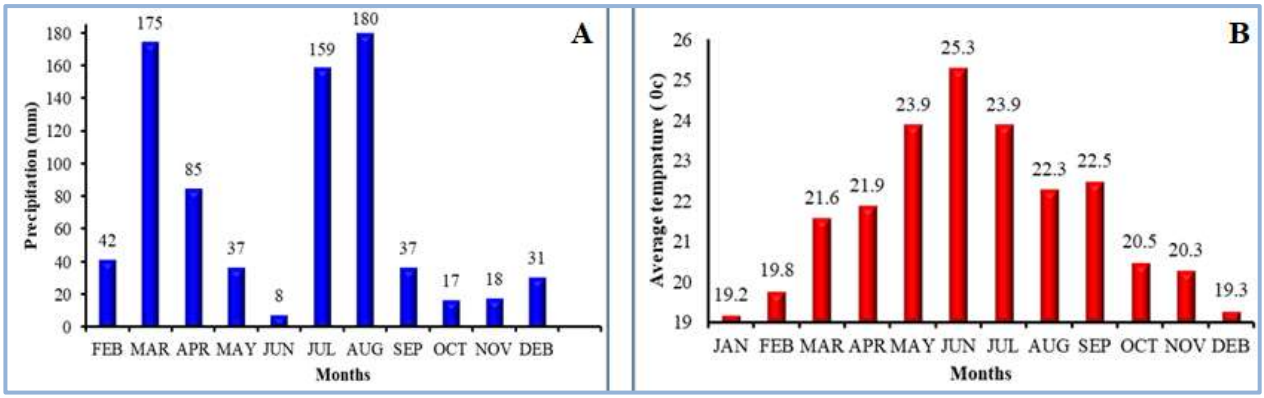

Figure 1.3: *The average precipitation and temperature of Raya valley displayed in A and B respectively (http://www.levoyageur.net/weather-city-ALAMATA.html)*

The distribution of vegetation in the study area is range from scarce to moderate and the plants of the area are unique indigenous types. These are almost indigenous plants of rare thorny bushes, moderately lengthen plants and few scattered longest trees. The local name of these few plants are Sebansa (Grar) and Agam are from the moderately lengthen, Beles or Kolkual is among the shrubs), Kinchib and Korora are among the longest plants. All these plants are

very common in the area. From the above listed plants, the dominant indigenous plants are Sebansa (Grar) and Beles (Kolkual).

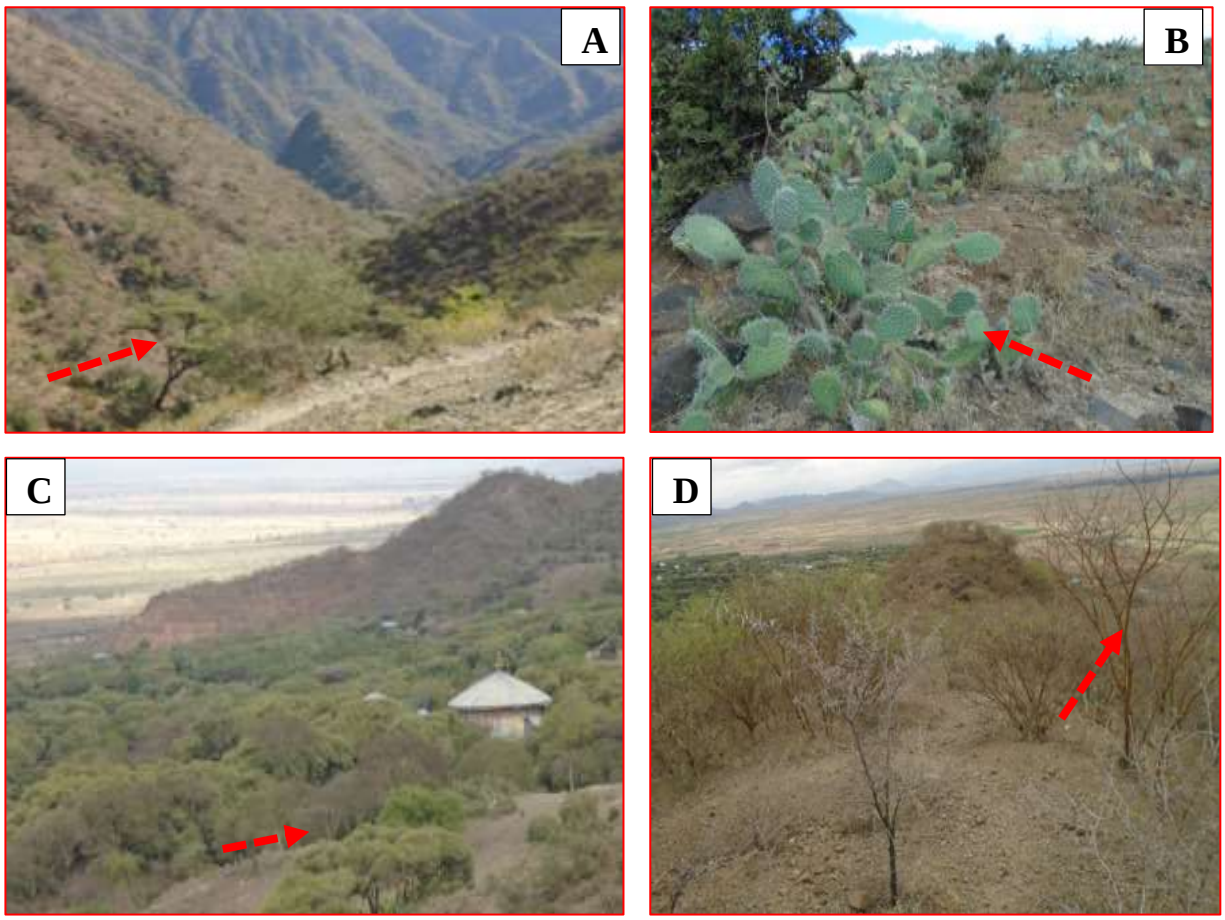

Figure 1. 4: The four dominant plants in the study area. (A and C) show 'Korora and Kinchib'. They are among the longest plants of the area. (B) shows 'Beles or Kulkual' and it is from shrubs found in the area and (D) Shows Sabansa and it is among the moderately lengthen trees.

1.2.4. Human settlement and land use

Gubana Mender is a village found in the study area in which relatively denser population are living together. This village is found in the west direction of the study area in Raya Alamata woreda. Similarly, Mesnokelewa is another village where denser population is living together. This village is found west of the study area in Raya Kobo woreda. But there are also few scattered villages such as 'Tigrie Mender' are found on top of 'Gubana' ridge.

Both mixed crop and livestock farming system are the common mode of agriculture in Raya area. Although the local people have practice both types of agricultural system, crop production has given great attention than raising livestock. Mostly, the local people have cultivated some types of crops on the plain of Raya valley. However, the mountain or hill as the whole is used as pasture for their livestock (cattle). The most common types of cereal

crops cultivated in the area are Teff, Sorghum and Maize while cattle (cows, sheep and goats), camels, donkeys are the most common livestock used by the local people of the study area (Yohannes, 2007 as cited in Gidey Yirga, 2010**)**.

1.3. Statement of the problem

According to Mohr (1962) and Solomon Tadesse (2009), The Ethiopian Cenozoic volcanic province is characterized entirely by pre-rift extensive flood basalt and rhyolites as well as by similar rift related volcanics. According to Gezahegn Yirgu (2010) rarely plutonic rocks of mafic and felsic compositions are associated with this Ethiopian Cenozoic volcanic province are very rare and occur in the form of dyke and minor intrusive bodies.

A small mafic-ultramafic exposure has recently been identified ad described at Selen Wuha river and its vicinity on the eastern margin of Raya marginal graben (Gezahegn Yirgu, 2010; Merhawi GebreEgziabher, 2011; WWDSE, 2011; Tenalem Ayenew et al., 2013; Ayele Almaw et al., 2015). This exposure of mafic- ultramafic unit is situated in Selen Wuha Tabia of Alamata woreda. According to the studies of Merhawi GebreEgziabher (2011), WWDSE (2011) and Tenalem Ayenew et al. (2013), these mafic-ultramafic rocks are considered to be Precambrian in age and they are assumed to be parts of the basement intrusive rocks. Specifically, Merhawi GebreEgziabher (2011) and Tenalem Ayenew et al. (2013) have considered them as Meta-igneous rocks of basement unit and described as metamorphosed intrusive rocks (meta-pyroxenite and meta-dunite). On the other hand, the petrography of the ultramafic body has been described by Gezahegn Yirgu (2010) as follows: olivine (~37%), orthopyroxene (~35%), clinopyroxene (~20%) and opaque oxide (~8%). It is holocrystalline, coarse grain and has inequigranular texture. Based on this petrographic result, the age of this massif is probably fall under the Oligocene. In addition, the result has no any sign that indicate the nature of metamorphism on the studied mafic-ultramafic massif. This shows that the massif has not been well studied in any detail so far and this results a very limited knowledge of this mafic-ultramafic body. Consequently, the massif requires further geological, structural and petrological investigation. In addition, the areal coverage and nature of emplacement of the massif is also not clear. Hence, the target of this study is to solve such uncertainty and related problems of this mafic- ultramafic massif. The overall objective of this study is making detail characterization on the aspect of petrographic, geochemistry and field relations of this mafic-ultramafic exposure.

1.4. Objective of the study

1.4.1. General objective

The main objective of this research study is to describe and characterize the mafic-ultra mafic body found in Selen Wuha area of Raya marginal graben as well as to assess the structural controls for its occurrence.

1.4.2. Specific objectives

The Specific objectives of this research study are:

- To characterize the lithologic variations within the study area.
- To determine the extent of the mafic-ultramafic massif and its exposed geometry (dyke, sill, obduct ophiolitic complex or any other) in relation with the surrounding country-rocks.
- To verify the contact relationships between the massif and the surrounding lithologic units.
- To identify the geological structures and deformational features affecting the mafic-ultra mafic massif as well as the country rocks.
- To determine the relative age of the mafic- ultramafic massif, whether it is Neoproterozoic or Cenozoic in age.
- To produce a geological map of the study area at the scale of 1:25,000 that shows the distribution of major lithological units and major geological structures.
- To characterize the petrographic features and mineralogical assemblages of the various lithologic units and determine whether the unit is metamorphosed or not.
- To investigate (assess) the occurrence of economic mineralization that may be hosted or associated with the massif.

1.5. Important research questions

There are a number of important research questions that need to be addressed about this massif. These are:

1. What are the lithological and mineralogical characteristics of the massif?
2. How wide and extensive is this massif? What is its geometry?
3. What are the contact and stratigraphic relationships of the massif with the surrounding rock units?

4. What is the relative age of the massif?
5. Is it part of a layered mafic/ ultramafic intrusive structure?
6. What type of internal structures, such as mineral layering exists within the massif?
7. What tectonic and deformational features are present affecting the massif and country rock?
8. Are there any economic mineral deposits hosted in the massif and if so what are these?

1.6. Expected outcomes and significance of the study

The expected results of this research project are:

- Complete description and lithologic characterization of Selen Wuha mafic-ultramafic body.
- The areal extent of the mafic-ultramafic rock body found in Selen Wuha area.
- Types and distribution of tectonic structures in the study area.
- A geological map and accompanying cross section of the study area at the scale of 1:25,000.

Some of the significances of research project are:

- It will have detail petrographic, geochemical and structural descriptions of the mafic-ultramafic massif found around Selen Wuha area. As a result, it will serve as initial or additional source for any beneficiaries of the thesis.
- It will have geomorphological, geological, petrological knowledge of the targeted massif and the area. Therefore, it will fill the existing gap on geological, geochemical and petrological knowledge of this mafic-ultramafic massif.

1.7. Research methods

1.7.1. Reviewing relevant literatures

Various relevant literatures are searched and utilized from the beginning to the end to make the work convincible based on the evidence. These literatures are either previously works on Raya valley and its vicinity or regional geological works which are relevant to the title of the problem.

1.7.2. Remote sensing and GIS techniques

Spot 5 satellite images, DEM 30 (digital elevation model), google earth map, previous regional geological maps and topographic map have been used. Spot satellite image (spot 5) is bought from Ethiopian mapping agency. This image is a recent image which has captured in 2016. Digital elevation model 30-meter resolution has been used to show topographic variation in 3D view and to visualize the structural alignments such as the alignment of faults and lineaments. In addition, different software's, such as ArcGIS 10.3, ERDAS IMAGE 9.2, Surfer10, and Global Mapper 12 are used to analyze these major structures, lithologies and contacts of the lithologies from images and models. Furthermore, different plotting software's, such as PetroGraph2beta.exe, WinRock, GCD kit tool and CIPW Norm Hollacher are used to plot and present geochemical and petrographic data of the analyzed samples.

1.7.3. Field work and Geological mapping

Data from the field have been collected during two phases of field works. During the first phase of field work detail sampling, recording of the various measurements and preliminary mapping of the lithologies and structures of the area are carried out. After the first phase of field work satellite images and previous works (particularly maps) have been reviewed to make cross check with the data gathered from the field. During the second phase of field work, lithologies, contacts between lithologies and tectonic structures have been studied and mapped.

1.7.4. Petrographic and geochemical studies

About fifty rock samples have been collected from the field during both phases of field work. From these 50 rock samples 20 thin sections have prepared for petrographic analysis. These thin sections are prepared at the Ethiopian geological survey. The thin sections are selected based on the objective of study, variety of the lithologies, their freshness (representativeness). About 10 rock samples have also been prepared for geochemical analysis (major oxide and trace element analysis). These ten geochemical samples have been sent to University of Leicester, UK, Department of Geology. Samples were analyzed for major elements on PANalytical Axios Advanced XRF spectrometer while Trace elements, including REE, were determined using Laser ablation Inductively Coupled Plasma Mass Spectrometer (LA-ICP-MS).

1.8. Reviewing previous works

There are a number of studies in Raya valley related to hydrogeology to evaluate the ground water potential, ground water flow dynamics, ground water quality for irrigation and ground water flow modelling of the valley. There are also hydrogeological studies related to hydraulic and aquifer characteristics of the Ashange formation and the Quaternary alluvial sediment deposited in the valley. These studies include WWDSE (2008; 2011), Mohammedsultan Abdella (2010), Merhawi GebreEgziabher (2011), Abdella Abdu (2011), Tenalem Ayenew et al. (2013) and Ayele Almaw et al. (2015).

There are few regional studies which describe the major lithological distribution of the valley. These include WWDSE (2008; 2011), Merhawi GebreEgziabher (2011) Gezahegn Yirgu (2010); and Melese Tadesse et al., (2011). These researchers have documented the occurrence of mafic-ultramafic unit in their report paper and have included it as mappable lithology in their geological map. Melese Tadesse et al. (2011) have produced a geological map and report of the Raya valley and its surroundings which is summarized here in chapter two. In this work, the occurrence of mafic intrusive bodies is described under Precambrian meta-volcanic unit

WWDSE (2008; 2011), Merhawi GebreEgziabher (2011) and Tenalem Ayenew et al. (2013) also provide some descriptions on the geology of the Raya valley. These works have identified and mapped mafic-ultramafic units, pyroxenite and gabbro, and have described them as metamorphosed igneous intrusive units under the Precambrian basement (Figure 1.6). In the work of Gezahegn Yirgu (2010) ultramafic rocks consisting of pyroxenites have been identified in Selen Wuha area and have been described as non- metamorphosed intrusive igneous unit.

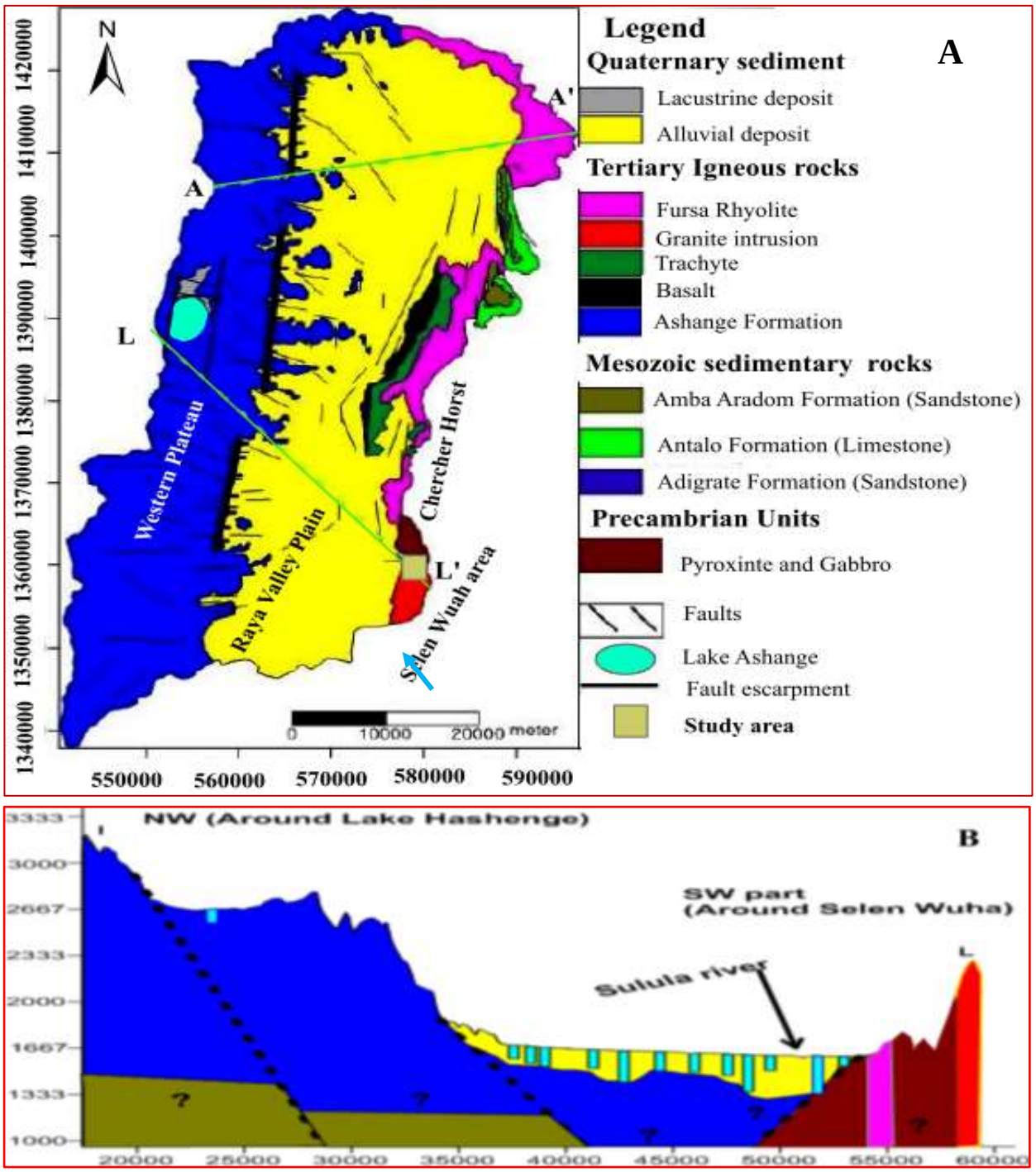

Figure 1. 5: Geological map and cross sectional map of Raya valley. (A) Geological map of Raya area. (B) Cross sectional map of Alamata sub-basin (after Merhawi GebreEgziabher, 2011).no modification is made on this cross section.

CHAPTER TWO

REGIONAL GEOLOGICAL SETTING

2.1. Introduction

The Precambrian basement rocks (metamorphic rocks), the late-Palaeozoic to Mesozoic marine and continental sediments, Cenozoic to Quaternary volcanic (dominant) with minor sedimentary rocks are the main Ethiopian rock types recording in the geological history of Ethiopia (Mengesh Tefera et al.,1996; Pik et al., 1998 as cited in Kurkura et al., 2012; Solomon Tadesse, 2009). Similarly, Asefawossen Asrat (2006) has subdivided the whole Ethiopian geological history in to Precambrian, Paleozoic, Mesozoic and Cenozoic eras. From his idea, Ethiopian Precambrian rocks are generally metamorphic rocks and have associated with intrusions. While the Mesozoic sedimentary succession form a group of rocks resting unconformably on the Precambrian basement rocks. Eventually, Cenozoic era is related to the formation of Ethiopian plateau as a result of extensive flood basalt eruption between 31-29 Ma. Therefore, the Cenozoic volcanic rocks produced from flow of flood basalt have rested over the Mesozoic sedimentary successions. This era is also related to the formation of Ethiopian rift valley as result of the subsequent breaking up of the uplifted dome. All these activities had happened from the early to the middle Cenozoic era.

On the basis of the grade of metamorphism, Ethiopian Precambrian basement rocks are divided in to three major groups (i.e. lower, middle and upper complex). Accordingly, low grade metamorphic rocks are related to upper complex, medium grade metamorphic rocks are grouped in to middle complex and the high grade metamorphic rocks are associated to lower complex group (Kazmin et al., 1978 as cited in Bheemalingeswara and Nata Tadesse, 2009). According to Kazmin (1971; 1975) as cited in Asefawossen Asrat (2001) lower complex group of metamorphic rocks are considered to be Archean in age, middle complex are lower to middle Proterozoic and upper complex are upper Proterozoic to lower Paleozoic.

Gerra (2000) and Teklay et al. (1998) as cited in Bheemalingeswara and Nata Tadesse (2009) have not confirmed with the Kazmin et al. (1978) Ethiopian Precambrian basement classifications. Gerra (2000) and Teklay et al. (1998) have suggested that the Precambrian basement rocks are dominantly Neoproterozoic in age and are grouped in to different grades of metamorphism. In addition, the basement rocks of Ethiopia have been classified by Asefawossen Asrat et al. (2001) in to Volcanic-sedimentary terrain and Gneisic - migmatitic terrain. These are separated by numerous Ophiolitic sutures.

According to Co-ESERAR (1997) as cited in Afework Desalegn (2011) the geology of northern Ethiopia is dominated by Tertiary volcanic rocks underline by Mesozoic sedimentary rocks. The volcanic rocks are predominantly fissural basaltic lava flows with silica varieties. The central type volcanoes have confined to the upper parts of this succession. The Tertiary volcanic successions of the northwestern Ethiopian plateau have been divided by Zanettin et al (1974) in to two main cycles. The first cycle is the formation of Ashange basalts and the second cycle is the formations of Aiba basalts, Alajae rhyolites and Tarmaber basalts. Ashange formation is a pre-Oligocene stage volcanic formation while Aiba, Alajae and Tarmaber formations are the Oligo-Miocene stage volcanics. Therefore, all the three formations have overlain Ashange formation. Based on their trace element and Ti concentrations, these north-western Ethiopian flood basalts (Ashenge, Aiba, Alaje basalt and rhyolite and Terma Bere formations) have later regrouped by Pik et al., (1998 and 1999) into three distinct groups. These are low-Ti basalts (LT), high-Ti1 (HT1) basalts and high-Ti2 (HT2) basalts. Generally, flood basalt volcanic, Amba-Aradam (upper sandstone) formation, Antalo super sequence, Adigrat Sandstone formation, Enticho Sandstone & Edaga Arbi Tillites and basement metamorphic rocks are the major general Stratigraphic sequence of northern Ethiopia. The sequence is written from the younger to the oldest geologic units (Arkin et al., 1971; Beyth, 1972b; Merla et al., 1979 as cited in Tesfamichael Gebreyohannes, 2010).

2.2. Geology of Raya marginal graben

Geologically, the northern part of Western afar depression is characterized by different aged lithologic units. The age of these outcropped lithologic units is range from late Precambrian (Neoproterozoic time) to present. Accordingly, the major lithologic units of the area are Neoproterozoic (Precambrian) basement complex (low grade metamorphic units), Paleozoic to Mesozoic sedimentary successions and Cenozoic volcano-sedimentary sequences (Redfield et al., 2003 as cited in Miruts Hagos et al., 2016). Similarly, Precambrian basement low grade metamorphic rocks, Mesozoic sedimentary rocks and Cenozoic volcanic rock units with undifferentiated lacustrine and alluvial deposit are some of the lithologic units exposed in Raya marginal graben (Melese Tadess et al., 2011; Merhawi GebreEgziabher, 2011; WWDSE, 2011).

2.2.1. Precambrian basement rocks

These Precambrian rocks found in Raya basin are low-grade meta-sediments and meta-volcanics. Meta-volcanic is exposed as uplifted block bounded by high-angle normal faults. The meta-volcanic consists of dominantly meta-basalt with subordinate mafic and felsic intrusive. Meta-sediments are exposed in the northwestern part of Maychew area. Lithologically, it is represented by varying proportions of slate and phyllite (RVDP, 1996 as cited in Mohammedsultan Abdella, 2010 and in Dessie Nedaw, 2003; Melese Tadess et al., 2011).

2.2.2. Mesozoic sedimentary formations

There are outcrops of Mesozoic sedimentary rocks in Raya valley. These abundantly outcropped Mesozoic sedimentary rocks are Adigrat Sandstone, Antalo Limestone and Amba-Aredom formation. According to the map prepared by WWDSE (2011) shown below most of these Mesozoic sedimentary rocks have outcropped in eastern escarpment of Mohoni sub-basin along the Chercher ridge. Particularly, Antalo limestone formations have exposed along the elongated ridge of Adi-Abdero village toward the south until Weyra Wiha River of the Chercher ridge while Amba-Aradom formation has outcropped in Adi-Abdero village to Adi Immbay and around Dalet village of the escarpment. Furthermore, it has outcropped at the foot of the western escarpment of the valley along the gravel road taking from Mohoni to Maychew. In Stratigraphic order, this formation has rested on top of Antalo limestone and beneath the Tertiary basalts. Adigrat formation which is located in the eastern part of the escarpment is the oldest formation relative to the above Mesozoic and Cenozoic units. It has covered by Antalo formation and it is concealed unconformably the Precambrian basement **(**WWDSE, 2011; Merhawi GebreEgziabher, 2011).

2.2.3. Tertiary to Quaternary volcanics and sediments

The Tertiary volcanics in Raya area are Eocene to Miocene plateau basalts, Miocene Kemissie rhyolite, Dalha formation, and Tertiary granite (syenite) while The Quaternary volcanics are dominantly basalt with minor rhyolites. In this area, Ashange formation has exposed within the dissected valleys and gorges of the plateau. In addition, it has outcropped in the western escarpment region and northern region of the Raya basin. It underlies unconformable the Aiba basalt and Alaje formation. The unconformity is commonly marked by paleosoils and deposition of 4 to 6 m thick sediments composed of sandstone and shale with coal seams.

Particularly, this much sediment deposition is located along Maychew-Adi Shiho highway. This formation has tilted from west to the east direction and this indicates the flow of this flood basalt was from west to the east direction (Melese Tadesse et al., 2011; WWDSE, 2011; Merhawi GebreEgziabher, 2011).

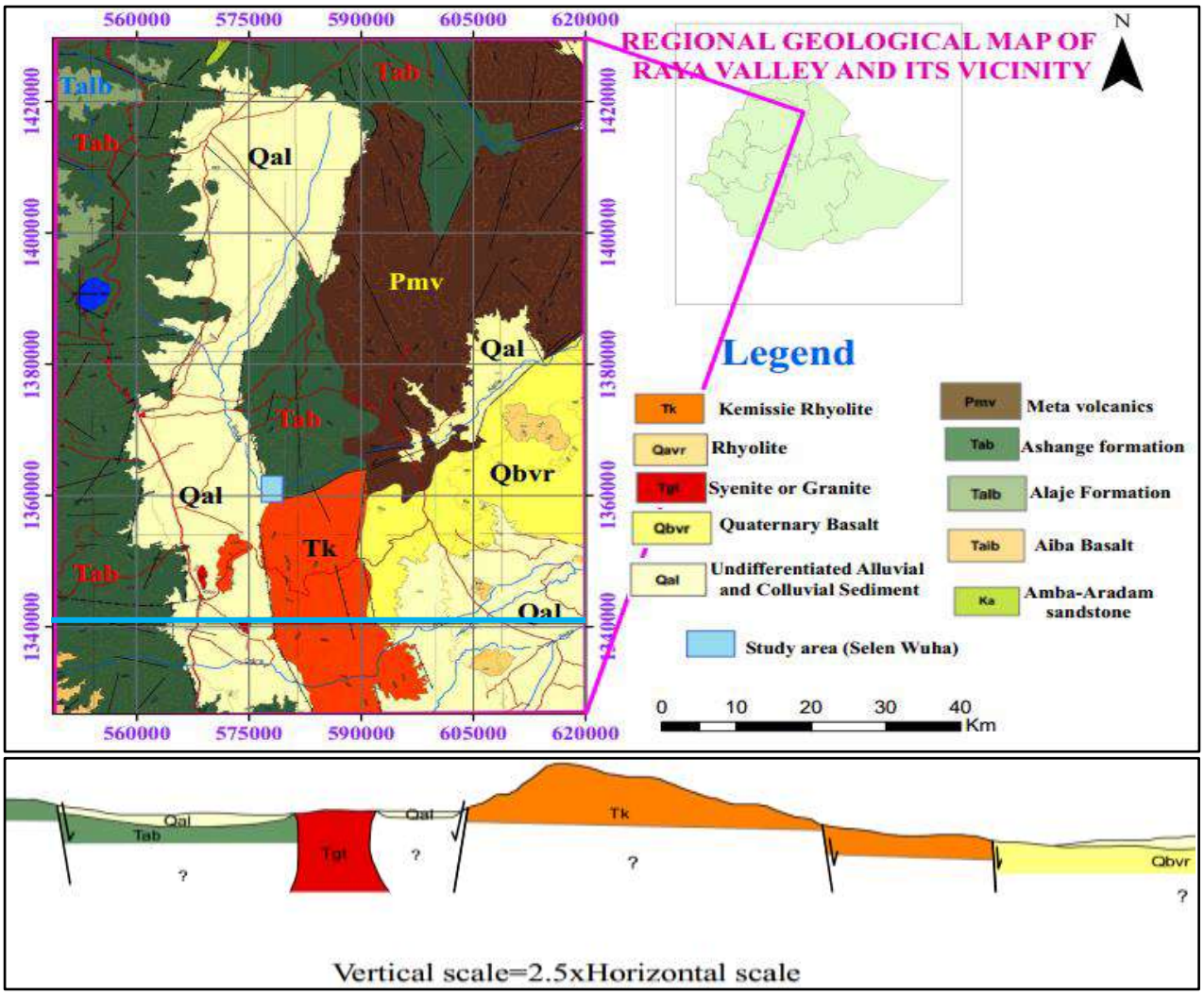

Figure 2. 1: Regional geological map and cross sectional map of Raya valley and its vicinity. It is prepared by Melese Tadess et al. (2011).

Granite, Kemissie rhyolite and Dalha Formation are also found in Raya area. Granite has exposed in north and southeast of kobo town by forming hilly topography. The lithologic characteristics of this unit is light grey and greyish brown color in fresh samples and light gray to yellowish brown in weathered samples. Kemissie rhyolite has exposed in the central southern part along the western margin of the Afar rift. It consists of rhyolite, ignimbrite, tuff and ash. The color of this fresh rhyolite unit is pink, brown and light greenish gray. Texturally, the rock is porphyritic and composed of phenocrysts of K-feldspar, quartz and

plagioclase and commonly it shows flow banding structures. Quaternary volcanics and sediments are basalts, felsic to intermediate volcanics, rhyolite, Fluvio-lacustrine sediments and undifferentiated sediments (Melese Tadesse et al., 2011; WWDSE, 2011).

2.3. Geological structures in Raya valley

According to WWDSE (2011) both primary and secondary structural elements are dominantly occurred in Raya valley. Among these structural elements faults, bedding, joints, fissuring and tilting are the main structures of the area. These geological structures are manly occurred and affect for the Mesozoic sedimentary rocks and tertiary volcanic rocks. According to Melese Tadesse et al. (2011) the faults widely found in the area are normal faults, revers faults, trust faults, strike-slip faults and lineaments. Among them the high angle and low angle normal faults are the dominant faults in the study area. These high angle faults found in the area are striking toward NNE, NNW, NE, NW and E-W directions. Among these NNE and NE striking faults are the dominant fault structures in the area. However, the faults are striking in NE (040°-050°) and dipping toward the west direction are commonly seen in the eastern side of the marginal graben.

In Raya graben, three prominent normal faults were recognized by (WWDSE, 2011). These faults have aligned or striking along NW, NE and N-S directions. These fault structures are mostly high angle normal faults and structurally related to the development of the Raya graben. The E-W striking fault is unknown fault and WWDSE (2011) is considered it as high angle normal fault while Melese Tadesse et al. (2011) has recognized it as left lateral strike-slip fault**.** The thrust faults are observed on Precambrian, meta-volcanic rocks, Mesozoic sedimentary rocks and Ashange volcanics. These faults are dipping in the west direction with moderate and steep angles (20°-60°) and their orientation is toward N, NE and NW. Jointing has affected almost all volcanic rocks found in the western mountain and eastern escarpment of the valley. These joints have nonsystematic arrangement. There are same moderately developed columnar joints in aphanitic basalt. Primary structures such as layering and bedding are clearly observed in Ashange basalt, Tertiary trachyte, and Mesozoic sedimentary rocks. These structures have been recognized via the change in composition and color (WWDSE, 2011).

CHAPTER THREE

GEOLOGY OF THE STUDY AREA

3.1. Introduction

Ultramafic, plagioclase-olivine phyric basalt, pyroclastic deposit and alluvial and lacustrine sediment deposit are the major lithologic units of the study area. Moreover, dykes of gabbro, micro gabbro and micro-granite rocks are recognized in the study area. The distributions of these major lithologies of the area including gabbro are shown below in figure 3.1. About fifty representative rock samples have been collected from all exposed lithologic units, dykes and veins of the area. From these fifty representatives rock samples about 30 are collected from the three major lithology of the area (ultramafic rock, plagioclase-olivine phyric basalt and pyroclastic material). The remaining are collected from dykes and veins found in the study area. Accordingly, about 20 representative ultramafic rock samples have been collected.

From the collected representative rock samples, 20 thin sections (10 from ultramafic unit, 4 from gabbro and micro gabbro units and 4 from plagioclase- olivine phyric basalt) have been prepared for petrographic analysis. The remaining two thin sections have been prepared from the veins hosted in ultramafic unit. In addition, 2 polished sections have also been prepared to identify the opaque minerals present in the ultramafic unit. These prepared thin sections and polished sections have been selected based on the objective of the study, lithologic variety and freshness or representativeness of the samples. The two polished sections have been prepared after the thin sections and geochemical data have been prepared and analyzed. On the other hand, they are prepared based on the weight percent of Fe_2O_3 present in the sample. Accordingly, ST1S11 and ST1S7 are the two ultramafic samples having high concentration of Fe_2O_3 and hence they are prepared for polished section analysis or opaque mineral identification. All these twenty thin sections and both polished sections have been prepared in geological survey of Ethiopia.

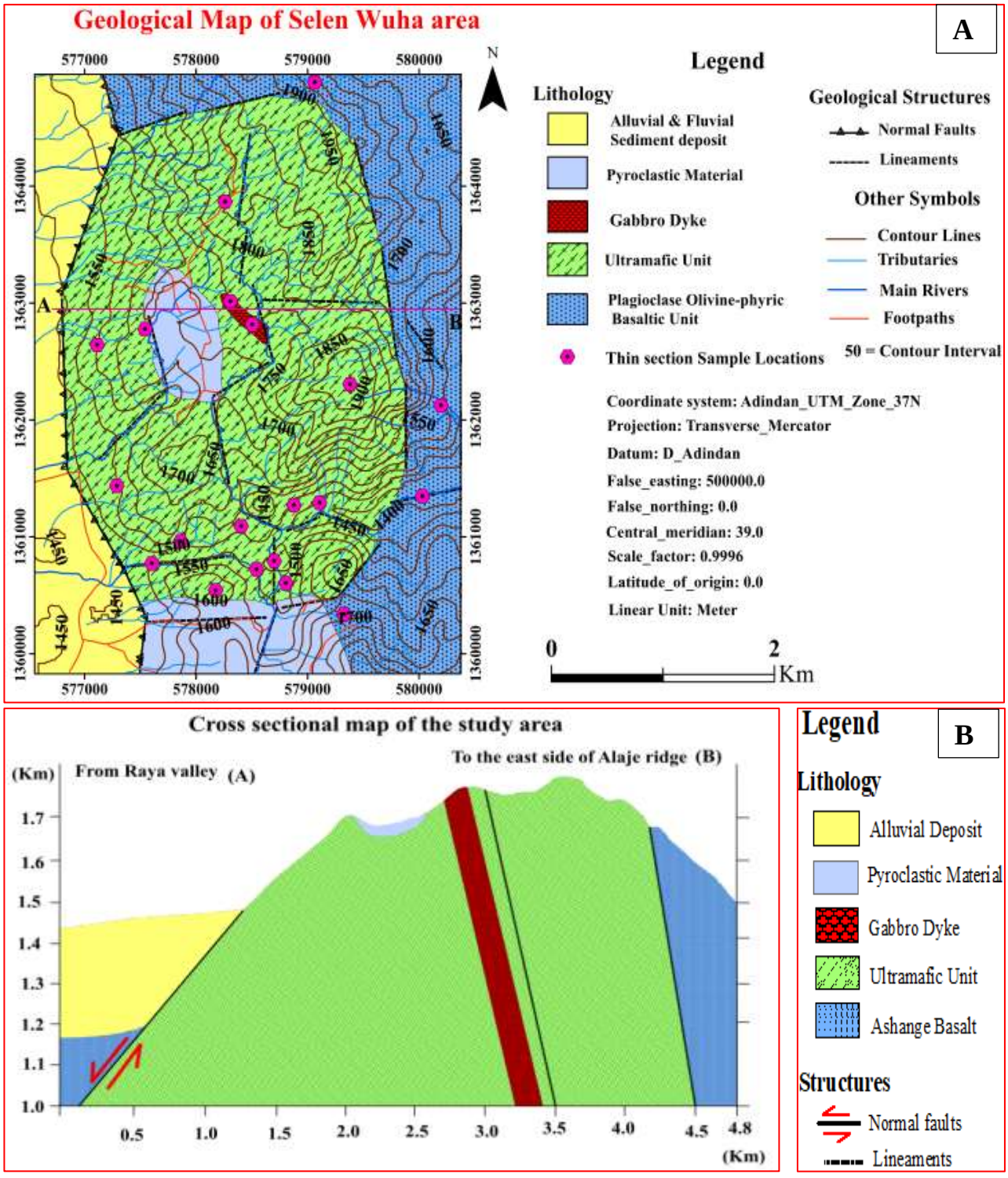

Figure 3. 1: Geological map and cross sectional map of the study area. Geological map is mapped with the scale of 1:25,000 and it shows lithologic and structural distribution of the study area. It also shows topographic variation of the area. (A) Geological map of the study area (B) cross sectional map along A-B profile line (the profile line is from Raya valley to the east side of Alaje ridge).

3.2. Lithology and petrography descriptions of the units

3.2.1. Ultramafic unit

This unit covers an extensive area and its areal extent is about 9.4km^2 (53.71%) of the mapped area. The particular localities where this ultramafic unit has extensively exposed are Alaje ridge, Amed Ager, Selen Wuha river, Gubana ridge and Kassie ridge (figure 1.1). The strength of the unit varies from very weak to very strong. This is due to the strong effect of fracturing and weathering (alteration). The strongly weathered ultramafic unit is exposed in all parts of the study area where this ultramafic unit is covered. It is well exposed on top and sides of hills and ridges. However, it is not found in the rivers where the strong dark colored relatively fine grained ultramafic unit is outcropped. The color of this weathered unit ranges from reddish brown to pale yellowish brown. Since fracture is high here, the unit is altered deeply. As a result, it is easily fragmented when hammered slowly and it has no fresh surface even in the interior of large broken samples (fig. 3.2 C). In this unit abundant large sized pyroxene minerals are present. The size of these pyroxene mineral grains reaches up to 1.8cm (fig. 3.2 A & B). These grains are also altered but not as high as their surroundings. As it has mentioned earlier, the strongly altered ultramafic unit is also affect by fracturing and some fractures of the unit have filled with sheeted light colored secondary materials (veins). These veins are abundant on the Gubana ridge and on the cliff found in both sides of Selen Wuha river (south and north ward of the river).

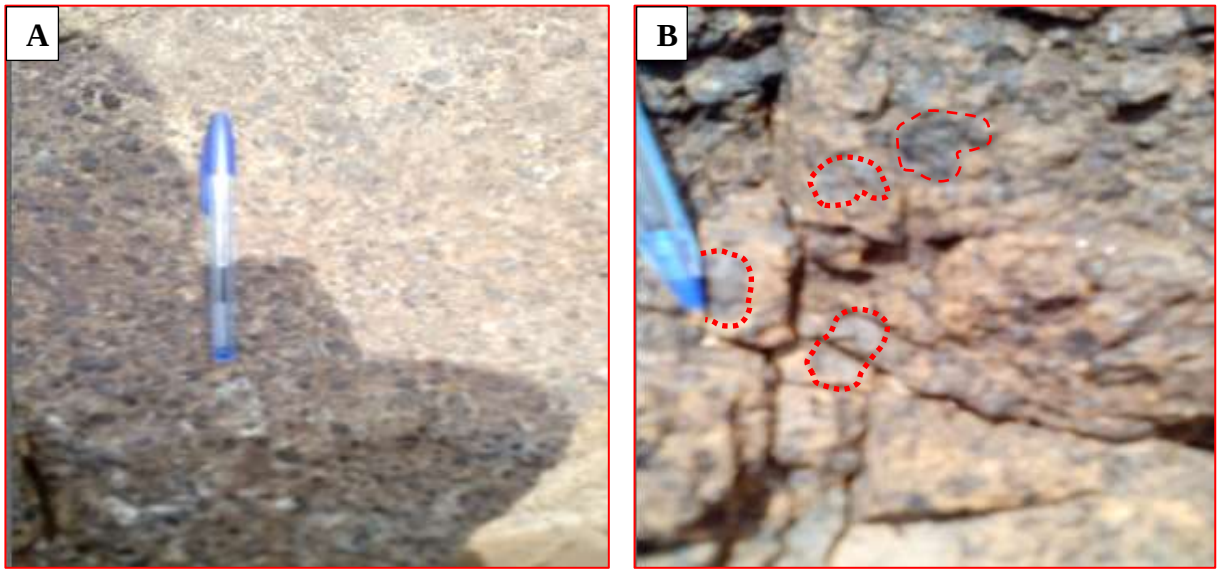

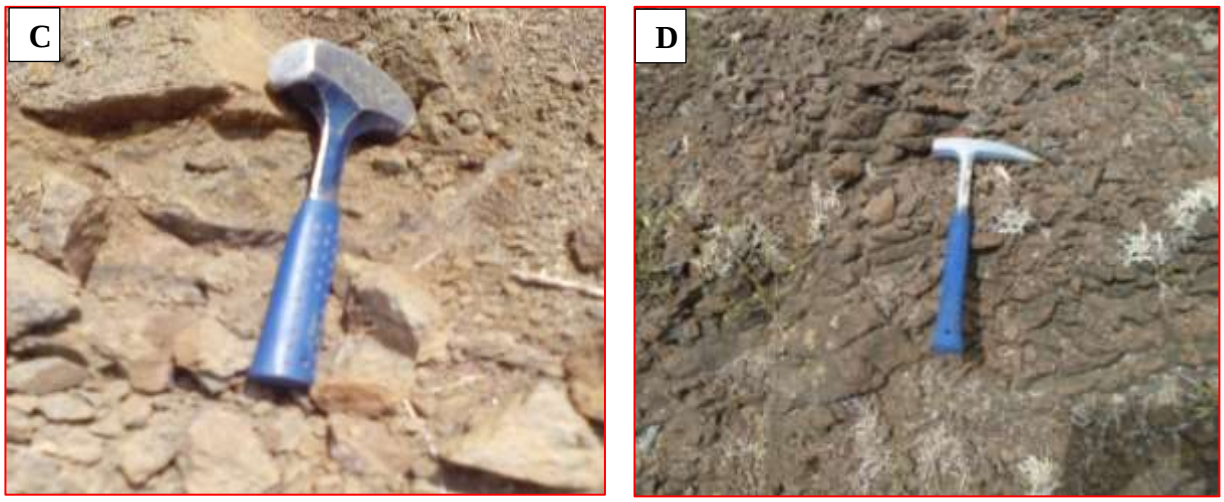

Figure 3. 2: Strongly weathered and fractured ultramafic unit exposed in different part of the study area. Figure (A) shows coarse pyroxene grains in weathered ultramafic unit. Figure (B) shows coarse pyroxene mineral grains via close-up view. Few coarse grains are incircled by broken line. Figure (C) shows strongly weathred and hence easily fragmented ultramafic unit. Figure (D) shows strongly weathred and fractured ultramafic unit.

The color of the harder (strong) ultramafic unit is very dark. This unit is well exposed in Selen Wuha river, Gorso river and Alaje river. Very dark unaltered coarse grained ultramafic boulders are also found on top of the ridges such as on top of Alaje ridge, Amed Ager ridge, Gubana ridge and near Melaku river (i.e. close to Tigrie Mender). The shape of these abundantly disseminated boulders dominantly ranges from sub-rounded to round. They usually coexist with strongly weathered and easily fragmented ultramafic unit. The boulders are too resistant to break with geologic hammer and their broken fresh surface is shiny (fig.3.3 A & F). Moreover, unaltered relatively fine grained dark colored ultramafic unit is exposed in Selen Wuha river, Gorso river and Alaje river. This strong (resistant) dark colored ultramafic unit is strongly fractured. The fractures are oriented non-systematically and some of them are filled by dark colored secondary materials (veins). These veins are altered strongly (fig.3.3 B). Uniquely, slight grain size variation is observed in the dark colored fine grained ultramafic unit outcrop in Selen Wuha river. This variation ranges from fine to medium coarse grained. The coarser grained unit outcrops at the beginning of Selen Wuha river (i.e. east of Raya valley) but as going down the river (i.e. Selen Wuha river), it becomes finer and finer. Particularly, very fine (almost similar to basalt) is found below the junction point of Alaje River and Selen Wuha river. In this exposure, the grains are indistinguishable with unaided eye (fig. 3.3 E). However, the color and petrographic characteristics of the coarser and finer

grained unit is similar. Furthermore, mineral layering (mineral segregation) is not observed throughout the lithology.

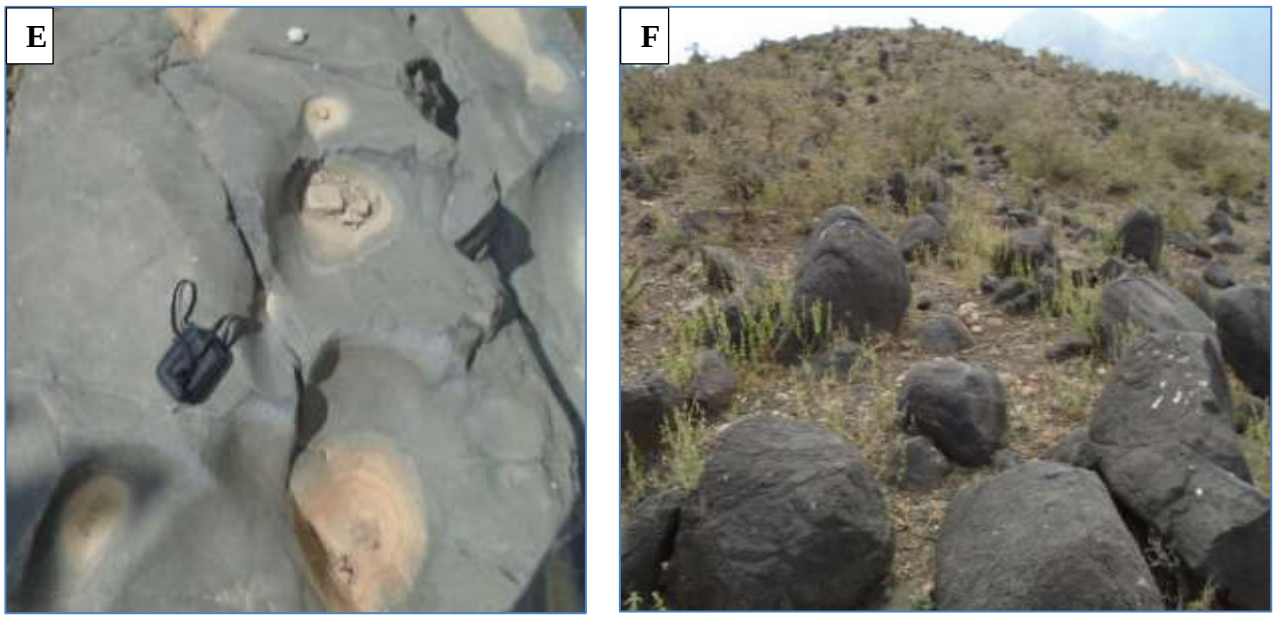

Figure 3. 3: Ultramafic units exposed in different part of the study area. Figure (A & F) shows less altered boulders and blocks of ultramafic unit. Figure (B) dark colored vein hosted in coarse grained ultramafic unit exposed at the begning of Selen Wuha river. Figure (C) strongly weathered and fractured ultramafic unit. Figure (D) strongly weathered and fragmented ultramafic unit found on Gubana ridge and figure (E) relatively fine grained ultramafic unit exposed in Selen Wuha river.

Ten ultramafic thin sections (ST3S6, ST5T5, ST3S4, ST3S5, ST2S3, ST3S2, ST1S11, ST1S7 TPAH and AAMU) have been prepared for petrographic analysis. Almost similar minerals (Ol, Cpx, Opx, and Fe-Ti oxides) are obtained in all these listed thin sections. In few thin sections, fractures filling secondary materials are also present. There is some variation in concentration of olivine mineral in all the ten thin sections. Accordingly, these ten ultramafic thin sections are classified in to olivine poor group, which are grouped under pyroxenite and olivine rich group which are grouped under peridotite. Only three thin sections (ST1S11, TPAH and ST2S3) show relatively high concentration of olivine mineral (>40%). The rest seven thin sections (ST3S6, ST5T5, ST3S4, ST3S5, ST3S2, AAUM and ST1S7) have relatively low concentration of olivine mineral grains (<40%). Clinopyroxene and olivine are the major mineral constituents of pyroxenite group. Hence, their modal proportion ranges from 50% (ST3S6) to 87% (ST3S2) and from 3% (ST3S2) to 35% (ST3S6) respectively. However, Opx and Fe-Ti oxides minerals are relatively the minor mineral constituents. The modal proportion of Opx is between 2% (ST5T5) and 19% (ST3S4) while Op (Fe-Ti oxides) minerals are very small in modal proportion. It ranges from almost 0% (ST3S4 and AAUM) to 7% (ST3S6).

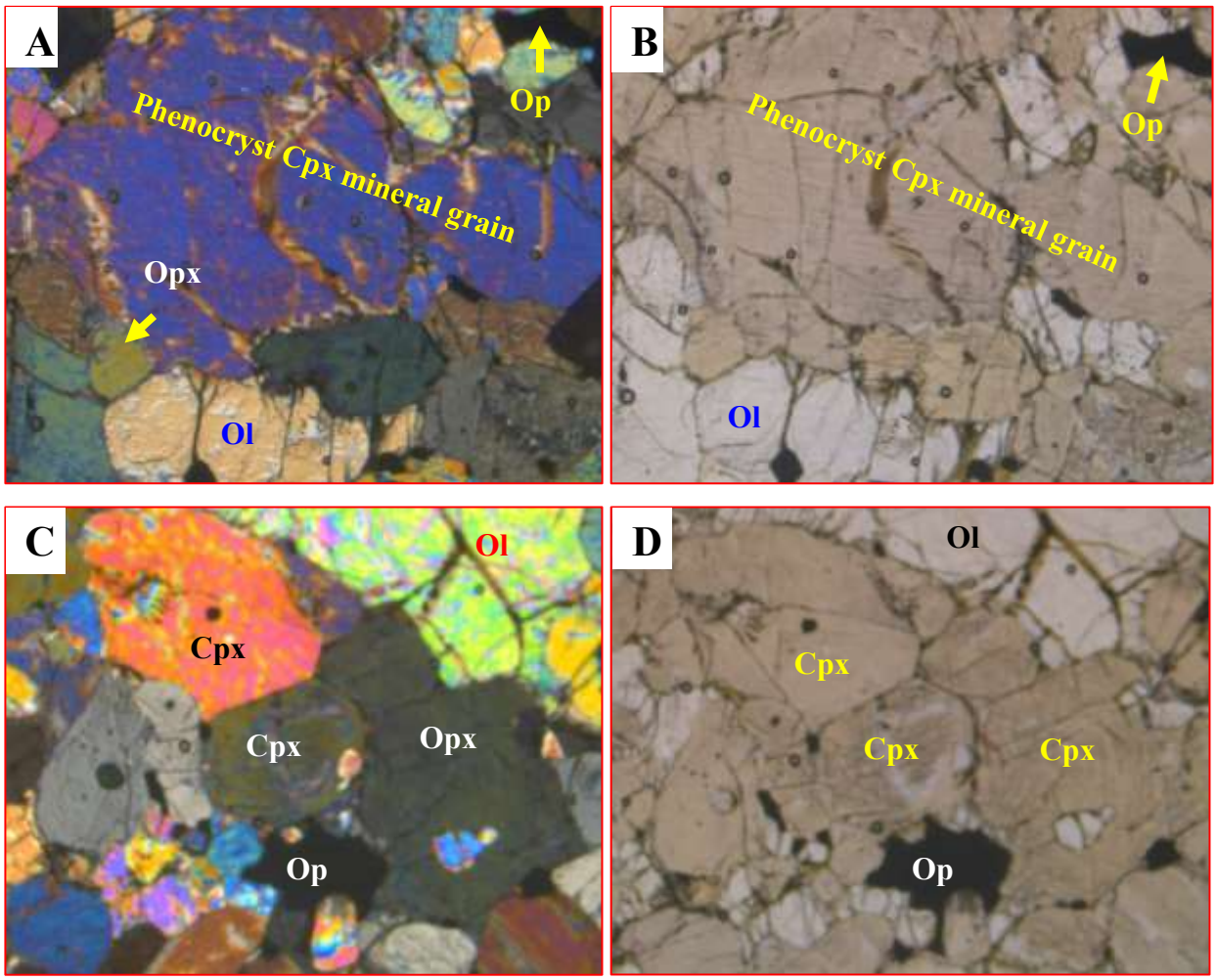

Figure 3. 4: Microphotographs showing the mineral contents of pyroxenite unit. Phenocryst of Cpx is shown in figure (A) and (B). Random arrangement and interlocking of mineral grains are shown in figure (C) and (D). Figure (B) and (D) are capture from PPL view while figure (A) and (C) are from XPL view. The photos are captured using lower magnification power (4x). Ol-olivine, Cpx-clinopyroxene, Opx- orthopyroxene, Op- opaque, PPL-plane polarized light, XPL- cross polarized light.

The concentration of olivine in the peridotite ranges from 75% (ST2S3) to 80% (ST1S11). In this group of ultramafic samples, clinopyroxene is the second dominant mineral and it is about 16% in modal proportion. This model proportion is very small as compared with its model proportion found in olivine poor group of ultramafic thin sections. Peridotite also shows low concentration of opaque and orthopyroxene minerals (table 3.1).

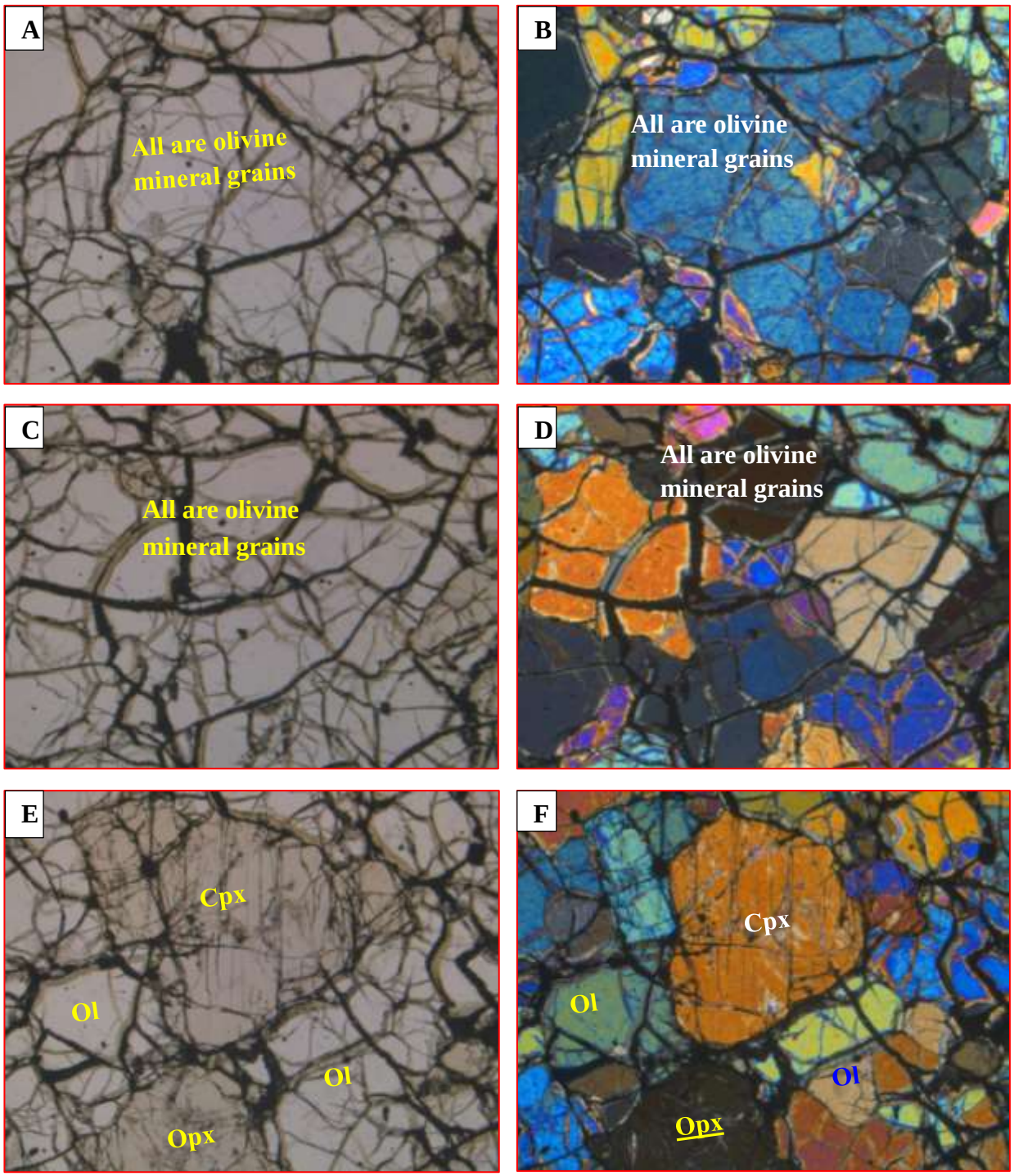

Figure 3.5: Microphotographs show abundant olivine mineral grains in peridotite samples. Figure (A and C) show only olivine mineral grains. However, few pyroxene minerals are shown in figure E. The grains are strongly fractured. The images are from both views (XPL and PPL) and they are captured using lower magnification power (4x).

	Estimated modal proportions (%)									
Mineral	ST5T5	ST3S4	ST3S5	ST2S3	ST3S2	ST1S11	ST1S7	ST3S6	TPAH	AAUM
Cpx	63	56	71	16	87	15	75	50	17	81
Opx	2	19	3	7	8	2	5	8	3	5
Ol	31	25	21	75	3	80	15	35	73	14
Op	4	0	5	2	2	3	5	7	7	0

Table 3.1: Shows estimated modal proportion (%) of the four identified ultramafic minerals. Estimated modal proportion (%) is the average proportion of each mineral from all field views

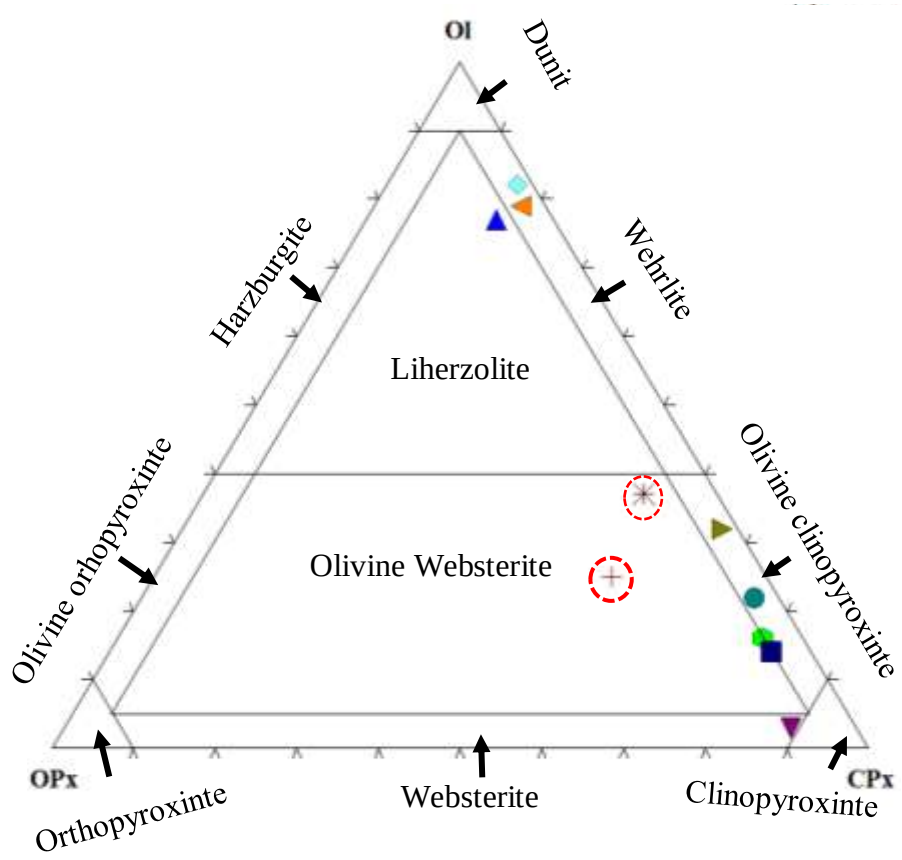

Figure 3. 6: IUGS ultramafic rock classification and nomenclature diagram made using the modal proportion of Ol, Opx and Cpx minerals. This rock classification diagram shows the position of ultramafic samples collected from different part of the lithology.

Olivine mineral grains are colorless (white). However, the color of Cpx and Opx are light brown. The relief difference among the four mineral grains is very small. The two pyroxene (Cpx and Opx) mineral grains have two sets of cleavages. One set of cleavage is a perfect cleavage which is clearly seen under PPL while the other set of cleavage is weak. In average, the angle between the two sets of cleavages is about 90º. In addition, rare clinopyroxene mineral grains have simple and penetrative twinning. Most grains of this mineral have no twinning. Cpx mineral grains have an inclined extinction and the extinction angles of the

measured grains are about 63º, 62º, 50º, 40º. However, these orthopyroxenes have parallel (straight) extinction angle.

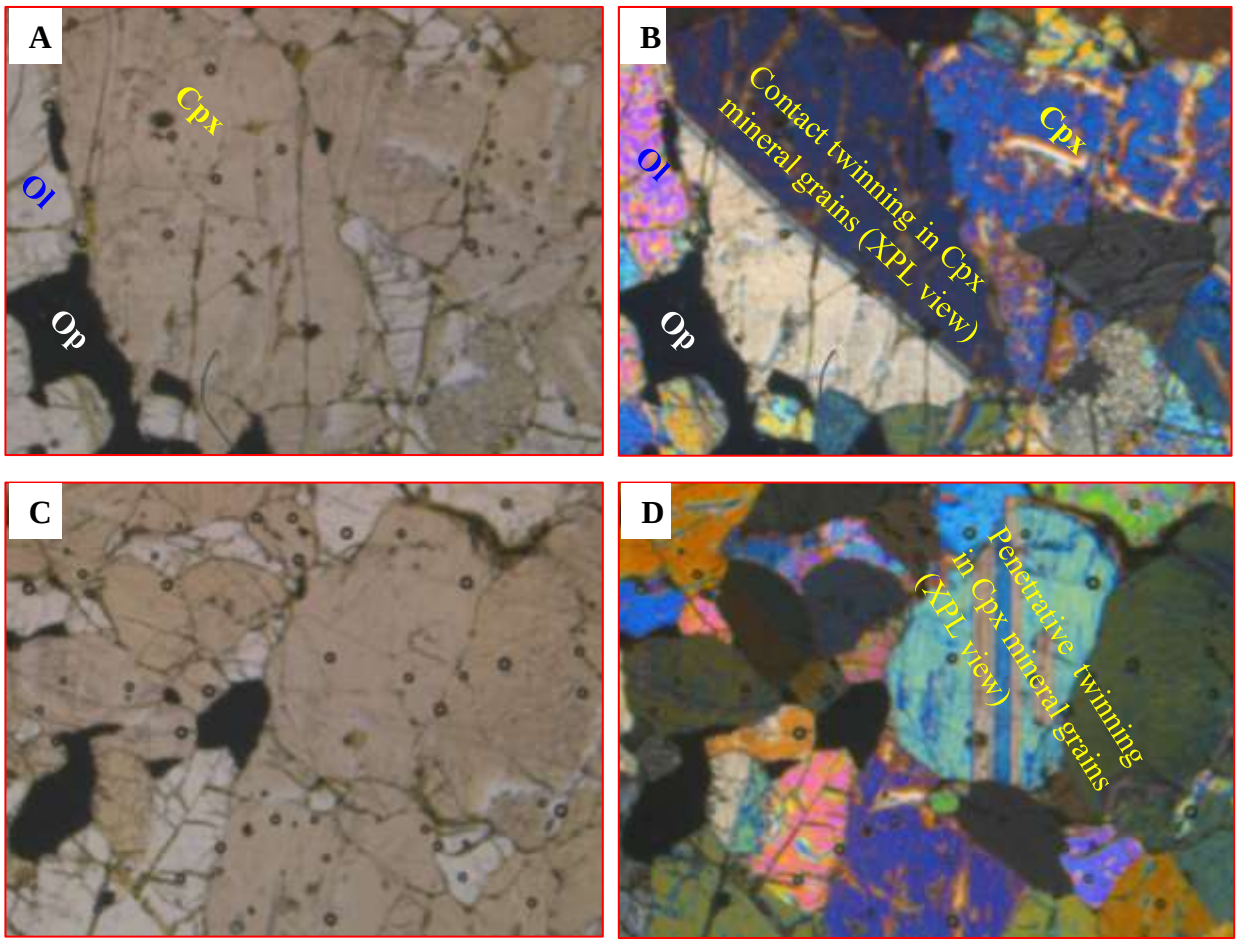

Figure 3. 7: Microphotographs of ultramafic thin sections illustrating mineral content and nature of twinning. Rare contact and penetrative twining is seen in Cpx mineral grains. The images are taken from both PPL and XPL views. Lower magnification power is used to capture the images (4x).

The grains of the minerals are holocrystalline and the unit show inequigranular texture. There is some variation in grain size and grain shape of the minerals. As it has shown in table 3.2, the dominant grain shape of all the mineral grains of the unit is anhedral. Almost all the grains have an irregular outline. The upper and lower limit of grain size distribution (range of grain size for fine, medium, coarse and very coarse grains of the phaneritic units) is documented in Gillespie and Styles (1999). Accordingly, the size of the fine phaneritic crystalline grains ranges from 0.032mm to 0.25mm, medium phaneritic (0.25mm to 2mm), coarse phaneritc (2mm to 16mm) and the size of very coarse phaneritic is greater than 16mm. The size variation of the mineral grains in the studied ultramafic unit ranges dominantly from medium phaneritic to coarse phaneritic (table 3.2). Overall, this unit shows Porphyritic-phaneritic texture. Even though Almost all the grains of the minerals are coarse grained, there are few

exceptional grains which are very large in grain size relative to the grains surrounding them. Mostly, these phenocrysts are olivine, clinopyroxene and orthopyroxene minerals grains.

Minerals	Mineral grain size (mm)		Dominant grains shape	Degree of fracturing
	Length	Width		
CPX	~3.7	~1.6	Anhedr	Less fractured
OPX	~2.5	~1.8	Anhedral	Less fractured
Olivine	~3.5	~2.7	Anhedral	Strongly fractured
Op	~1.5	~0.6	Anhedral	Fracture filling

Table 3.2: Mineral forms and grain size variations present in the four ultramafic minerals. Lower magnification power (4x) is used to measure the size of the mineral grains. Cpx=clinopyroxene, Opx= orthopyroxene, Op= opaque

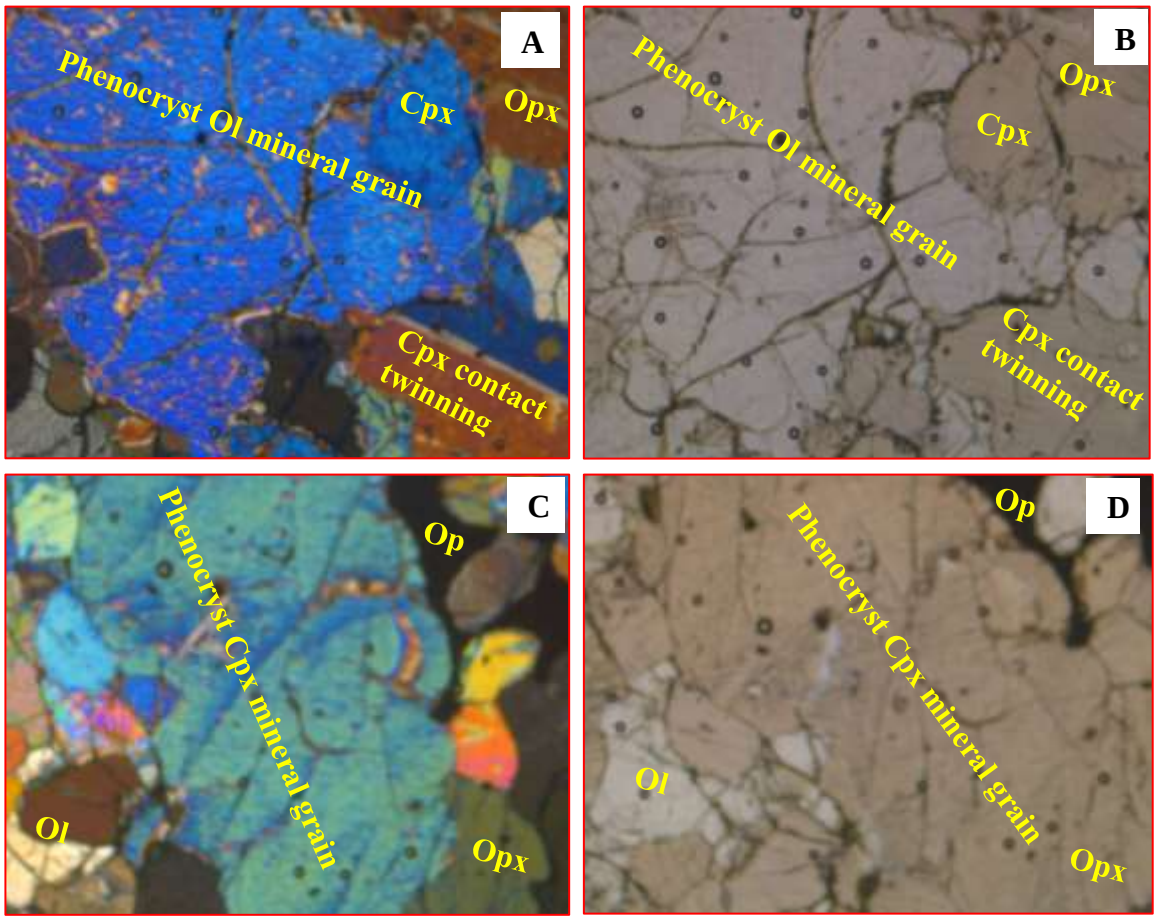

Figure 3. 8: Phenocryst of Cpx and Ol from both XPL and PPL views. The large grains are surrounded by the smaller phaneritic grains of Ol, Cpx, Opx and Op. Olivine phenocryst is shown in figure(A & B) while clinopyroxene phenocryst is shown in figure (C & D).The images are captured using lower magnification power (4x).

All the grains of the minerals have arranged randomly without having preferred alignment. They are interlocking each other and form boundary of triple junctions. Furthermore, metamorphic texture is not observed in all ultramafic thin sections (figure 3.9).

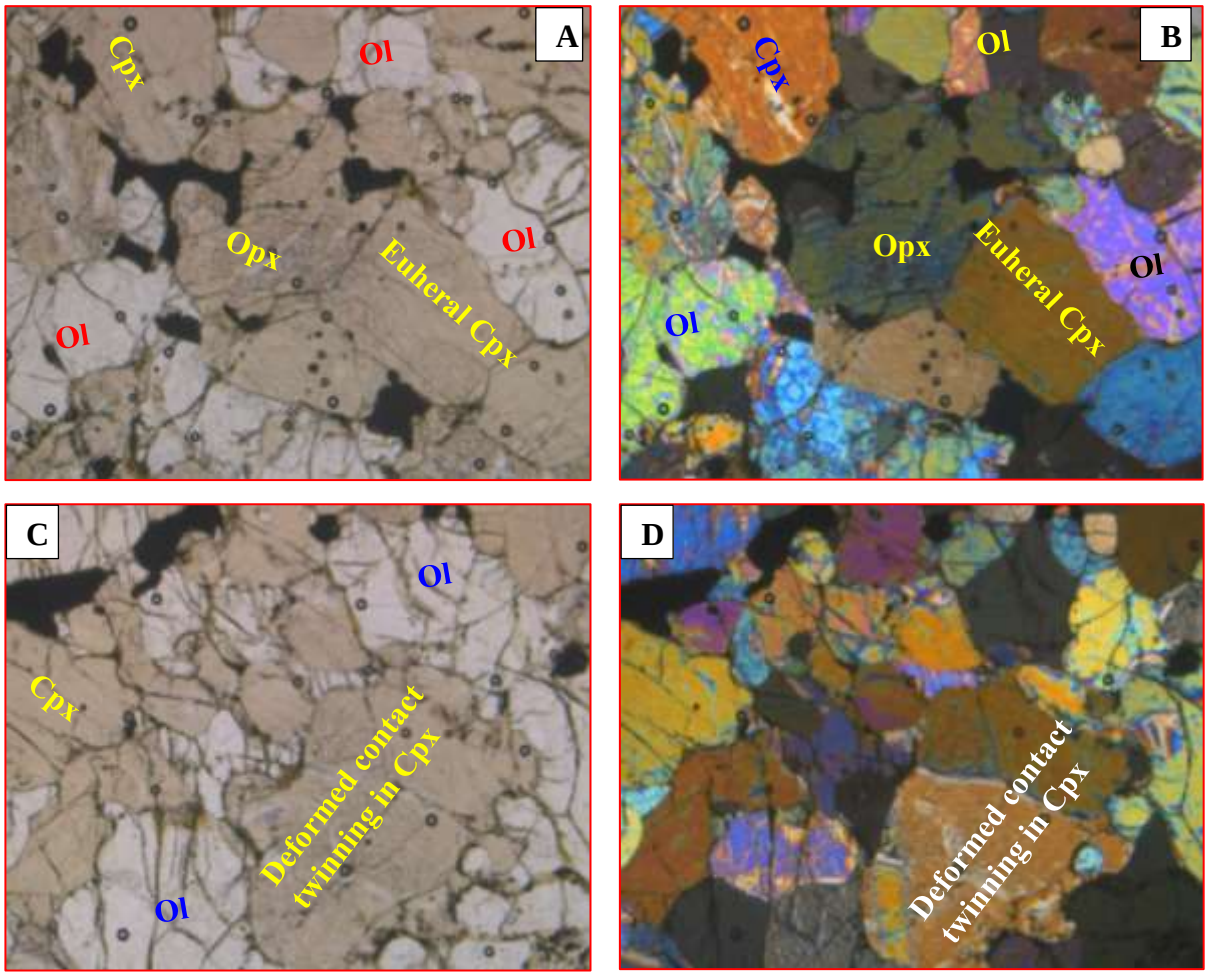

Figure 3. 9: Random arrangement of mineral grain. Contact twinning produced by deformation is also shown in lower image (C & D). Euhedral shaped of Cpx mineral grain is shown in figure (B). These images are captured using lower magnification power (4x).

As it has been stated above in the lithologic description of this study, ultramafic unit of Selen Wuha area is strongly affected by fracturing. These fractures are clearly seen in the outcrop of the unit as joints and veins and in the microscopic scale. Almost all minerals of the unit are affected by fracture. Mineral grains in the seven thin sections (ST3S3V, ST3S2V, ST1S11, ST1S7, ST3S4, ST3S2 and ST5S5) show strong and dense fracture. In few of these thin sections such as ST3S3V, ST3S2V, ST3S4 and ST3S5, Fine opaque mineral grains and other pale yellowish green colored secondary material have filled the fracture. The secondary material is only found in this fracture and it has the shape of that fracture. With this material, there are fine opaque mineral grains (figure 3.10). ST3S3V and ST3S2V are ultramafic thin

sections prepared from the veined ultramafic unit. This veined ultramafic unit is hosted in the relatively less altered ultramafic units. Although fracture filling secondary materials is present in same thin sections (ST3S4 and ST3S5), it is more common in these veined ultramafic samples (ST3S3V and ST3S2V). Fracture filling secondary material shown in figure 3.10 (C & D) is captured from these veined ultramafic samples (ST3S3V and ST3S2V).

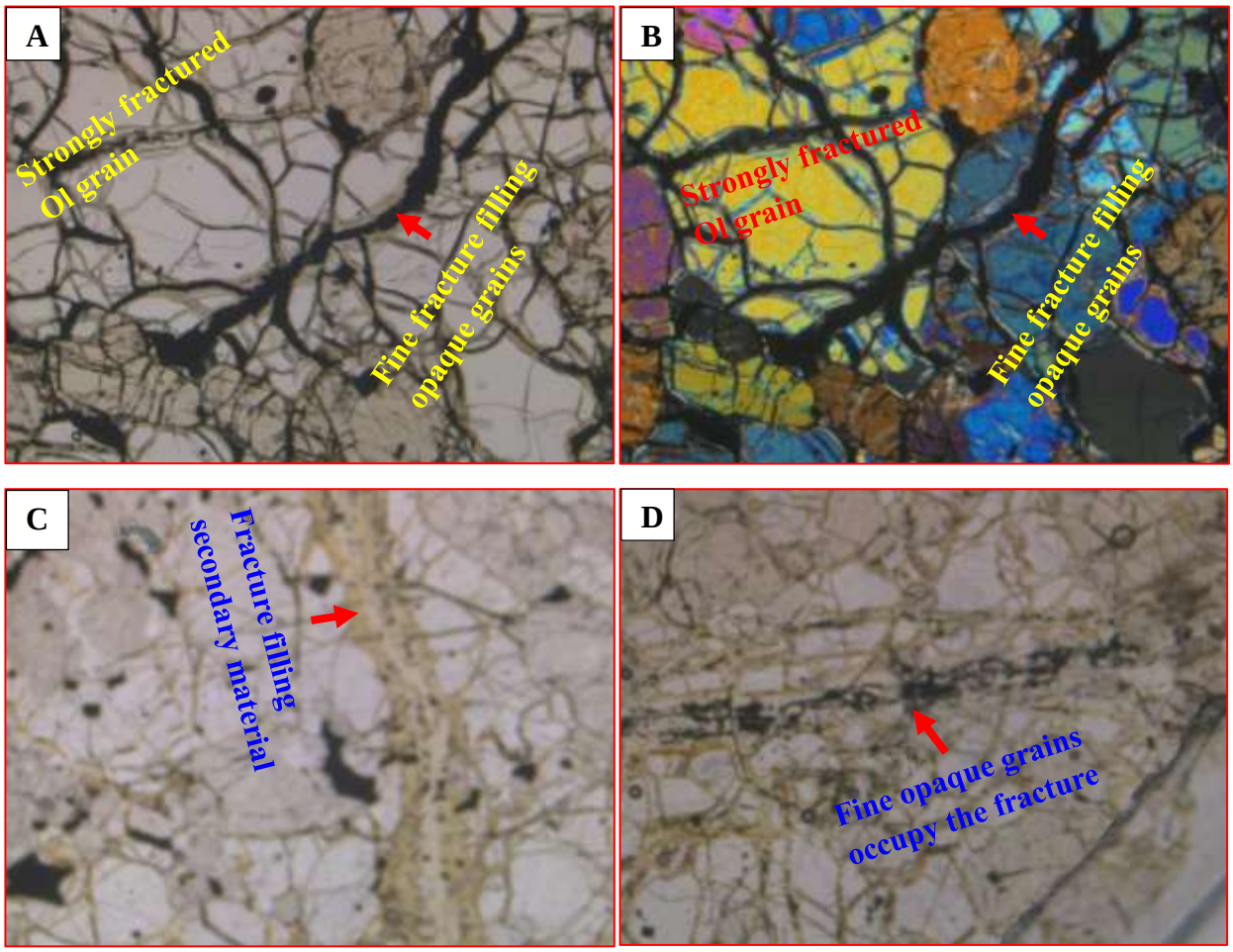

Figure 3. 10: Effect of fracture on olivine mineral and secondary materials filled the fracture. Figure (A & B) are from PPL and XPL views. They show strong fracture on olivine minerals and the fractures are filled by fine opaque minerals. Figure (C & D) are captured from PPL views and they show alteration in the fracture of olivine mineral grain and clustering of fine opaque in fracture. Microphotographs are captured using lower magnification power (4x).

From the petrographic analysis few Fe-Ti oxide minerals are identified. These minerals are mostly obtained in fractures and between mafic mineral grains. In addition, high amount of Cr and considerable concentration of Fe_2O_3 is obtained in geochemically analyzed ultramafic samples. Particularly, the concentration of Cr and Fe_2O_3 is high in ST1S11 and ST1S7 and hence they are prepared for polished section study. The purpose of preparing these polished

sections is to identify the opaque minerals or ores present in the unit. From the study of polished section, identified opaque minerals are magnetite, hematite and very few chromites. Relatively hematite is abundant than the other two identified ores (magnetite and chromite). Slight to strong effect of alteration is seen in magnetite mineral grains while hematite grains are not affected by alteration. In general, insignificant amount of ore minerals are found in both polished sections.

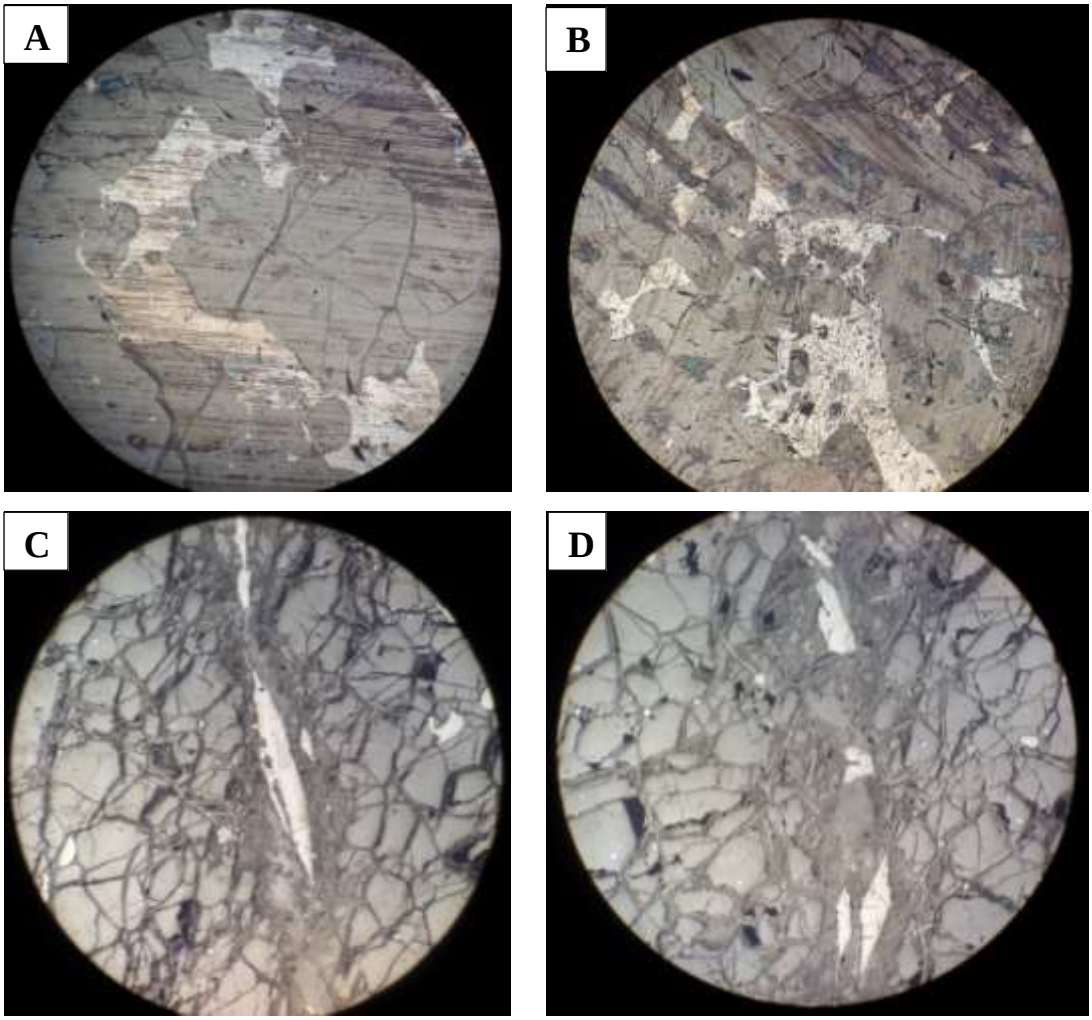

Figure 3.11: Polished section photos showing the ore mineral grains. Figure (A) slightly altered magnetite grain. Figure (B) strongly altered magnetite grain. Figure (C & D) Hematite mineral grain occupied the fracture. The photos are captured using 20X.

3.2.2. Gabbro

Gabbro with altered plagioclase mineral grains is intruded in the weathered ultramafic unit. This plutonic dyke has exposed in three distinct locations. One exposure is found above Tigrie Mender (Tigrie village) in a very close to the margin of upper part of Alje river. This is at

GPS location of X: 0578644 and Y: 1362863. The extent of this exposure is wider than the other two gabbro exposures. It is about 250m and it dips toward east with an angle of about 75^{O} to 80^{O}. Since it is coarse grained, minerals of the unit are easily distinguishable with unaided eye. The two dominant minerals are well identified via their color contrast. Thus, the white colored minerals are plagioclase while the dark colored minerals are pyroxenes. In this dyke, pyroxene minerals are looking dominant over plagioclase minerals and therefore it is pyroxene rich gabbro unit. The other two exposures are found on the Gubana ridge in the west side of Melaku river. In this ridge, very small dykes of this unit are outcropped at very close to Gubana mender (GPS X: 0577309 and Y: 1362495). The size of these dykes ranges from 60cm to 1.0m. These dykes are also grouped in pyroxene rich gabbro unit. In this dyke, plagioclase minerals are strongly affected by alteration. The third exposure of this unit is found in similar ridge at the pathway taking from Raya Mender to Amed Ager village. This is at GPS location of X: 0577181 and Y: 1363176. It is exposed with micro-gabbro and they are outcropped as densely disseminated boulders. They are found on top and side of the hill. In this unit, plagioclase minerals grains are looking dominant over pyroxenes and therefore it is plagioclase rich gabbro unit (fig.3.12 A & D**)**. All these dykes have almost the same orientation. They are oriented in northwest direction.

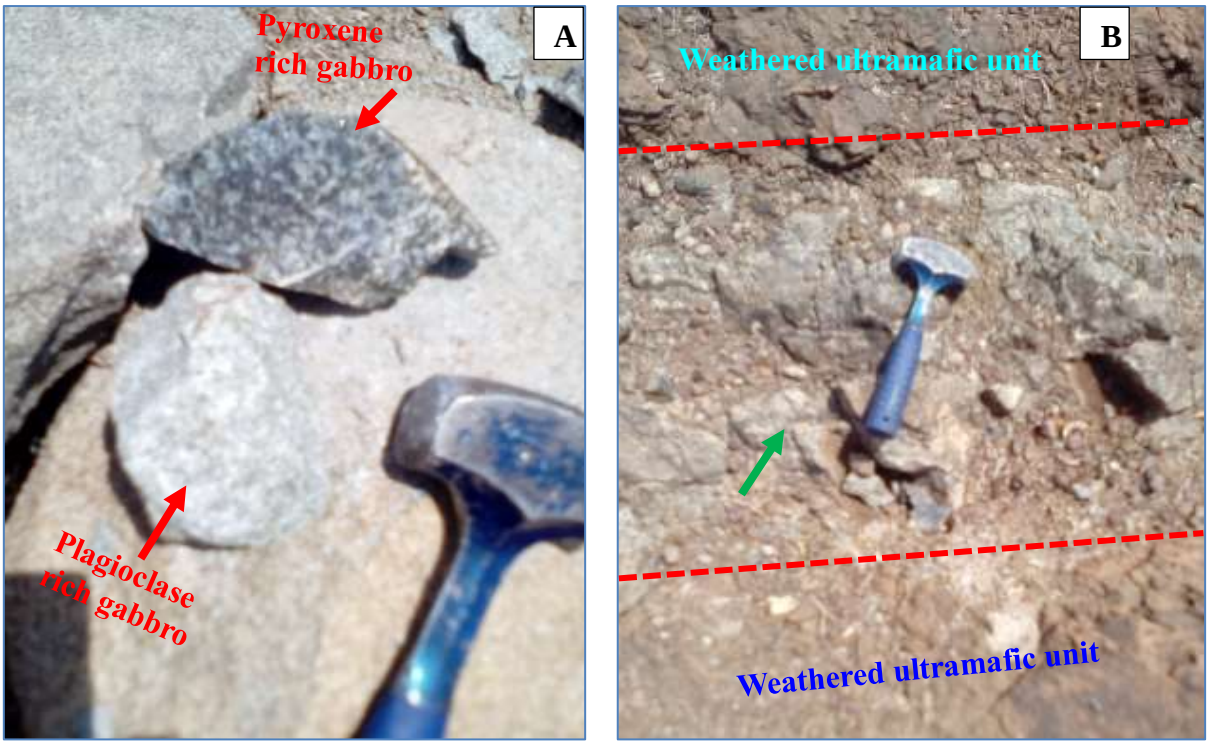

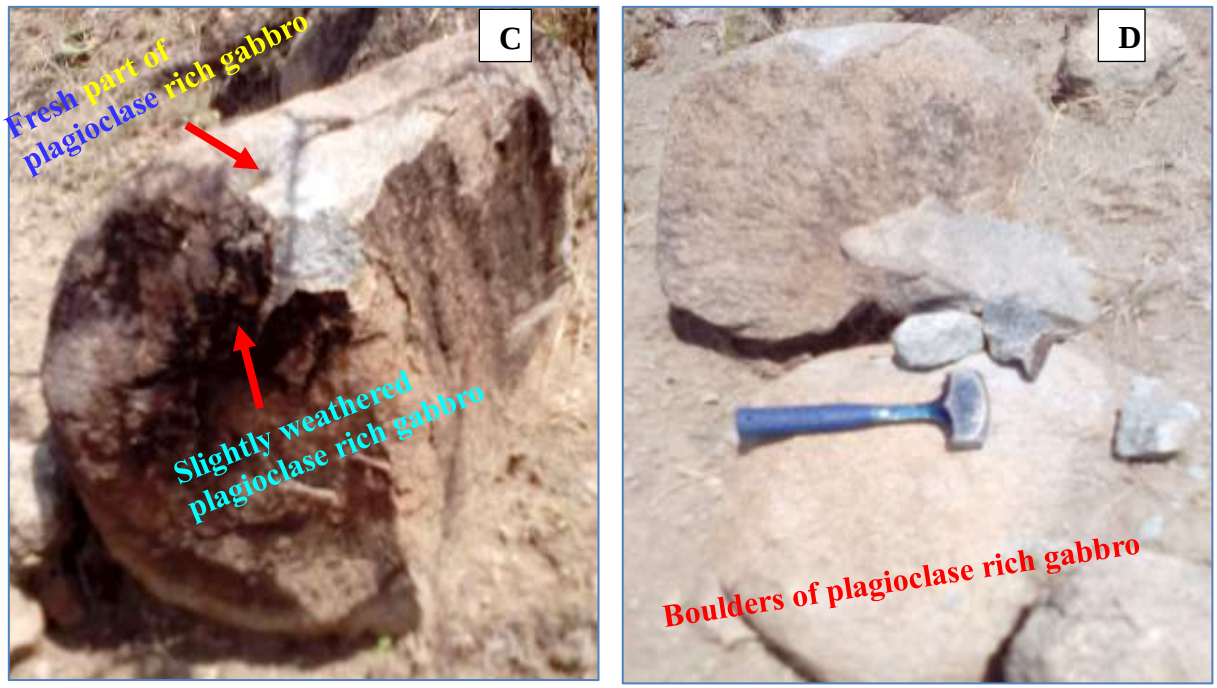

Figure 3. 12: Pyroxene rich gabbro dyke and different type of gabbro units. Figure (A) pyroxene rich and plagioclase rich gabbro. Figure (B) small dyke of pyroxene rich gabbro. The dyke is indicated by green arrow. Figure (C) fresh and slightly altered part of plagioclase rich gabbro. Figure (D) exposure of plagioclase rich blocks and boulders.

Both plagioclase rich and pyroxene rich gabbro are outcropped as boulders and blocks. They are moderately weathered and hence their weathered part is relatively weak in strength than the unaltered unit. Rare strongly weathered blocks of pyroxene rich gabbro are also found in the area (fig.3.13B). The color of the weathered unit is range from pale yellowish gray to grayish dark. Since both minerals of the unit are coarse and easily visible with the naked eye, the texture of the unit is phaneritic.

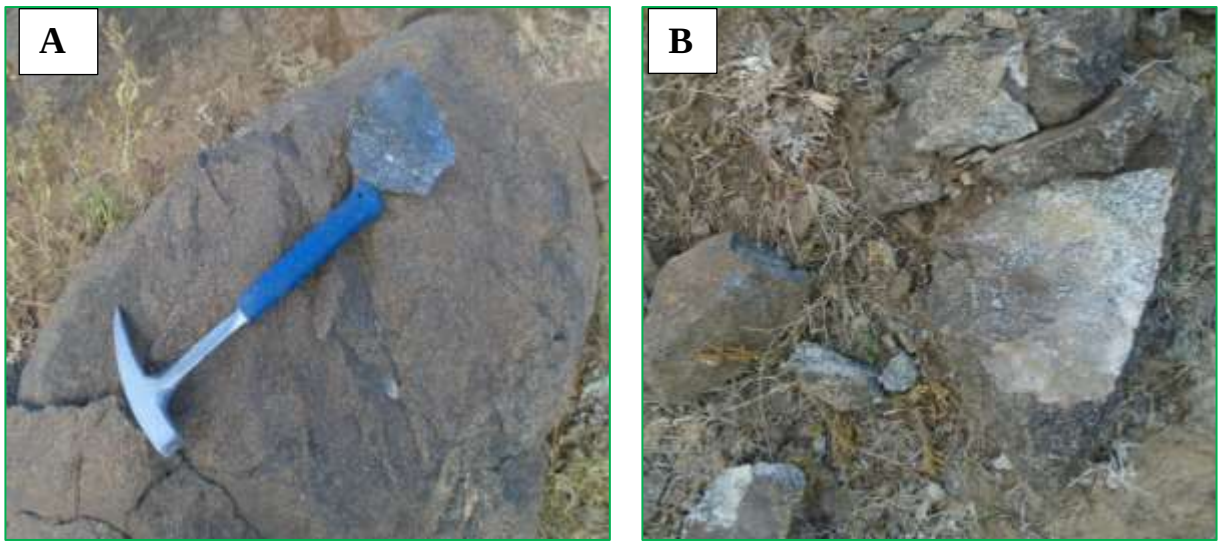

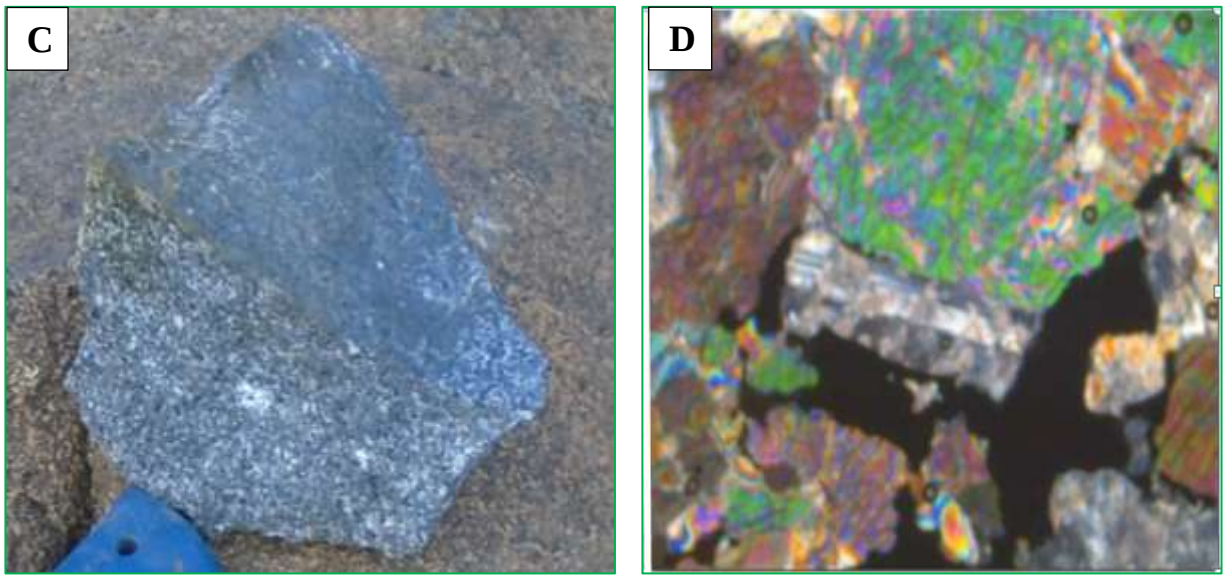

Figure 3. 13: Strongly to moderately weathered gabbro. *Figure (A) slightly weathered gabbro and piece of fresh gabbro is shown on top of it. Figure (B) strongly altered gabbro unit. Figure (C) minerals of the unit are shown on piece of fresh gabbro by close-up view. Figure (D) minerals of the unit in thin section. This microphotography is captured via lower magnification power (4x) of petrographic microscope.*

Two thin sections (ST4S4 and ST4S6) have been prepared for petrographic analysis. The identified mineral constituents of the unit are plagioclase, clinopyroxene, olivine and Fe-Ti oxides. Among these mineral constituents, plagioclase and clinopyroxene gets dominant and their modal proportion ranges from 40% to 55% and from 30% to 40% respectively. While Fe-Ti oxides and olivine minerals are minor constituents of the unit. Opaque minerals constitute up to 20% while olivine minerals are composed of less than 5% (table 3.3).

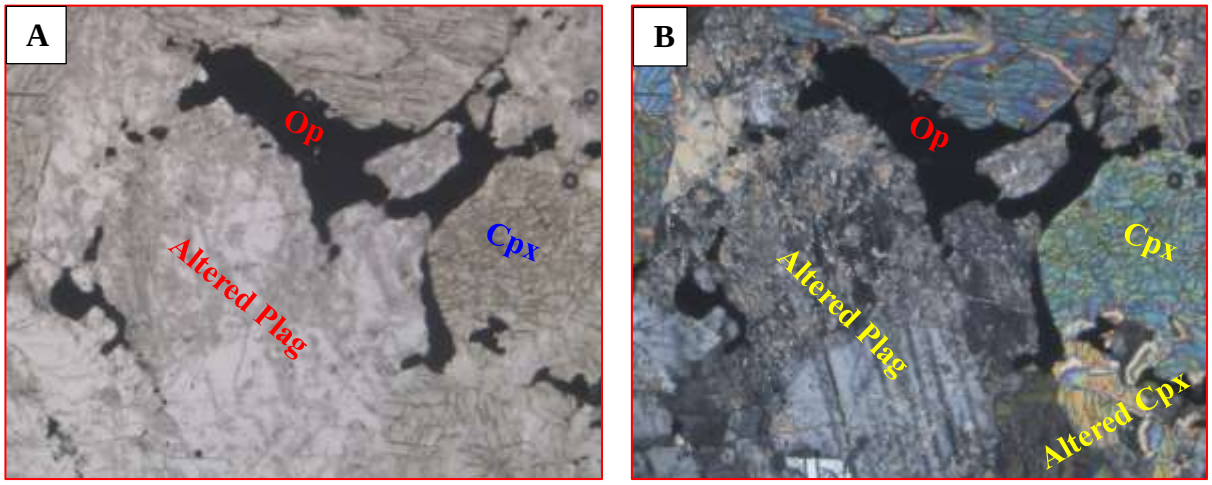

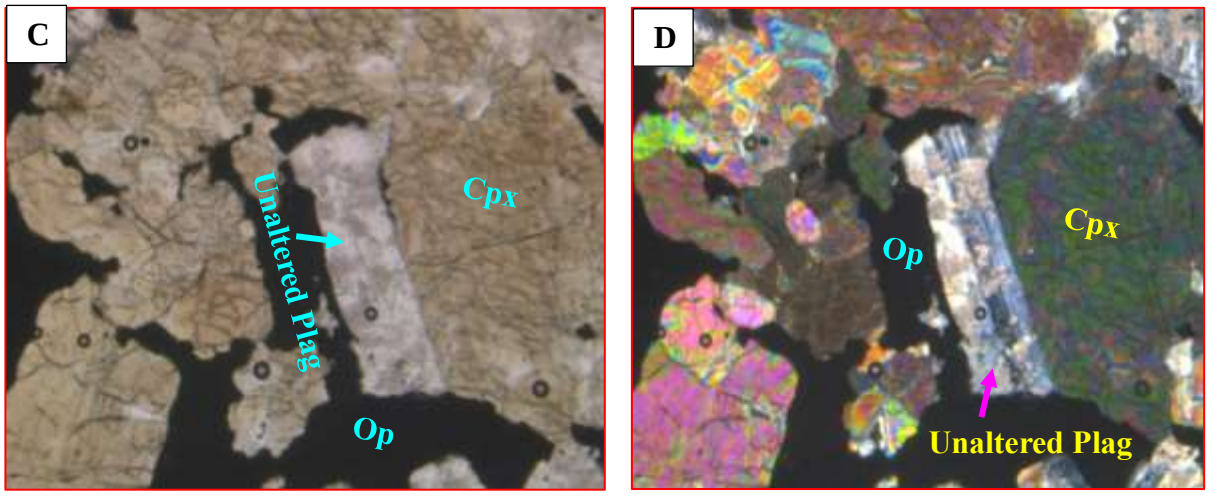

Figure 3. 14: The photos are taken from both PPL and XPL views to show the mineral constituent of the unit. Figure (A) is a photo taken from PPL view and it shows the mineral constituent of the unit. Figure (B) is a photo taken from XPL view to show the alteration effect on minerals of the unit. Figure (C and D) are also from both PPL and XPL view and show the shape of mineral mineral grains. Lower magnification power (4x) is used to capture the microphotography images. Cpx = clinopyroxene, Plag = plagioclase, Op = opaque

The unaltered grains of plagioclase minerals show polysynthetic twinning and few Cpx mineral grains exhibit contact twinning. In addition, there are two sets of cleavages in Cpx mineral grains. These are intersecting at an angle of approximately 90^{O}. One set of cleavage is perfectly seen while the other set of cleavage is relatively weak or not seen perfectly. These mineral grains have inclined extinction angle with an approximate angle of about 50º, 46º, 42º, 47º, 55º.

There is variation in the shape or habit of the mineral grains. Consequently, skeletal shape is the dominant shape of Fe-Ti oxides. But there are few relatively small isolated grains having anhedral shape. This skeletal shape is developed due to partially or completely enclosing of other mineral grains such as Cpx and plag. As it has illustrated in the table 3.3**,** the dominant crystal shape of clinopyroxene and olivine grains are anhedral but few crystals of clinopyroxene grains show subhedral and euhedral shapes. On the other hand, plagioclase crystal grains have dominantly anhedral shape but significant numbers of plagioclase mineral grains are euhedral and subhedral in crystal shapes. Plagioclase mineral grains have affected strongly by fracture and hydrothermal alteration. Generally, the quality of the plagioclase grains is reduced due to the effect of this hydrothermal alteration (figure 3.15).

Minerals	Modal (%)		Grains Size (mm)		Dominant grains Shape
	ST4S4	ST4S6	Length	Width	
Plag	48	44	~3.0	~1.0	Anhedral
Cpx	37	35	~3.0	~2.4	Anhedral
Op	13	18	~3.0	~1.0	Skeletal and branched
Ol	2	3	~1.5	~0.6	Anhedral

Table 3.3: This table shows modal proportion of minerals, grains size (maximum and minimum length and width of representative grains) and dominant shape of the grains of the minerals forming the gabbro unit.

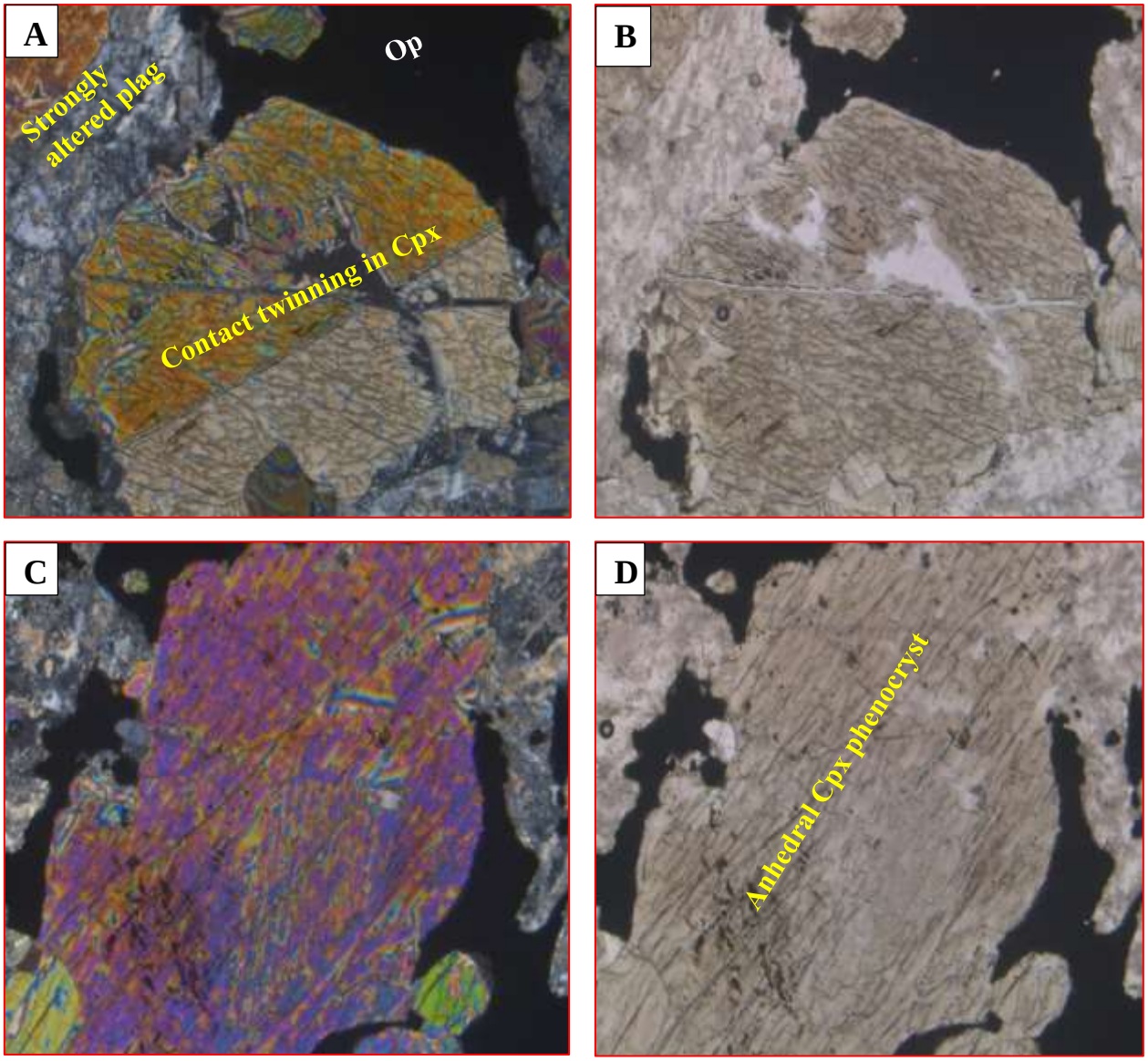

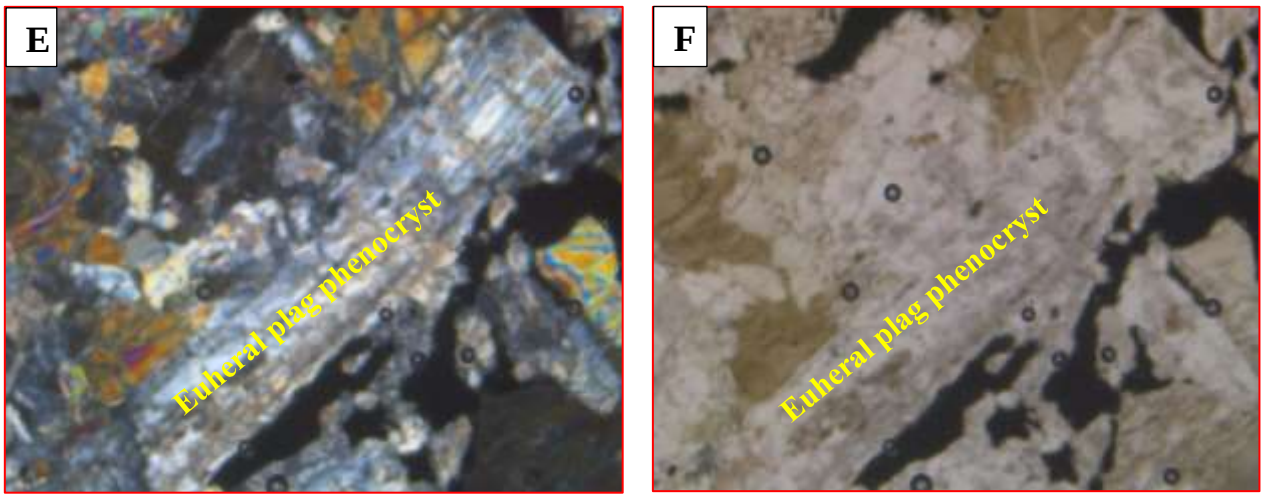

Figure 3.15: Microphotographs showing contact twinning and Porphyritic-phaneritic texture. Figure (A & B) are from PPL and XPL view and it shows contact twining in slightly altered euhedral Cpx mineral grain. Figure (A) Figure (C and D) phenocryst of anhedral CPX mineral grain. Figure (E & F) phenocryst of moderately altered plag. Lower magnification power (4x) is used to capture these images. Cpx = clinopyroxene, Plag = plagioclase, Op = opaque

Mineral grains of plagioclase, pyroxene, olivine and opaque have randomly interlocked in each other without forming preferred alignment. Accordingly, they have an igneous texture rather than metamorphic texture. The overall texture of the unit is phaneritic texture.

Since the unit is built from holocrystalline coarse mineral grains, its minerals are easily recognized one from the other using lower magnification power (4x). Although they are coarse in size, there is a variation in grain size among them. This variation is range from medium phaneritic to coarse phaneritic. Accordingly, they are inequigranular in texture. The size variation is range from about 1.5mm to 3.0mm. There is also an intergranular texture between clinopyroxene and plagioclase. In this case Fe-Ti oxides mineral grains fill the gap in between plagioclase and clinopyroxene grains (Figure 3.16).

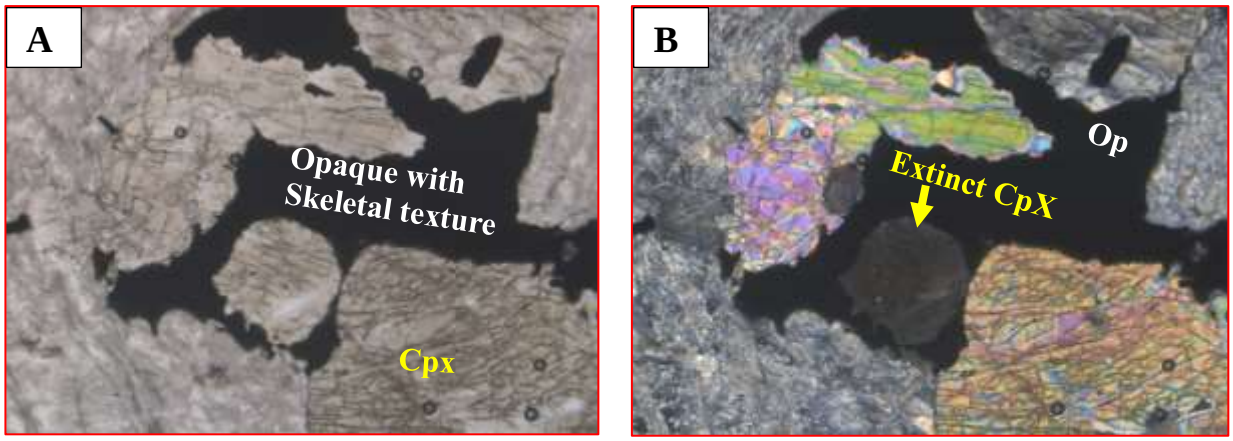

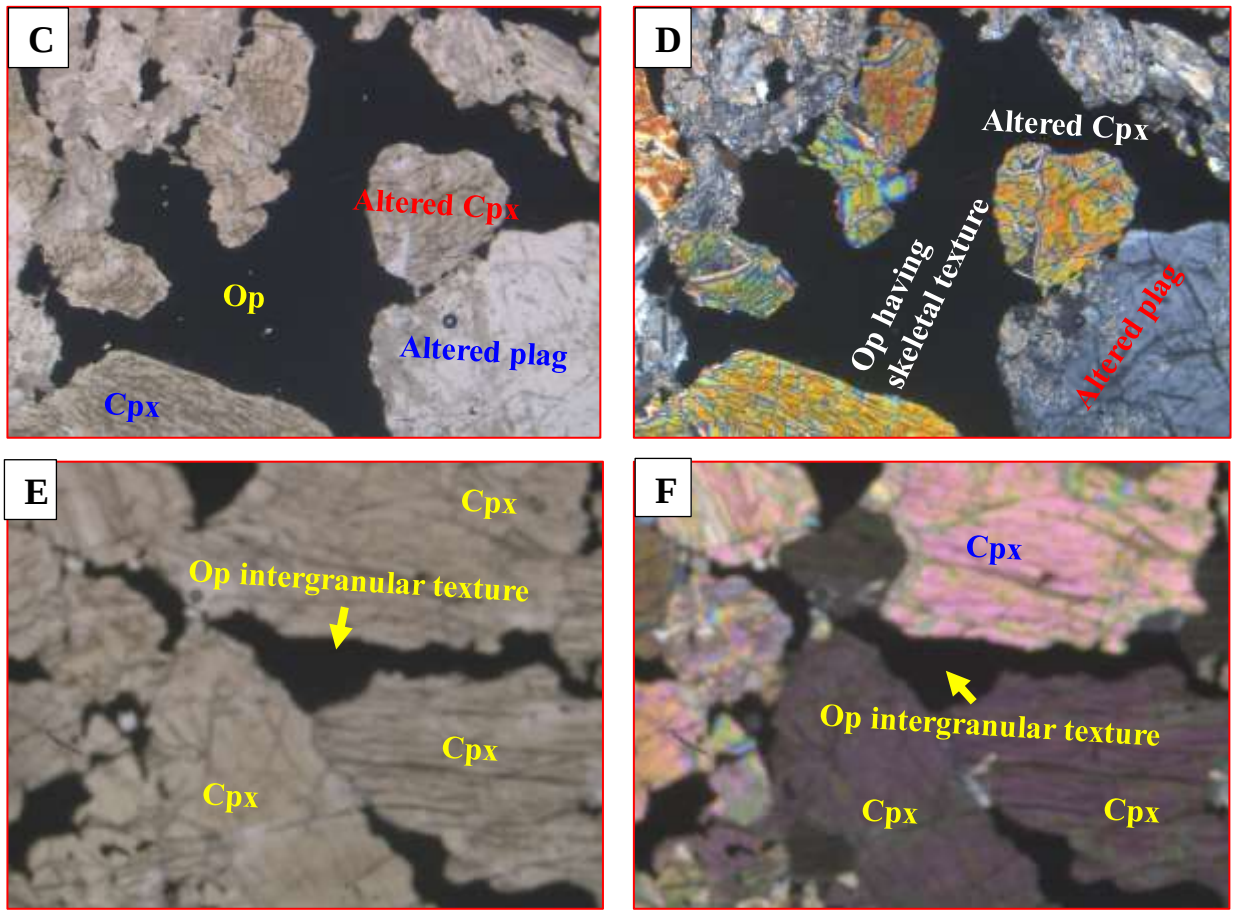

Figure 3. 16: These microphotographs show mineral texture (intergranular and skeletal texture) and the effect of alteration on both plagioclase and pyroxene mineral grains. *Figure (A), (C) and (E) are microphotographs from PPL view and Figure (B), (D) and (F) are microphotographs from XPL view. Altered plag is clearly seen in Figure (B) and (D)*

3.2.3. Plagioclase olivine-phyric basalt

In the study area, this basalt unit is exposed in the north, east and south-east side of the target unit (ultramafic unit). It is the second abundantly exposed lithologic unit. It covers about 3.95km^2 (22.57%) of the mapped area. Although rare massive unaltered outcrops are present, strong fracturing and jointing are the main characteristics of this basaltic unit. On the other word, this plagioclase-olivine phyric basaltic unit is strongly fractured and moderately weathered. The weathered color of the unit is pale yellowish to yellowish gray. Dark and dark grayish color is the common color of the fresh unaltered basalt. This texturally aphanitic (fine grained) unit is well exposed on the top of hills and ridges and in the river cut areas (i.e. on both side of the river banks). The basaltic unit exposed on the banks of the rivers is relatively less weathered and mostly it is not weathered. It is also outcropped in the form of dykes. Dykes of the basalt unit are also intruded in the ultramafic unit and in the pyroclastic

materials. The width of the outcropped dykes ranges from few centimeters to about 1.6m. The largest basaltic dyke is intruded in this plagioclase-olivine phyric basalt unit that outcropped in the east of Alaje ridge while the smallest dyke is intruded in the ultramafic unit and outcropped around Amed Ager ridge. The detail about these basaltic dykes exposed in different part of the study area is described in chapter four.

Figure 3. 17: Massive and strongly fractured basaltic unit exposed in different part of the area. *Fugure (A & B) shows massive unaltered dark to dark gray colored basaltic unit outcropped in the southeast direction of Gubagalla ridge and in the east ward of Alage ridge to the lower part of Selen Wuha river respectively. both pictures are capured from river bank exposures. figure (C & D) shows strongly fratured basaltic unit exposed in various part of the mapped area. mainly it is exposed in the east ward of Alaje ridge, Amed Ager ridge and to the south direction of lower SelenWuha river.*

Four thin sections are prepared for petrographic analysis. All these four thin sections show porphyritic texture and the unit they built is holocrystalline porphyritic rock unit. Phenocryst minerals are dominantly plagioclase, olivine and opaque (Fe-Ti oxides) mineral grains. In addition, very rare pyroxene (Cpx) phenocryst mineral grains also present. All these collectively make up about 30% of the studied unit and generally the unit is moderately porphyritic unit. From these phenocryst minerals, plagioclase gets dominant and it consists about 70% of the phenocryst abundancy. The second abundant phenocryst mineral is olivine and its estimated modal proportion is about 20%. Opaque and pyroxene microcrystalline phenocrysts use the remaining 10%. As it has mentioned, pyroxene phenocrysts are the least and very rare in concentration. Hence, they are about 2% in abundancy.

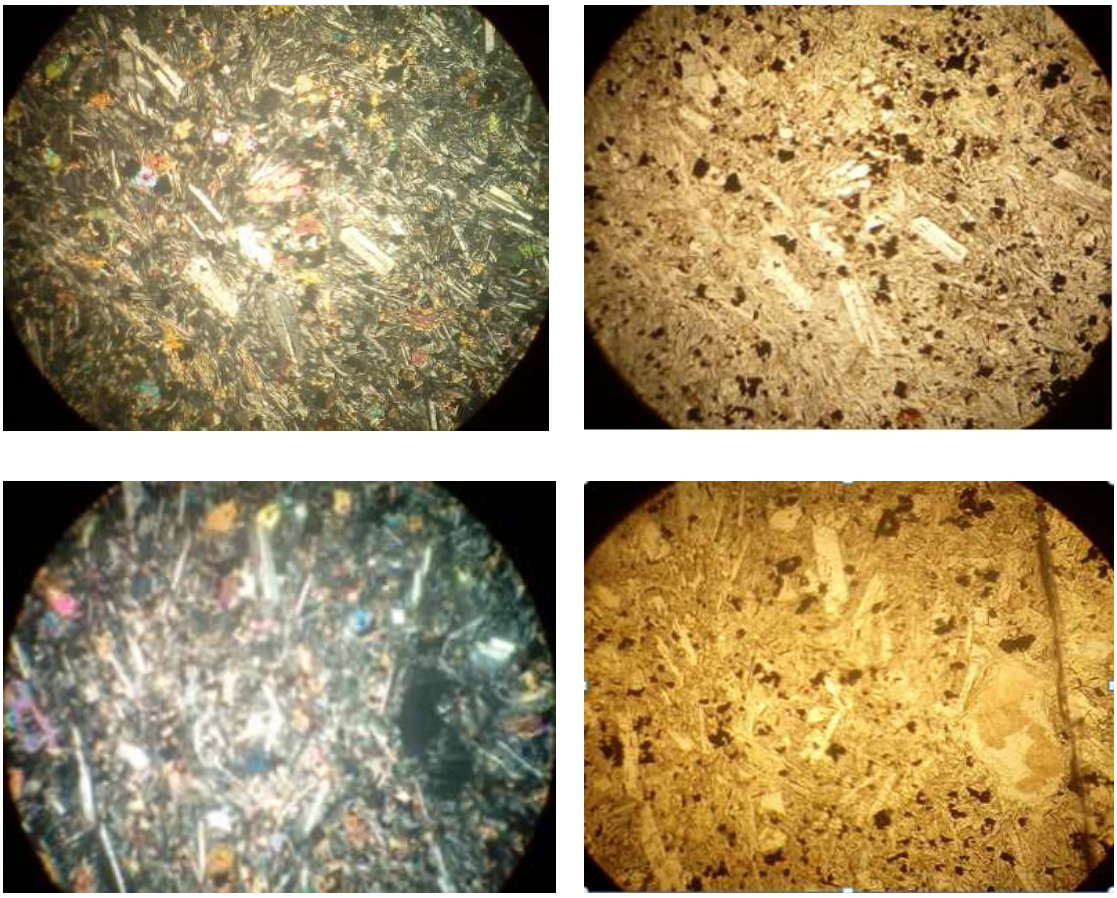

Figure 3. 18: Mineral content and porphyritic texture of the unit. *These photos are captured using medium magnification power (10X)*

Plagioclase phenocrysts are the largest in size and their maximum size reaches up to 3mm. In addition, almost all the large grains of this mineral are elongated and tabular in habit. These elongated plagioclase minerals show some sort of alignment. On the other hand, the elongation of both plagioclase phenocrysts and ground mass are aligned almost in specific

direction. This indicates the flow direction of the melt (magma). These elongated and tabular shaped grains of plagioclase mineral are not totally euhedral in grain shape. Microcrystalline Opaque and few olivine mineral grains are embedded in these elongated tabular shaped grains of this plagioclase mineral. Due to this inclusion and reaction effect, considerable grains of this mineral have developed subhedral grain shape. Accordingly, the overall shape of these plagioclases phenocrysts is euhedral to subhedral. Moreover, these plagioclase mineral grains have multiple twinning and very rare grains of this mineral show concentric zoning and this zoning is probably normal zoning.

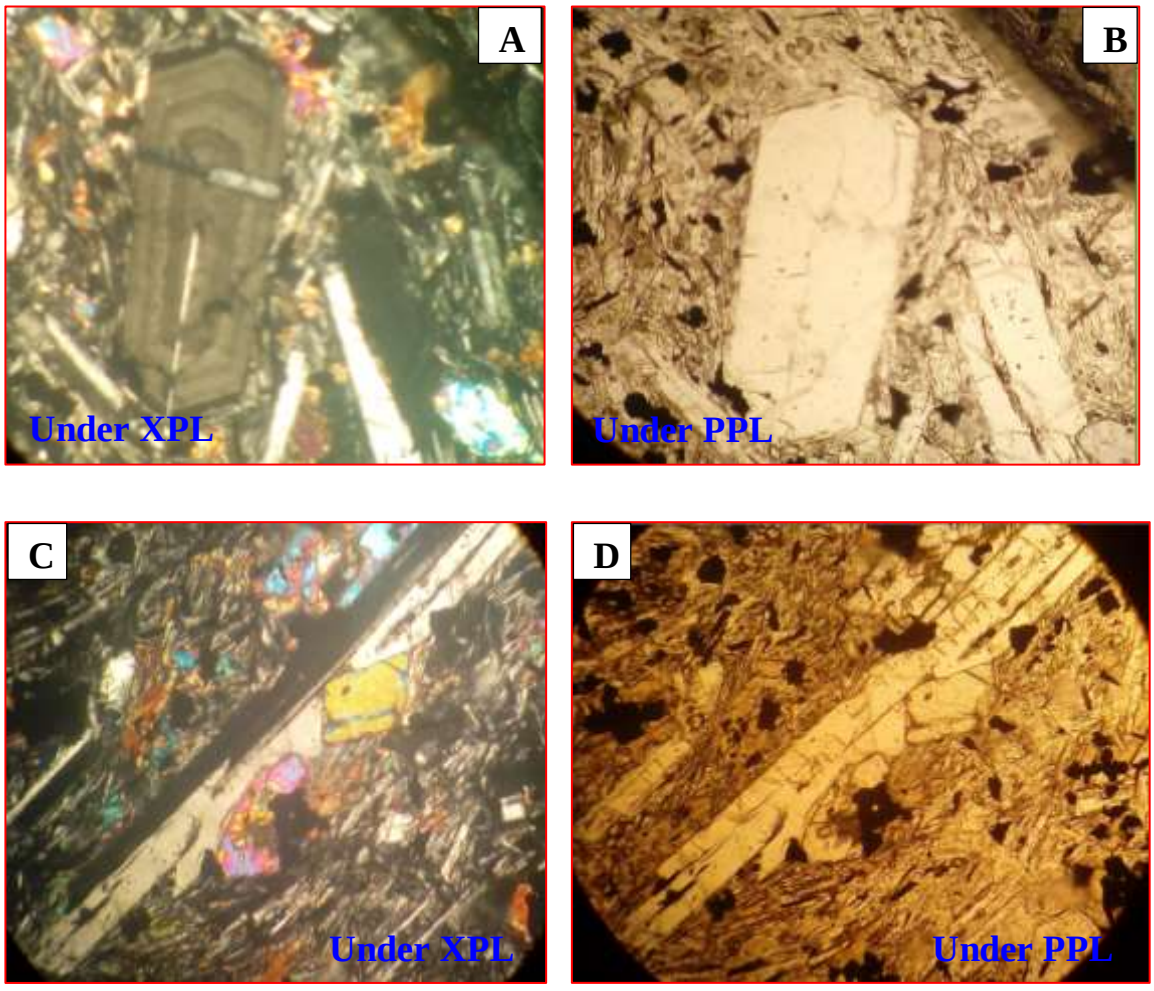

Figure 3. 19: Mineral zoning and mineral inclusions. *Figure (A & B) shows plagioclase zoning. It also shows phenocryst grains of Plag, Ol and Pxn. Figure (C & D) shows mineral inclusions. Ol and Op phenocrysts are embedded in Plag phenocryst. The pictures are captured using higher magnification power (40X).*

As it has already mentioned, Olivine and pyroxene phenocrysts (coarse and visible in grain size) are present in all thin sections. Olivine phenocrysts are the second abundant mineral

grains in the unit and they are smaller in size as compared with plagioclase phenocrysts. The largest olivine phenocrysts are measured up to 1.5mm. Moreover, olivine phenocrysts are affected by fracture and inclusion of Fe-Ti oxide minerals are seen in all thin sections. Significant plagioclase grains are also embedded in these olivine phenocrysts. As a result of these factors, the dominant shape of olivine phenocrysts is anhedral. Furthermore, significant sub-hedral grains of this phenocryst mineral are present in all thin sections.

Microcrystalline Opaque minerals are identified and mostly they are present as inclusions in the olivine and plagioclase phenocrysts. They make up about 8% of the phenocryst abundance. These dark coloured microcrystalline phenocryst grains are found sparsely. On the other hand, opaque minerals are not clustered rather they are spread out sparsely and found everywhere close to uniform distribution. They are far smaller as compared with plagioclase and olivine phenocryst grains. Accordingly, the dominant size of these grains is about 0.8mm. Even though considerable subhedral grains of these mineral are observed in all thin sections, they are dominantly anhedral in grain shape. In addition, very few euhedral opaque grains are present in the analysed samples.

Similar to the phenocryst phases, the identified ground mass minerals of the analysed samples are plagioclase, olivine, pyroxene and Fe-Ti oxides. These ground mass minerals cover about 70%. From these ground mass phases, plagioclase mineral laths are dominant. In modal proportion, they occupy about 65%. These plagioclase laths are thinly elongated tabular grains and they are aligned in the same directions by surrounded to those phenocryst minerals found in all analysed samples. They are also found as inclusion in olivine, plagioclase and opaque phenocrysts. Olivine and pyroxene collectively are the second abundant minerals and they are about 25%. The remaining 10% is occupied by fine opaque ground mass mineral. Since plagioclase and olivine are dominant phenocryst minerals, the studied rock unit is named as plagioclase olivine-phyric basalt or porphyritic plagioclase olivine basalt.

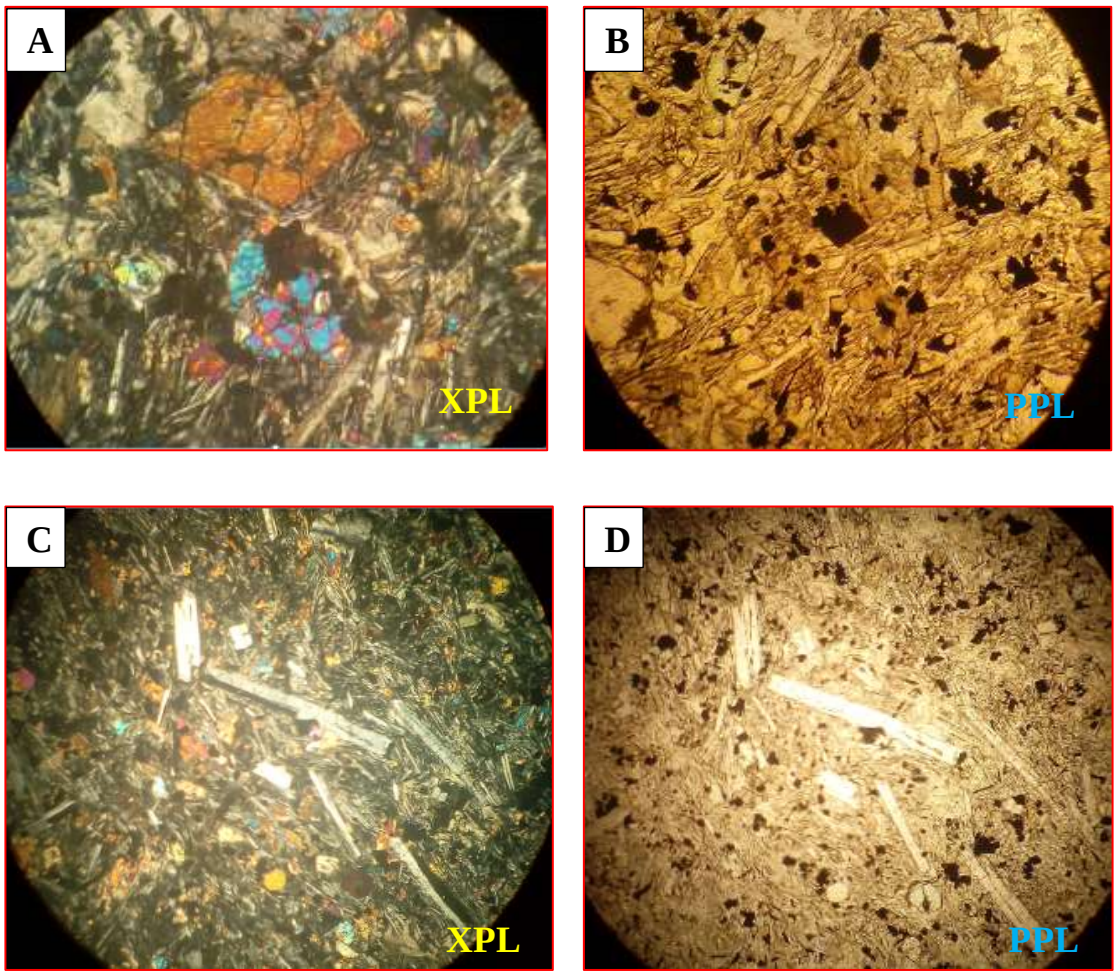

Figure 3. 20: Mineral shapes and arrangement. Figure (A) subhedral and anhedral olivine grains. Figure (B) anhedral and subhedral shape of opaque mineral grains. Figure (C & D) subhedral and euhedral shape of plagioclase minerals. The pictures are captured using higher (40X) and medium magnification power (10X)

3.2.4. Pyroclastic material

Outcrops of pyroclastic materials such as volcanic ash and slight to moderately welded ash (tuff) are present in the study area. Slight to moderately weld volcanic ash outcrops above Mesnokelowa village and around Kassie ridge. It also expose around Tigrie Mender (i.e. between Melaku river and Alaje river). Accordingly, the slightly welded volcanic ash is found around Tigrie Mender while the moderately welded volcanic ash is exposed above Mesnokelowa and around Kassie ridge. Collectively, their areal coverage is estimated to 1.75km^2 or 10.0% of the mapped area.

The moderately welded volcanic ash (tuff), outcrops above Mesnokelowa village and around Kassie ridge, is mainly characterized by hill side or ridge side exposures. However, it is also

found on top of hills and ridges. Unconsolidated fine grained volcanic ash (loose ash) is also present with this moderately welded volcanic ash (tuff). The color of the unconsolidated (loose) ash is light to grayish light while the color of the moderately welded volcanic ash is vary from pinkish (reddish) gray to gray. Few pinkish to reddish colored pyroclastic materials are also coexist with this moderately welded volcanic ash. These pinkish to reddish colored materials have smooth surface and slightly harder than the grayish moderately welded pyroclastic materials. This moderately welded pyroclastic material has rough surface and weak strength and hence it is easily fragmented when hammered with geological hammer.

This pyroclastic unit (loose and slightly welded ash) is contacted with the weathered ultramafic unit in the Kassie ridge. This is in the south side of Selen Wuha river. However, the contact between the two units is gradational contact. The ultramafic unit found on the south margin of Selen Wuha river (i.e. toward Kobo side) has intercalated with this fine ash material and this pyroclastic material is becoming thicker and thicker as going southward (i.e. toward the Mesnokelowa village). Eventually, the exposure of ultramafic unit is terminated in Kassie ridge at GPS location of Easting (X): 578120 and Northing (Y): 1360298 and it becomes the boundary of the two units.

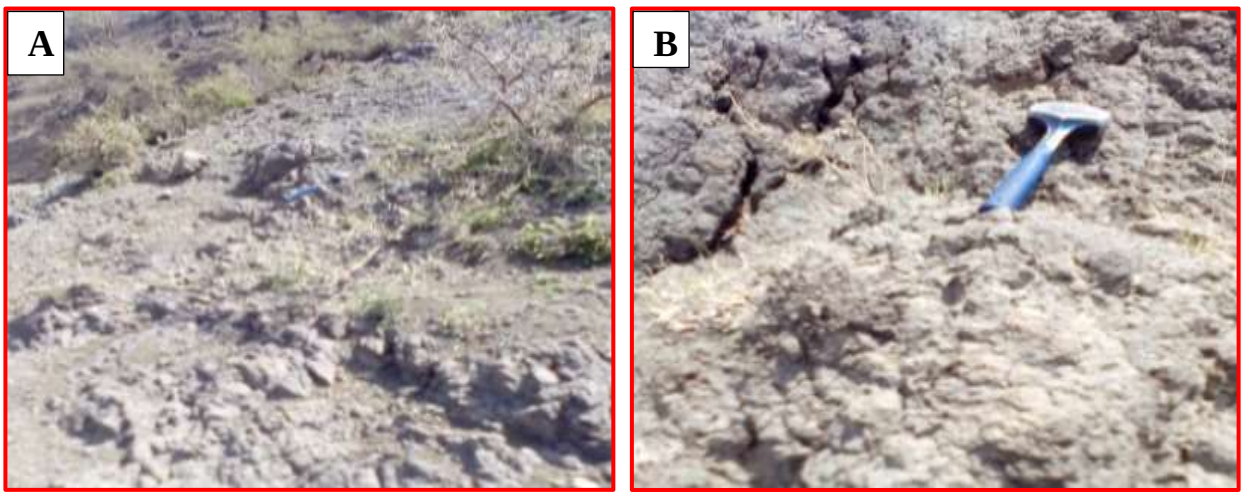

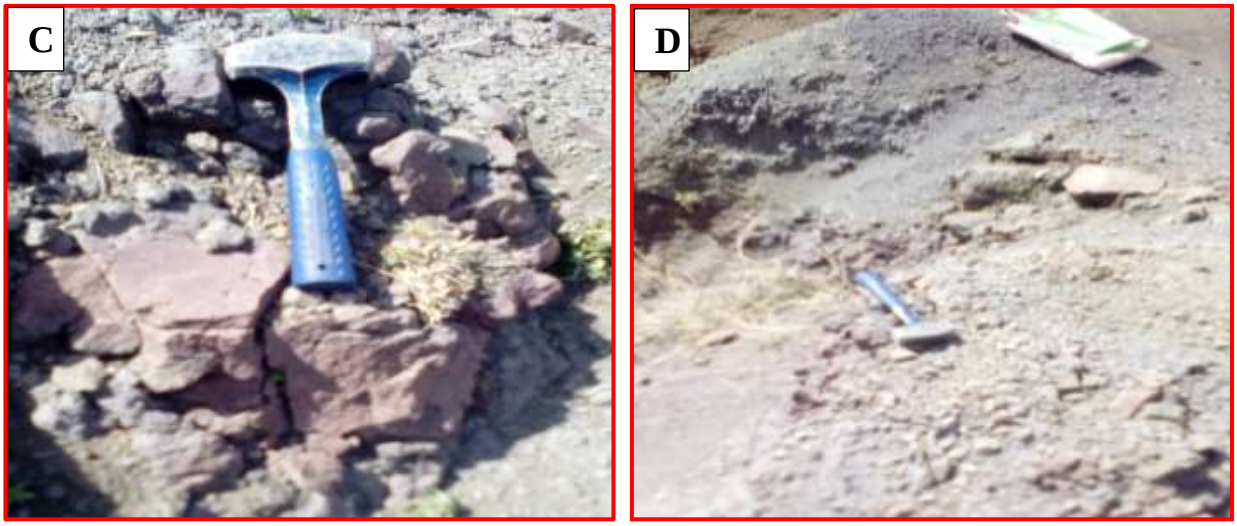

Figure 3. 21: Loose volcanic ash and moderately welded ash (tuff) exposed above Mesnokelowa village and near Kassie ridge. Figure (A) exposure of both loose volcanic ash and moderately welded ash (tuff). Figure (B) moderately welded ash (tuff). Figure (C) pinkish and gray pyroclastic material exposed together. Figure (D) shows loose fine grained volacnic ash

As it has mentioned above, Small exposure of pyroclastic deposit is also found to the north of Selen wuha river around Tigrie Mender (i.e. between Melaku river and Alaje river). Its areal extent is estimated to 0.75km^2 (4.29%) and its thickness is about 50m. This pyroclastic deposit has very fine grained unconsolidated pyroclastic material (volcanic ash) and slightly welded volcanic ash (altered tuff). In this slightly welded pyroclastic deposit, altered structures are present and these structures are distinguished via the color contrast. The color of these altered structures is light and they made reaction with diluted hydrochloric acid (HCl). On the other hand, the color of pyroclastic material is pale yellowish light and never reacts with HCl. The degree of its compactness is too small as compared with the moderately welded ash exposed near Kassie ridge and above Mesnokelowa. It is rested above ultramafic unit and it forms sharp contact with the surrounding ultramafic unit.

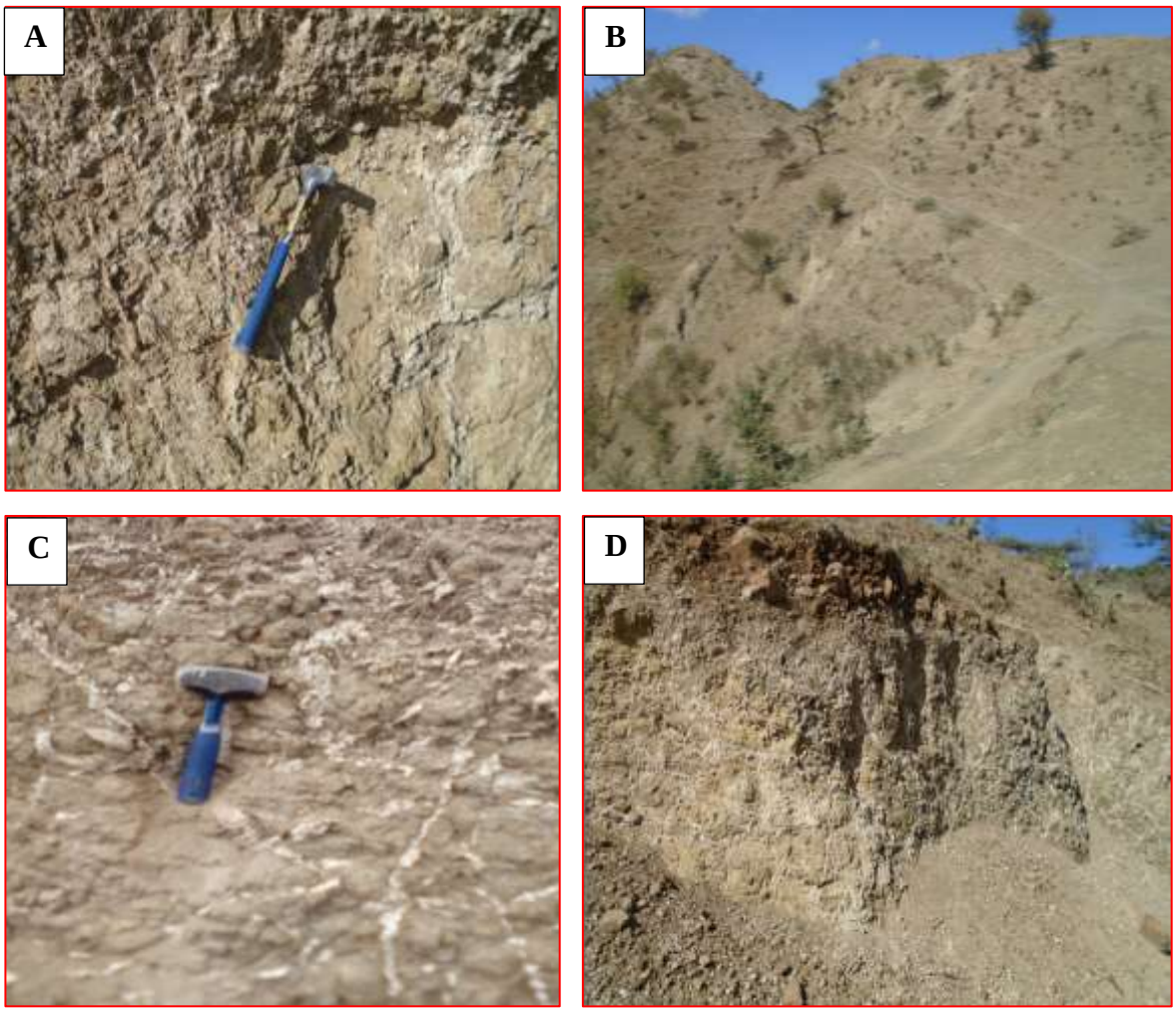

Figure 3. 22: Unconsolidated pyroclastic deposit (volcanic ash) outcropped around Tigrie Mender. Figure (A) and (C) are the close-up pictures and they show the difference between secondary material and the unconsolidated ash. Figure (A). Figure (B) and (D) thickness of the pyroclastic deposit.

3.2.5. Undifferentiated Alluvial and lacustrine sediment deposit

This undifferentiated alluvial and lacustrine sediment deposit is found in the valley of the study area. As part of the study area, it covers 2.45km^2 or 14% of the mapped area. It is formed as a result of erosional activities in the western and eastern high angle escarpment of the valley. It is obvious that the energy of the flood (runoff water) decreases as it flows from the ridge or escarpment area to the valley axis. Thus, the degree of coarsening decreases as going down to the valley axis. For this reason, the coarse sized materials like boulders, pebbles and cobbles are found at the base (foot) of the escarpment while sand and smaller sized materials are deposited within the plain of the valley. The alluvial sediment deposit is very thick in the plain of the valley.

According to REST (1997) as cited in Asmelash Abay (2003), Dessie Nedaw (2003), Mohammedsultan Abdella (2010) and Merhawi GebreEgziabher (2011), the thickness of this sediment varies from both escarpments to the axis of the valley. Accordingly, the minimum thickness of the sediment is found at the flank of both escarpments and the maximum thickness is found at the axis of the valley. Merhawi GebreEgziabher (2011) has noted that the average thickness of the sediment in the valley is about 150m and the maximum thickness is around 276m. This is based on the existing drilled borehole data. Dessie Nedaw (2003) has revealed that the lower unit of the basin fill is believed to be a lake deposit while the upper one is a river deposit. According to Tenalem Ayenew et al. (2013) and Mohammedsultan Abdella (2010) this thick Quaternary undifferentiated alluvial and lacustrine sediment deposit is composed of intercalating layers of gravels, gravelly sand, silty sand, silty clay and clay. According to the cross sectional map of Merhawi GebreEgziabher (2011) and Melese Tadesse et al. (2011), this alluvial sediment has directly rested on Ashange basalt and Ashange basalt On the other hand has covered Amba Aradom formation (upper sand stone) (figure 1.6 and 2.1)

Figure 3. 23: Quaternary alluvial deposit in the axis of Raya valley. The photo is taken from Bedeno Loko found near the study area (Raya Alamata sub-basin).

CHAPTER FOUR

GEOLOGICAL STRUCTURES OF THE STUDY AREA

4.1. Introduction

Raya valley is located at the margin of Afar depression. Because of its location, it is named as Raya marginal graben. Afar rift (Afar depression) is a rift where tectonic process is very active and volcanic eruption is also common (Miruts Hagos, 2010). Even though deformational metamorphic structures (ductile structures) are present in the basement units of Raya valley, brittle tectonic structures such as faults, lineaments, joints, dykes and veins are dominant geological structures of the valley **(**Melese Tadesse et al., 2011 and WWDSE, 2011). Since the study area is part of Raya marginal graben, it is affected by the internal earth processes which causes brittle tectonic structures. As a result of these reworking tectonic processes, there are different geological structures in the study area. The major geological structures which are identified in this study are normal faults, lineaments, joints, dykes and veins.

The normal faults as main geological structures are found in western side of the study area. This is at the contact of the valley and the eastern escarpment of the graben. They are series of normal faults generally aligned in N-S directions. Undifferentiated geological structures (i.e. lineaments) are also found in the area. Individually, these discontinuities are aligned in different directions. However, their overall alignment is nearly north-south and east- west directions. Furthermore, joints and veins are abundantly found in the study area. In addition, considerable amount of felsic and mafic dykes are intruded in the ultramafic and basaltic units. The detail field description for these individual geological structures of the study area is provided as follows.

4.2. Faults and lineaments

Series of normal faults are found in study area and they are oriented (striking) along the NE-SW, N-S, NW-SE, NNE-SSW and NNW-SSE directions. All these series of normal faults are dipping toward the graben (Raya valley). As a result, they have formed the eastern escarpment of the graben. Since the valley is found in the west direction of the ridge or the escarpment, they all are dipping in the range of SW to NW directions. On the other word, they are collectively dipping toward the west direction. Accordingly, the NE-SW striking normal fault

is dipping toward the NW direction with an approximate dip angle (amount) of about 45º to 65º. Similarly, the NW-SE oriented normal fault is dipping toward the SW direction with an angle of about 45º to 55º. The NNE-SSW striking normal fault is sloped along the WNW direction. Its dip amount is about 40º to 50º. Moreover, the NNW-SSE and N-S striking normal faults are tilted toward the WSW and W directions respectively. Their dip amounts are range from about 50^{O} to 70^{O} and from 40^{O} to 55^{O} respectively**.** These measurements are the average measurements (values) of the overall trend of each fault. Therefore, all these escarpments are an indication of high angle normal faults forming moderate to steep slope of fault planes.

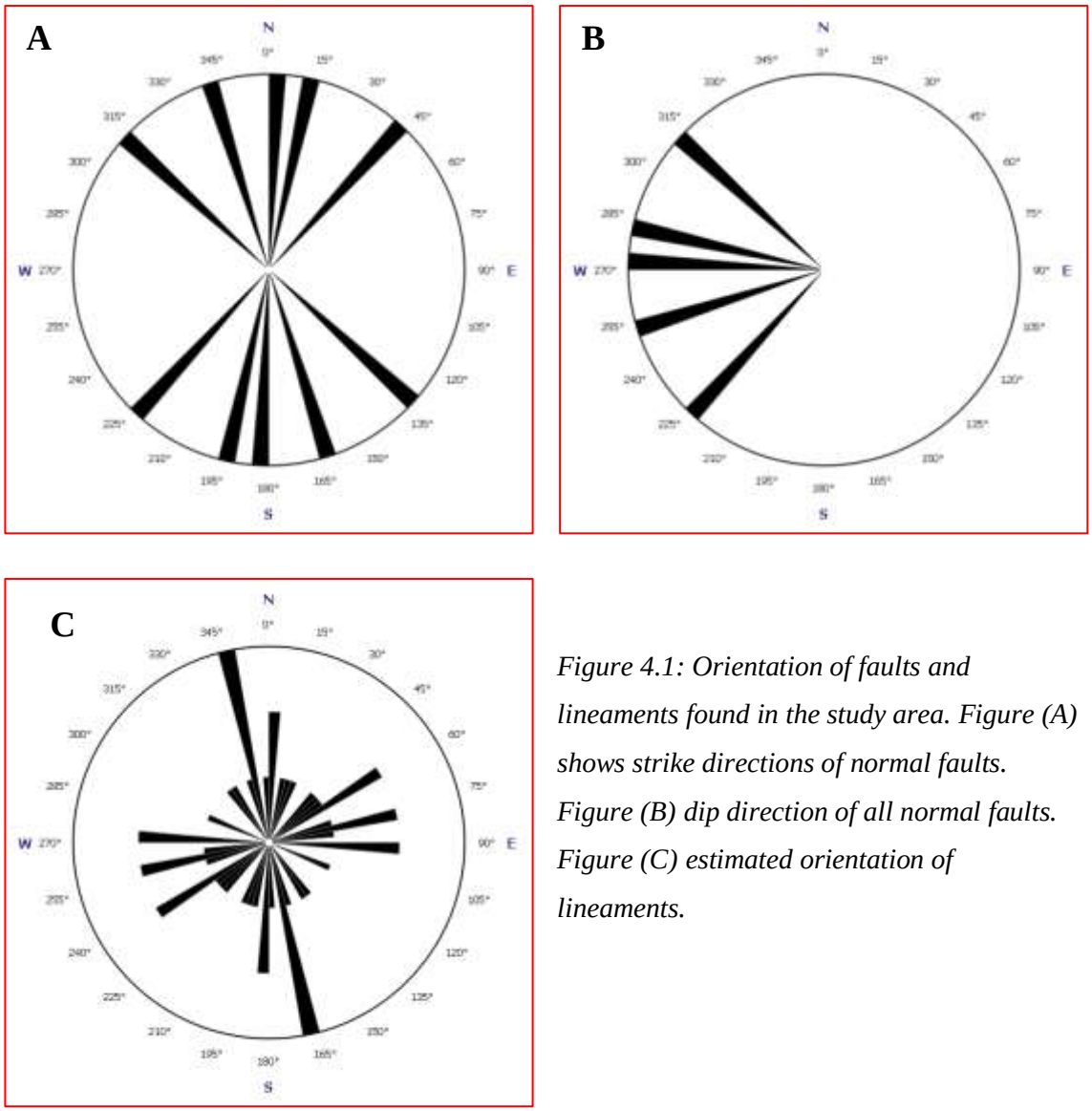

Figure 4.1: Orientation of faults and lineaments found in the study area. Figure (A) shows strike directions of normal faults. Figure (B) dip direction of all normal faults. Figure (C) estimated orientation of lineaments.

There are also unrecognized fractures that are aligned in different directions and they are studied using google earth map, digital elevation model and spot-5 satellite image. These lineaments are studied mainly using google earth map and digital elevation (DEM). Because

of its complexity, very limited information is obtained from spot-5 satellite image. Basically, these unrecognized discontinuities have oriented in to two significant directions Even though they individually aligned in different directions. In a regional view, some of the lineaments are aligned in the east-west direction while the others have oriented in north-south direction. Selen Wuha river and its main tributaries such as Alaje, Gorso and Melaku rivers are developed flowing these discontinuities (lineaments) and therefore, they are indications of these major unrecognized discontinuities. Consequently, Alaje, Gorso and Melaku rivers are developed along the lineaments which orients from northeast to north–south. However, Selen Wuha river is a river developed along the major discontinuities oriented in the east- west direction.

4.3. Joints

As it has been mentioned above in the introduction part of this chapter, the study area was affected by tectonic processes. Geological structures of joints, lineaments and faults found in the area are the manifestations of the tectonic processes that have occurred in that area. Both Systemic and non-systematic joints are dominantly found in the area. Comparatively, nonsystematic joints are looking dominant over systematic joints.

Systematic joints are clearly seen in the unaltered ultramafic unit exposed in Selen Wuha river and Alaje river. They are also common in some basalt dykes. Two and more sets of systematic joints are the most common joints in the study area. However, very rare one set of joints, which resemble to moderately develop columnar joints, are also observed in the unaltered ultramafic unit and the basaltic dykes. These are dipping in different angles. Some are dipping with about 20º and others have dip with 60º to 80º. In these one set of joints, there are small (fine) joints crossing for these major one set of joints. These are an indication of the successive fracturing event that had happened in the area through its geologic time. In two sets of systematic joints, the joints are not mostly intersected perpendicularly but they are intersected at an angle less than 90º. However, there are rare two sets of joints intersected at perpendicular angle (~90º). The orientations (strike) of these perpendicularly intersected joins are E-W and N-S. Their dip angle ranges from 60º to 80º. While the average orientations (strike direction) of the dominant two sets of joints, which are intersected at less than 90º, are NW and NE. These all joints are generally dipping in the same direction with their lithology or topography of the area. For example, most of the joints in Selen Wuha river are dipping toward the river (i.e. toward the south or north directions). Individually, some two sets of

joints as shown in the figure 4.3 are dipping in NW and NE with an angle of 60º to 75º. This is clearly observed in figure "D". There are NE dipping joints having low dip angle. Numerically, it is about 10 to 15 degrees. The average joint spacing is about 30 to 50cm and the average joint aperture is about 40 to 60cm. This is an average value of the measured few representative joints.

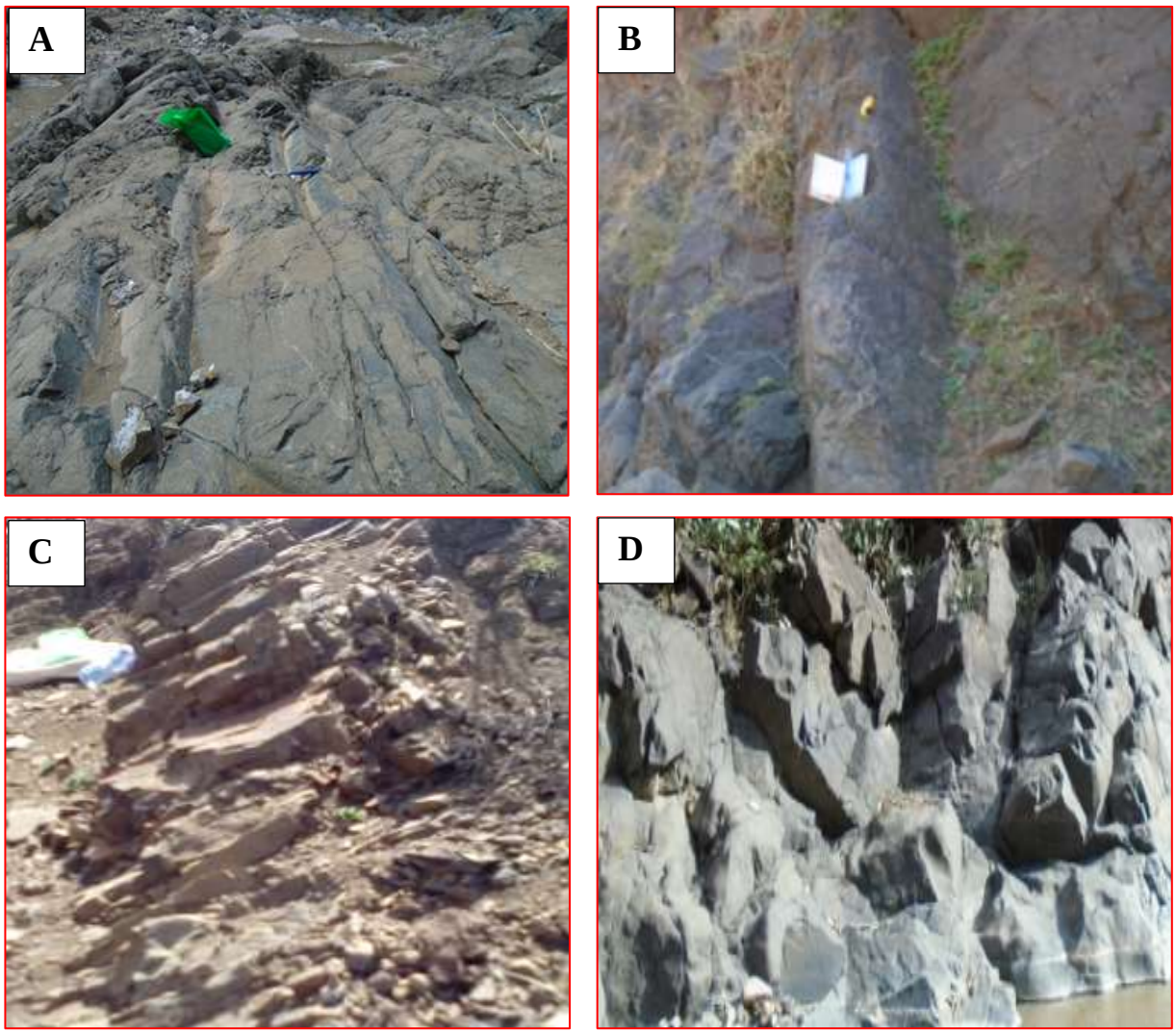

Figure 4.2: one and two sets of systematic joints hosted in ultramafic and basalt units. Figure (A) low angle one set of joints. Figure (B & C) high angle one set of joints. Figure (D) two sets of joints.

As it has been mentioned above, nonsystematic joints are the dominant joints in the study area. They are abundant in the basalt unit and strongly weathered ultramafic unit. These joints are dense joints and oriented in different directions. Nonsystematic joints found in the weathered ultramafic unit are filled by white colored secondary materials.

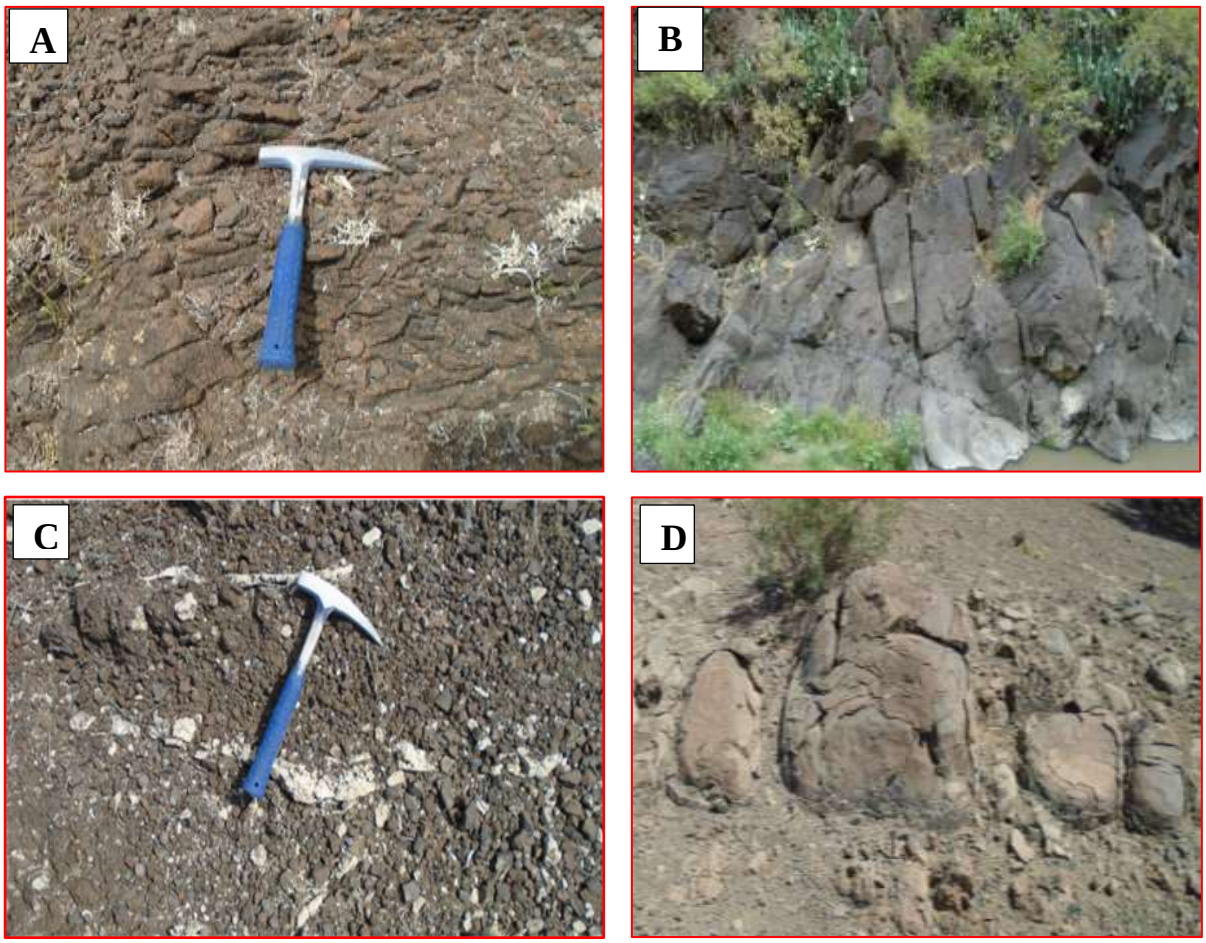

Figure 4.3: nonsystematic and exfoliation joints found in ultramafic and basaltic units. Figure (A) nonsystematic joints in weathered ultramafic unit. Figure (B) nonsystematic joints in basaltic unit. Joint filling light colored vein in weathered ultramafic unit. Figure (D) exfoliation joints found in basaltic dyke.

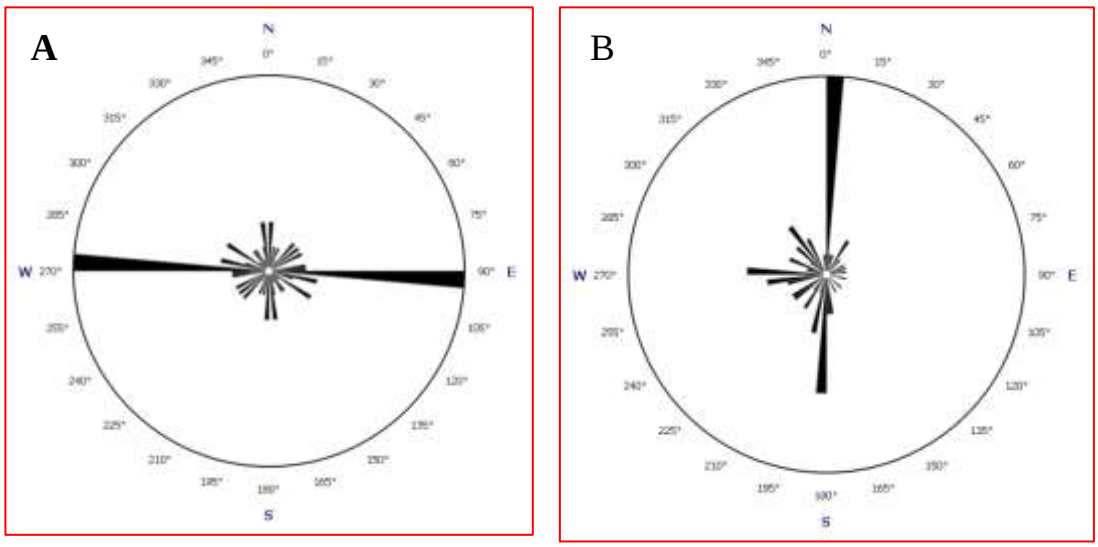

Figure 4.4: Rose diagram showing the orientation of measured joints. Figure (A) shows the overall strike direction of measured joints and Figure (B) dip direction of the measured joints.

4.4. Veins

Joints (fracture) may be open fractures or filled by various materials. Joints, which are filled by precipitated minerals, are called veins and joints filled by solidified magma are called dikes. These veins are dominantly situated in the study area where the ultramafic unit has extensively exposed. Hence, they are hosted in the dark colored relatively unaltered (fresh) ultramafic unit, in pyroclastic material and in the strongly weathered ultramafic unit. According to their color and their sensitivity to diluted hydrochloric acid, two types of veins (dark colored and light colored) are identified. The light colored veins have made reaction with HCl but the dark colored veins never made reaction with HCl. Most of These veins have no preferred orientation. They are arranged in nonsystematic way following the nonsystematic joints or fractures. This makes difficulty to measure the spacing and orientations of these veins. The dominant measured orientations of these veins are NE, NW, SW and SE.

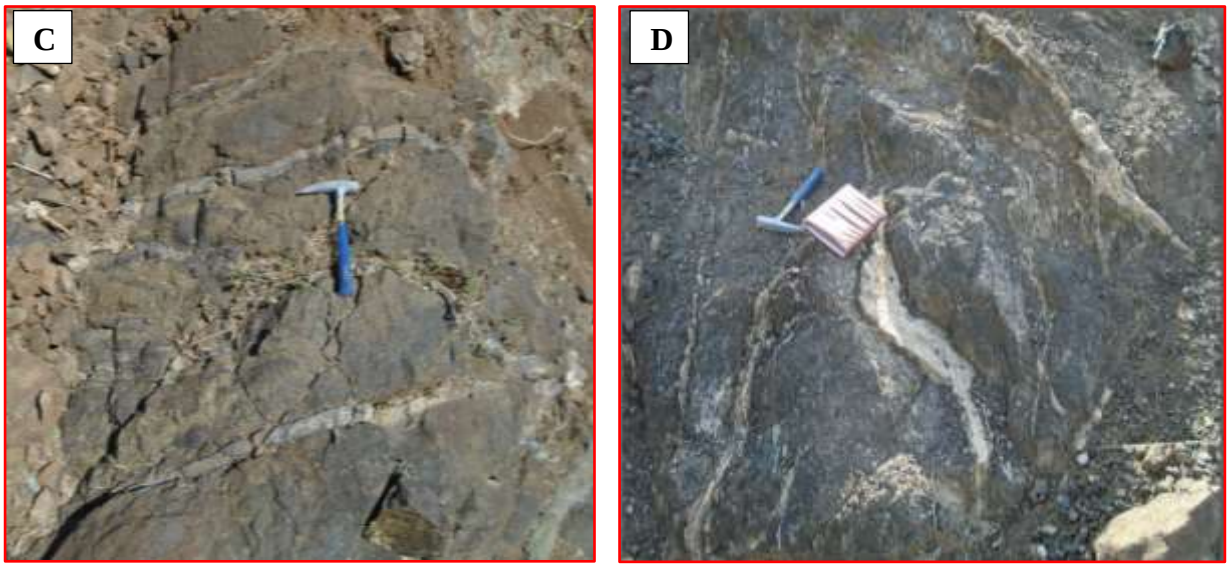

Figure 4.5: light and dark colored veins hosted in ultramafic unit, basaltic unit and pyroclastic material. Figure (A) light colored vein hosted in pyroclastic material. Figure (B) light colored vein hosted in weathered ultramafic unit. Figure (C) shows dark colored vein hosted in altered and strongly fractured ultramafic unit. Figure (D) sheeted light colored vein hosted in basaltic unit.

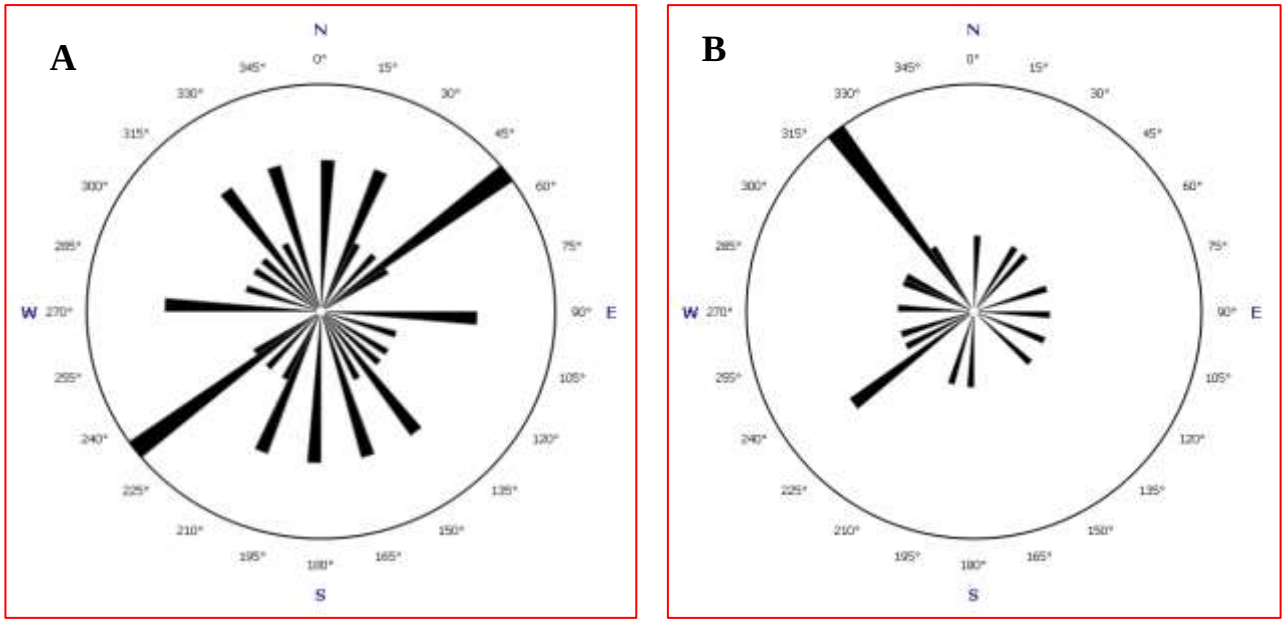

Figure 4.6: Rose diagram showing the orientation of both measured veins. Figure (A) shows the overall strike direction of measured veins and Figure (B) dip direction of veins.

4.5. Dykes

The common dykes recognized in the study area are gabbro, micro-gabbro, basaltic and microgranite. Basalt and micro-gabbro dykes are intruded in ultramafic unit and in plagioclase olivine–phyric basalt which has exposed in the east side of Alaje ridge and Amed Ager ridge. However, dykes of microgranite are rare and intruded in ultramafic and plagioclase- olivine

phyric basalt. Considerable Outcrop of basaltic unit is also coexisting with the pyroclastic material near Kassie ridge and hence basaltic dykes are also found within these basaltic exposures. Gabbro as a dyke is intruded in ultramafic unit only and its detail field and petrographic description is provided in chapter three.

Basalt dykes are abundantly exposed in the study area. Mainly they are intruded in ultramafic and basaltic units. The exposures of this basaltic dyke are also found within the pyroclastic outcrop. Generally, they are fractured and moderately to strongly altered. Their color ranges from grayish to dark grayish. There are also light gray and dark colored basaltic dykes. Moderately developed columnar joints and exfoliation joints are the common characteristics of these dykes. The dark colored basaltic dykes are small in size and commonly they are intruded in the ultramafic unit that has exposed in Selen Wuha river and Alaje river. However, the dark gray and grayish colored dykes are plentifully disseminated in the area where the basalt unit and pyroclastic material are extensively exposed. Geographically, they are situated on the ridge found above Mesnokelowa toward the south of Selen Wuha river and in the east of Alaje ridge within the plagioclase-olivine phyric basalt unit. As they are found abundantly, most of them are crisscrossed each other. The width of these relatively large dykes range from about 2.20m to 2.70m and their length is about 150m. While the size (width) of these smaller dykes, which are found together with these relatively large dykes, ranges from about 30cm to 1.20m and their length is about 15m.

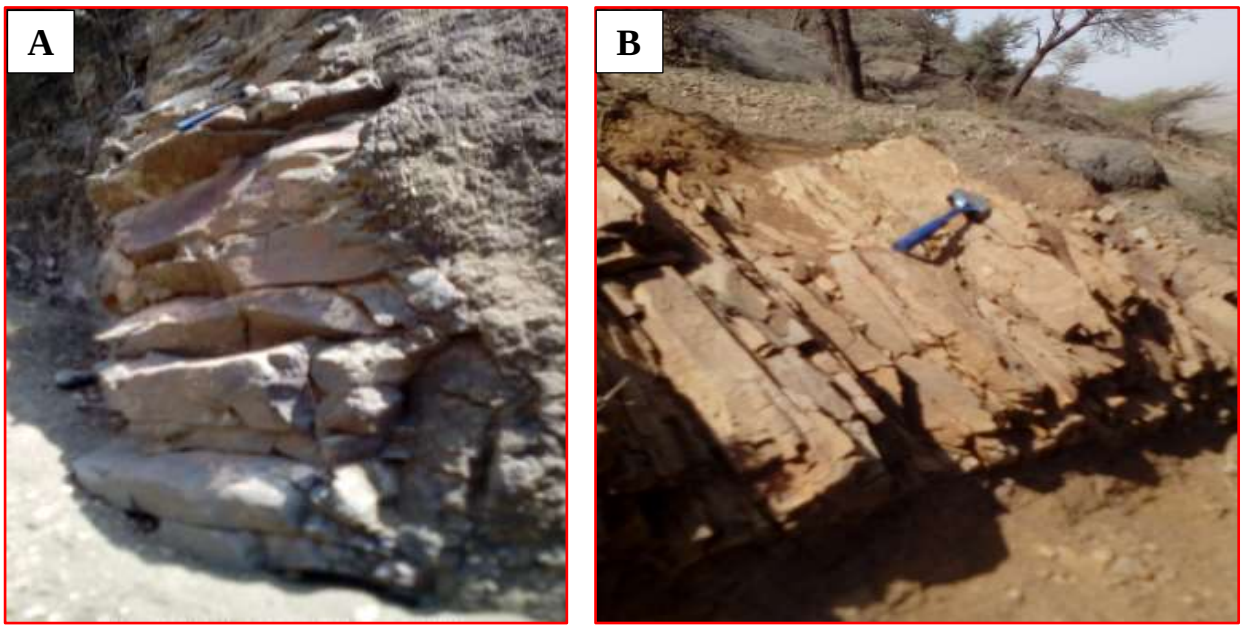

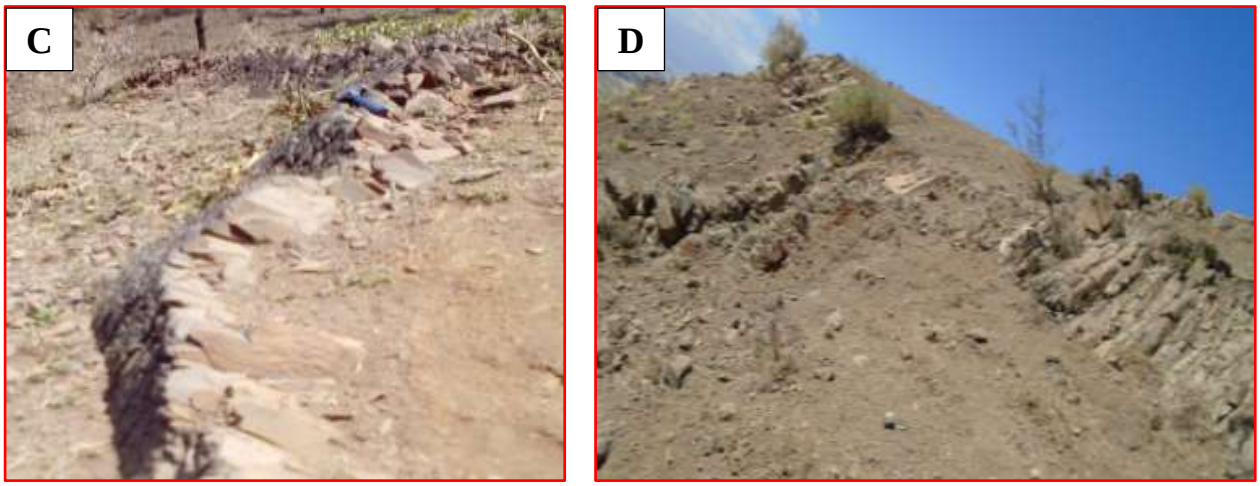

Figure 4.7: Basaltic dykes outcropped in different part of the study area. Figure (A) shows fractured basaltic dyke intruded in basalt unit exposed at the back of Alaje ridge. Figure (B & C) are basaltic dykes found at the contact of ultramafic and pyroclastic material. Figure (D) crisscrossed basaltic dykes outcropped above Mesnokelowa village.

All these dykes have different orientation. Some of these dykes oriented in north-south direction while others have oriented in east-west direction. There are also other dykes which have been oriented in different directions other than E-W or N-S direction. For example, there are two dykes on the ridge found above Mesnokelowa at GPS location of X=0577881 and Y=1359888. These dykes are crisscrossed each other and they are oriented in NW and NE strike directions (fig. D). The NW striking dyke is dipping toward SW with about 50º-65ºdip amount. The second dyke is dipping to the NW by about 35º to 55º dip angle. Similarly, another dykes found in the southwest direction of these crisscrossed dykes are oriented in NW direction. The dip amount of these dykes ranges from 50º-65º and their dip direction is toward NW. The orientation of the smaller dark colored dykes found in Selen Wuha river is E-W, N-S, NE-SW and SE-NW.

As it has mentioned above, considerable dykes of micro gabbro are intruded in both ultramafic and plagioclase-olivine phyric basalt unit. The color of the fresh micro-gabbro unit is range from dark grayish to dark. This dyke is intruded in weathered ultramafic unit exposed on Gubana ridge (i.e. northwest of Melaku river) and in the plagioclase-olivine phyric basalt unit exposed on the east side of Alaje ridge. All these dykes of this unit have variable orientations. The dykes outcropped on Gubana ridge (intruded in weathered ultramafic unit) and Amed Ager village are porphyritic in texture. The phenocrysts (pyroxene mineral grains) are dark in color and they are easily recognized with unaided eye. However, the color of the dykes is dark grayish. The width of the dykes ranges from few cm to about 1.50m. Even though it has rough

(unsmooth) surface, its minerals are indistinguishable to unaided eye. Hence, it is nearly similar to basaltic dyke in color and texture. In thin section study, the minerals of micro-gabbro are coarser and porphyritic. The size of the phenocryst mineral grains is different from one thin section to another.

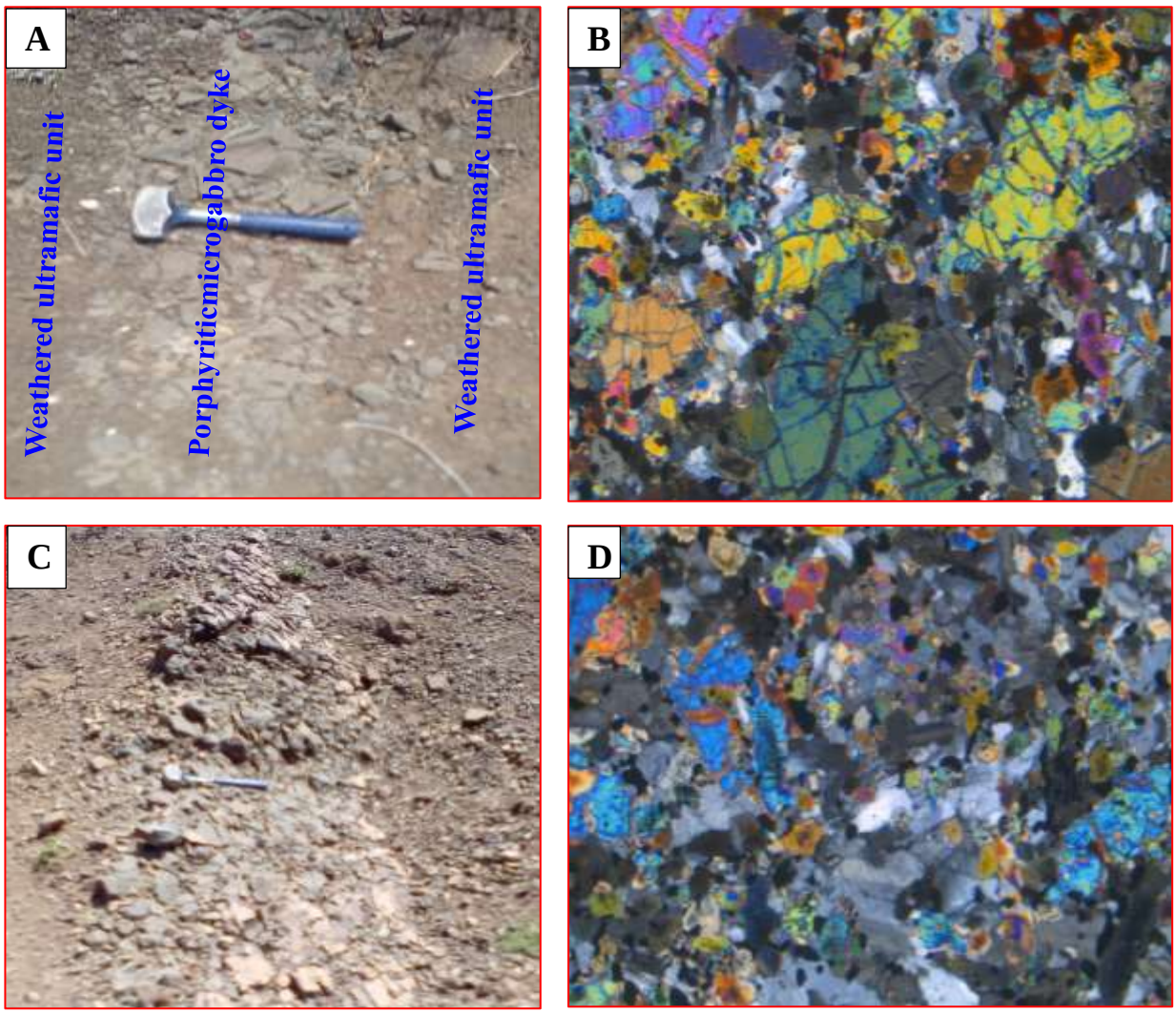

Figure 4.8: Fractured and porphyritic micro-gabbro dykes and their microphographs. *Fugure (A) porphyritic microgabbro dyke intruded in weathered utramafic unit. It is found near Amed Ager village. Fugure (B) thin section photo showing mineral content and phenocryst phases of the porphyritic dyke. Fugure (C & D) fractred microgabbo dyke and its microphotography. The dyke is intrudeded in the basalt unit found in the east side of Alaje ridge. Thin section photo shows the phenocryst phases and minerals of the dyke.*

This unit is composed of relatively fine and coarse grained minerals. Hence, the texture of the unit is porphyritic with phenocrysts of olivine and plagioclase minerals. The average modal proportion of the fine phaneritic (avarage grain size <0.5mm) and phenocryst grains is about 80% and 20% respectively.

Phenocryst phases are olivine and plagioclase minerals grains. From these two phenocryst minerals, Olivine grains are the dominant phenocryst grains and their modal proportion covers about 90% of the modal proportion of the phenocryst of the thin sections while the remaining 10% is occupied by plagioclase phenocrysts. Overall, the phenocryst mineral grains (particularly olivine phenocryst) is more abundant in thin section ST4S3B than ST4S2B. The minerals are affected by alteration. The length and width (size) of these olivine phenocryst is about 1.5mm and 1.0mm respectively. However, the size of phaneritic groundmass (matrix) of the sample is much less than this. The modal proportion of the fine phaneritic ground mass (matrix) is about 50% plagioclase, 10% olivine, 25% pyroxene and 15% opaque. Almost all Fe-Ti oxide mineral grains are relatively finer in size and all of them are anhedral in grain shape. The overall shape of olivine and pyroxene mineral grains is anhedral. In addition, Both mineral grains are strongly fractured.

Rare micro-granite dykes are also intruded in ultramafic unit and in plagioclse-olivrine phyric basalt. Specifically, these dykes are located in selen wuha river above the narow canvnture of the river. The color of these dykes is vary between pale yellowish light, light gray and lightish. Since they have rough surface, their grains are slightly visible with the help of hand lense. the micro-graintic dykes hosted in plagioclse olivrine phyric basalt are strongly fractured and sligtly weathered. The weathered color of the dykes is pale yellowish light. Moreover, they have variable orientations and hence some of the measured dykes have oriented in WSW, NW and SW directions.

From the petrographic analysis, mineral constituents of the dyke are alkali feldspar (orthoclase and sanidine), plagioclase, Fe-Ti oxides and few of quartz. There is slight grain size variation among the grains of these minerals. Accordingly, very few large sized grains of alkali feldspar and plagioclase minerals are available. These large sized grains are elongated and most of them are subhedral to euhedral in grain shape. The maximum length of these tabular shaped grains is range from about 0.75mm to about 1.5 mm. Even though most grains of Fe-Ti oxides and quartz are smaller in size and anhedral in shape, considerable thinly elongated opaque mineral grains are available and they are measured from about 0.4 mm to 0.8 mm in length. The dominant shape of Fe-Ti oxides and quartz mineral grains are anhedral but there are very few euhedral Fe-Ti oxides grains. However, the dominant shape of plagioclase and alkali feldspar mineral grains is subhedral to euhedral. All these mineral grains are arranged randomly. Therefore, the overall texture of this holocrystalline dyke is porphyritic-phaneritic and the overall grain size range is between fine phaneritic to medium phaneritic.

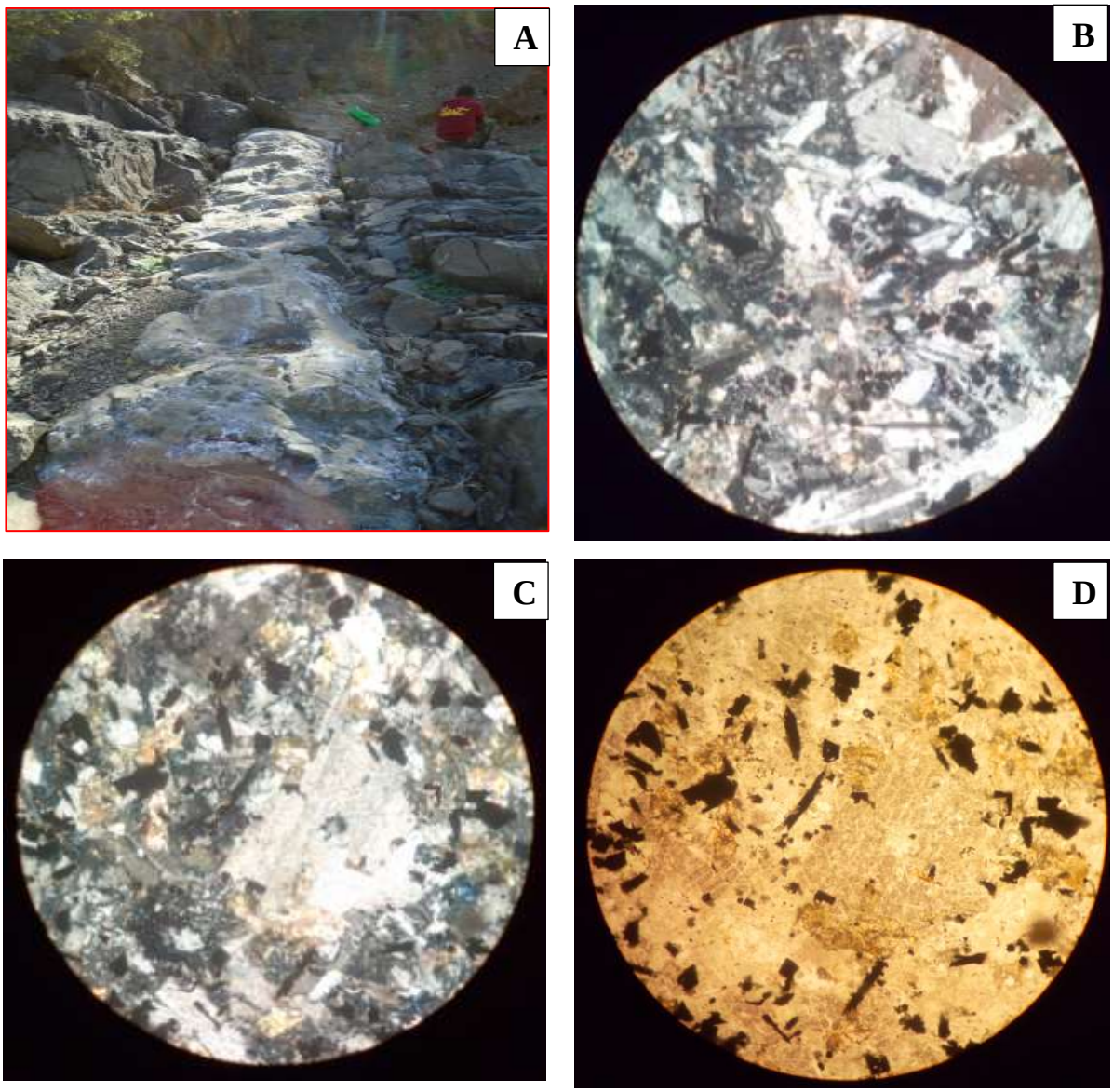

Figure 3.9: Micro-granite dyke and its thin section photo. (A) microgranite dyke outcropped in Selen Wuha river. Fig (B & C) XPL photo show porphyritic – phaneritic texture and mineral grain arrangement. Fig. (D) PPL photo shows shape of opaque grains.

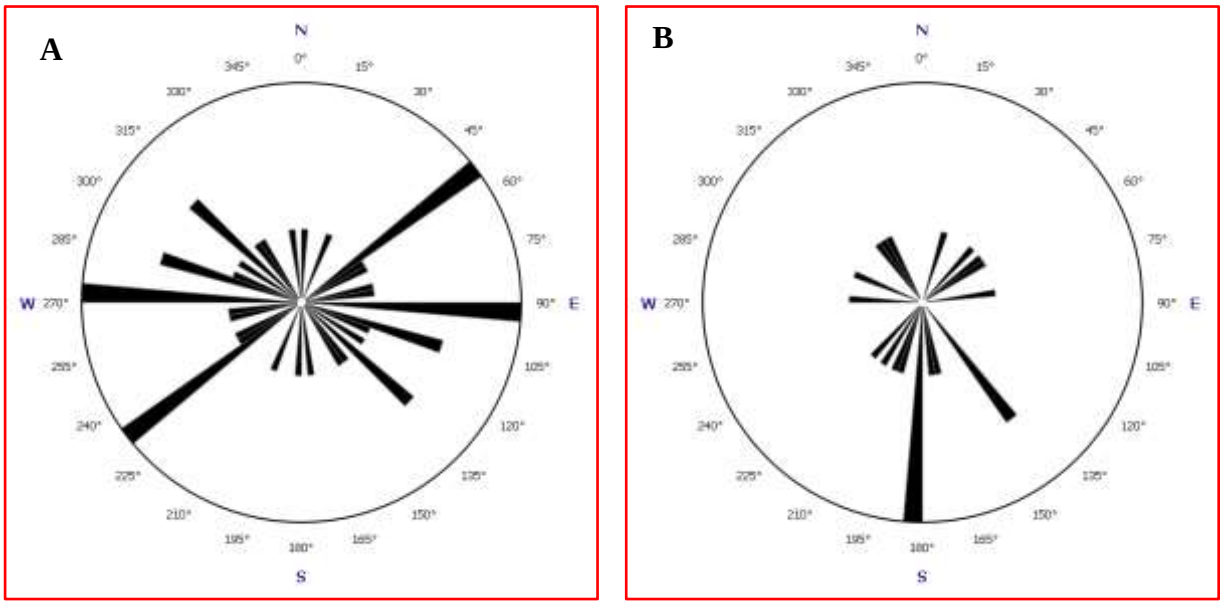

Figure 4.10: Rose diagrams showing the overall orientations of various dykes of the study area. Figure (A) shows the overall strike direction of the measured dykes and figure (B) dip direction of the the measured dykes

CHAPTER FIVE

GEOCHEMISTRY OF SELEN WUHA MAFIC-ULTRAMAFIC UNITS

5.1. Introduction

A total of 10 fresh samples (6 ultramafic and 4 gabbroic) were selected for whole rock geochemical analyses. The selected samples were cut in to slabs and trimmed to remove surface alteration. The slabs were then crushed using a porcelain jaw-crusher and powdered with a tungsten carbide

The powdered samples were sent to the University of Leicester, UK, Department of Geology. Samples were analyzed for major elements on PANalytical Axios Advanced XRF spectrometer. Major elements determined on fused glass beads prepared from ignited powders sample to flux ratio 1:5, 80% Li metaborate: 20% Li tetraborate flux. Results quoted as component oxide weight percent. Trace elements, including REE, were determined using Laser ablation Inductively Coupled Plasma Mass Spectrometer (LA-ICP-MS).

All these six ultramafic samples show high concentration of MgO, Mg number (Mg #), Fe_2O_3, Cr, Ni and Co. They exhibit also low concentration of SiO_2, Na_2O, K_2O and P_2O_5, Rb, Ba, Nb, Zr, Y, Hf and REEs. Analyzed ultramafic samples have low value of LOI content. Numerically, it ranges from -0.14(ST1S7) to 2.95 wt. % (ST1S11 and ST3S2).

In contrast to ultramafic samples, all these gabbroic samples demonstrate low concentration of MgO, Mg #, Fe_2O_3, Cr, Ni and Co. In addition, they display relatively high concentration of SiO_2, Na_2O, K_2O and P_2O_5, Rb, Ba, Nb, Zr, Y, Hf and REEs as compared with ultramafic samples. On the other hand, the value of LOI in these samples ranges from 0.58 (ST4S4) to 2.76 (ST5S3) wt. %. This value is not high enough however it is low and imply no excess post-crystallization hydrothermal alteration and low grade metamorphism is carryout on the unit. Hydrothermal alteration and metamorphism processes disturb the abundance of the constituted chemical elements.

The geochemical data (major oxides and trace elements geochemical results) of these 10 analyzed samples is presented in table 5.1. In that table, the value of Mg # is calculated using CIPW Norm Hollacher and it is checked manually using its general formula given here.

$$\left(\frac{\frac{MgO}{40}}{\frac{MgO}{40}+\frac{Fe2O3}{80}}\right)\times 100 = Mg\#$$

5.2. Geochemistry of ultramafic unit

The concentration of MgO in the analyzed ultramafic samples ranges from 22.31 wt. % in ST3S3 to 37.08 wt. % in ST1S11. The highest Fe_2O_3 is obtained in ST1S7 (17.59 wt. %) and its lowest concentration is acquired in ST5T5 (12.12 wt. %). Furthermore, high Mg # is reported in ST1S11 (81.94%), ST5T5 (81.81%), ST3S2 (79.94%) and ST3S5 (79.25%). In general, the amount of Mg # in these analyzed ultramafic samples ranges from 72.63 (ST1S7) to 81.94 in (ST1S11). Likewise, the concentration of Cr, Ni and Co ranges from 1690ppm (ST3S3) to 3000ppm (ST1S11), 1030ppm (ST3S3) to 1980ppm (ST1S11) and 96ppm (ST5T5) to 143ppm (ST1S11) respectively. In contrast, low concentration of SiO_2 is obtained in these ultramafic samples. It ranges from 39.22 wt. % (ST1S11) to 45.55 wt. % (ST5T5). Similarly, Na_2O and K_2O have very low concentration and it is below 1wt. %. Moreover, these two major oxides are not detected in few ultramafic samples such as ST1S11, ST3S2 and ST3S5 and hence they are reported as below detection limit. Similarly, Rb, Ba, Th and U are also reported as below detection limit in all ultramafic samples. Some other incompatible trace elements such as Sr, Y, Zr, Hf, Ta and most of REEs are recognized in better concentration. However, their concentration is very low as compared with their concentration reported in gabbroic samples (table 5.1).

5.3. Geochemistry of gabbroic units

The gabbroic samples show low concentration of MgO, Mg#, Fe_2O_3 and CaO as compared with ultramafic samples. Numerically, their abundance is range from 3.16 wt. % to 8.14 wt. % (MgO), 36.3 to 56.3 (Mg#), 10.99 wt. % to 13.24 wt. % (Fe_2O_3) and 5.44 wt. % to 9.22 wt. % (CaO). An exceptional high concentration of CaO (about 13.12 wt. %) is obtained in one sample (ST4S4). The concentration of this sample (ST4S4) is even higher than the concentration of CaO reported in ultramafic samples. Furthermore, compatible trace elements (Cr, Ni and Co) show low concentrations. This is range from <20 ppm (below detection limit) to 30 ppm (ST4S4), from 30 ppm (ST4S8 and ST5S3) to 90ppm (ST4S4) and 21ppm (ST5S3) to 42ppm (ST4S4) respectively. Conversely, high concentrations of SiO_2, Al_2O_3, TiO_2, Na_2O and K_2O are obtained. In number, they range from 41.64wt% to 45.21wt% (SiO_2), 12.59 wt. % to 14.41 wt. % (Al_2O_3), 2.78 wt. % to 8.71 wt. % (TiO_2), 1.5wt% to 3.7wt% (Na_2O) and 0.6wt% to 1.2wt% (K_2O). Moreover, incompatible trace elements such as Rb, Ba, Nb, Sr, Y, Zr, Hf, Ta, Th, U and almost all of REEs show relatively high concentration as compared with ultramafic samples. As an example the concentration of Sr, Ba, Zr and Rb is range from 308

ppm (ST2S5) to 2730ppm (ST4S4), 363 ppm (ST2S5) to 938 ppm (ST4S4), 287 ppm (ST4S4) to 505 ppm (ST5S3) and 6 ppm (ST4S4) to 29 ppm (ST2S5) respectively.

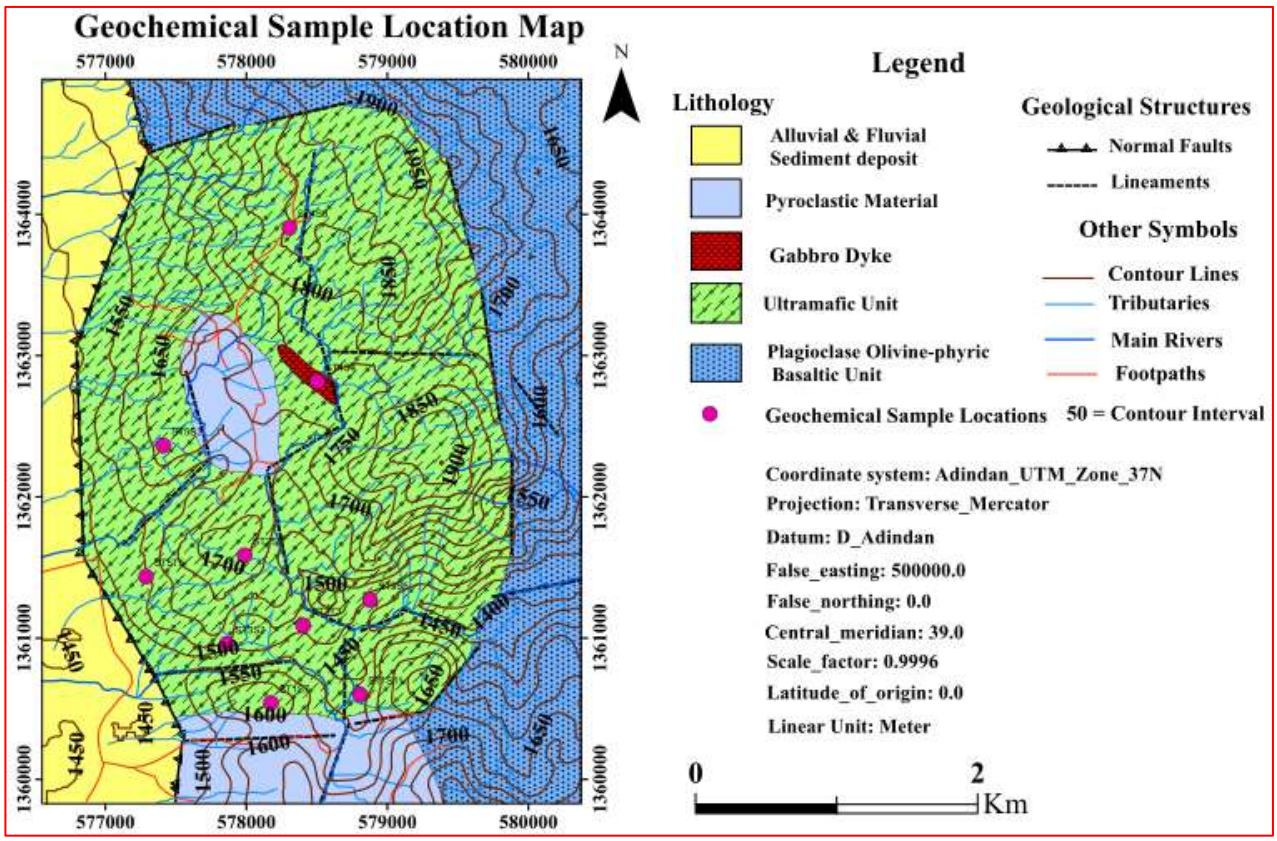

Figure 5.1: Geochemical sample location map.

Table 5.1: Major element (Wt. %) and trace element (ppm) abundancy of Selen Wuha gabbroic and ultramafic samples. The geochemical data of the 10 samples is normalized to volatile free base. The ratios of Eu/Eu, $(La/Sm)_N$, $(La/Yb)_N$ and $(Tb/Yb)_N$ are calculated using Boynton (1984).*

	Ultramafic samples						Gabbroic samples			
Samples	ST1S11	ST1S7	ST3S2	ST3S3	ST3S5	ST5T5	ST4S4	ST2S5	ST4S8	ST5S3
SiO_2	39.22	40.13	41.59	41.70	43.46	45.55	41.64	47.61	47.84	51.27
TiO_2	0.43	5.20	0.86	4.51	1.76	0.88	8.71	3.58	3.82	2.78
Al_2O_3	0.87	1.84	1.16	4.60	1.65	1.47	12.59	14.1	14.3	14.41
Fe_2O_3	16.19	17.59	14.69	15.29	14.31	12.12	12.51	12.63	13.24	10.99
MnO	0.21	0.20	0.18	0.18	0.18	0.15	0.12	0.18	0.19	0.17
MgO	37.08	23.56	29.54	22.31	27.58	27.52	8.14	4.32	4.07	3.16
CaO	3.69	11.02	8.53	10.44	11.00	12.01	13.12	9.27	8.2	5.44
Na_2O	<0.007	0.151	0.067	0.449	0.130	0.159	1.643	3.658	3.994	4.464
K_2O	0.010	0.004	<0.001	0.038	<0.001	0.008	0.661	1.658	1.664	2.897

P_2O_5	0.017	0.014	0.008	0.012	0.010	0.017	0.053	0.91	0.823	0.878
Total	97.717	99.709	96.625	99.529	100.08	99.884	99.187	97.785	98.141	96.459
SO_3	0.032	0.011	0.025	0.005	0.01	0.012	0.012	0.021	0.012	0.013
LOI	2.95	- 0.14	2.94	0.5	0.1	0.43	0.58	2.14	1.79	2.76
Mg #	81.94	72.63	79.94	74.30	79.25	81.81	56.31	40.4	37.8	36.3
FeOt	14.57	15.83	13.22	13.76	12.88	10.91	11.26	11.36	11.91	9.89
V	73	408	135	337	186	113	415	328	333	225
Cr	3000	1800	2750	1690	2280	2600	30	<20	<20	<20
Co	143	108	121	96	99	95	42	30	36	21
Ni	1980	1060	1410	1030	1300	1170	90	70	30	30
Zn	120	130	100	120	100	80	150	150	160	150
Ga	2	8	4	8	5	4	21	29	26	26
Rb	< 0.1	< 0.1	< 0.1	< 0.1	< 0.1	< 0.1	6	29	22	53
Sr	16	43	25	215	37	38	2730	308	820	752
Y	2	11	5	9	9	6	35	44	42	49
Zr	8	111	13	73	35	20	287	461	471	505
Nb	< 1	13	< 1	11	2	< 1	42	56	58	56
Ba	< 3	< 3	< 3	10	< 3	< 3	938	363	368	395
Hf	0.2	3	0.5	2.4	1.3	0.6	7	10.2	10.4	13.3
Ta	0.1	1.3	0.2	1.2	0.3	0.1	3	3.9	4.2	4
La	0.8	2.6	0.9	1.4	1.5	1.7	38.6	51.4	53.3	57.7
Ce	2	9.6	3.4	5.2	5.9	5.5	94.2	122	127	134
Pr	0.35	1.87	0.71	1.14	1.28	1.02	13	16.4	16.7	17.9
Nd	1.9	10.7	4.2	7.2	7.8	5.8	60.5	70.8	72.6	76.5
Sm	0.6	3.6	1.5	2.7	2.7	1.9	14	15.9	15.8	17
Eu	0.2	1.18	0.5	1.02	0.94	0.63	4.56	4.89	4.95	5.27
Gd	0.6	3.6	1.6	2.9	3	1.9	12.2	13.9	13.6	14.7
Tb	< 0.1	0.5	0.2	0.4	0.4	0.3	1.7	1.9	1.9	2.1
Dy	0.5	2.9	1.3	2.2	2.3	1.5	8.6	9.9	9.8	11
Ho	< 0.1	0.5	0.2	0.4	0.4	0.2	1.4	1.7	1.7	1.9
Er	0.2	1.1	0.5	0.9	0.9	0.6	3.5	4.3	4.2	4.8
Tm	< 0.05	0.13	0.06	0.11	0.11	0.07	0.44	0.55	0.53	0.62
Yb	0.2	0.8	0.3	0.6	0.6	0.4	2.6	3.2	3.2	3.6
Lu	< 0.01	0.1	0.05	0.08	0.09	0.06	0.34	0.42	0.44	0.51
Th	< 0.1	< 0.1	< 0.1	< 0.1	< 0.1	< 0.1	0.4	4.6	4.8	5.4
U	< 0.1	< 0.1	< 0.1	< 0.1	< 0.1	< 0.1	0.1	1.4	1.5	1.6
Eu/Eu*	1.00902	0.9922	0.98093	1.10829	1.00586	1.00371	1.04359	0.98413	1.00868	0.99628
$(La/Sm)_N$	0.83871	0.4543	0.37742	0.32616	0.34946	0.56282	1.73433	2.03348	2.12199	2.13501

$(La/Yb)_N$	2.69677	2.19113	2.02258	1.57312	1.68548	2.86532	10.00918	10.82923	11.22954	10.80582
$(Tb/Yb)_N$	1.98198	2.7558	2.93952	2.93952	2.93952	3.30696	2.88299	2.61801	2.61801	2.57208

5.4. Variation diagrams for gabbroic and ultramafic samples

The geochemical data of ultramafic and gabbroic samples presented above in table is also displayed below in variation diagrams. Three common type of variation diagrams are identified by petrologist and geochemists (Best, 2003). Among the three common variation diagrams, binary and normalized (spider and REE pattern) variation diagrams are used here to characterize the analyzed rocks of the study area. In Cartesian variation diagrams MgO and Zr are used as index of differentiations. Hence, MgO is plotted against selected major oxides and compatible trace elements while Zr is plotted against compatible and incompatible trace elements. The selected incompatible trace elements (mobile and immobile trace elements) chosen here are according to their susceptibility for hydrothermal alteration and low grade metamorphism effects. This helps to visualize the post-crystallization processes of the analyzed units. Normalized variation diagrams such as multi element spider diagrams and REE patterns are also used here to understand the magmatic processes of the studied mafic-ultramafic massif (Rollinson, 1993; Willson, 1989).

5.4.1. Binary variation diagrams

MgO as index of differentiation is plotted against selected major oxides since it display wide range of variation in the analyzed ultramafic samples (Rollinson, 1993; Willson, 1989). This helps to understand the response of those oxides in basaltic magma processes (differentiation). From the diagrams shown below negative correlation of ultramafic samples is presented in MgO versus TiO_2, Al_2O_3, and CaO and slight decreasing to constant (horizontal) trend is shown in MgO versus Na_2O, K_2O and P_2O_5. The noticeable slightly decreasing trend is shown in MgO versus Na_2O diagram. Inflection trend is established by MgO versus SiO_2. Slight Inflection trend is also shown in the diagram formed by MgO versus CaO. In gabbroic samples positive trend is formed by MgO against TiO_2, CaO and Fe_2O_3 and negative trend is shown in MgO versus SiO_2**,** Al2O3, Na2O, K2O and P2O5.

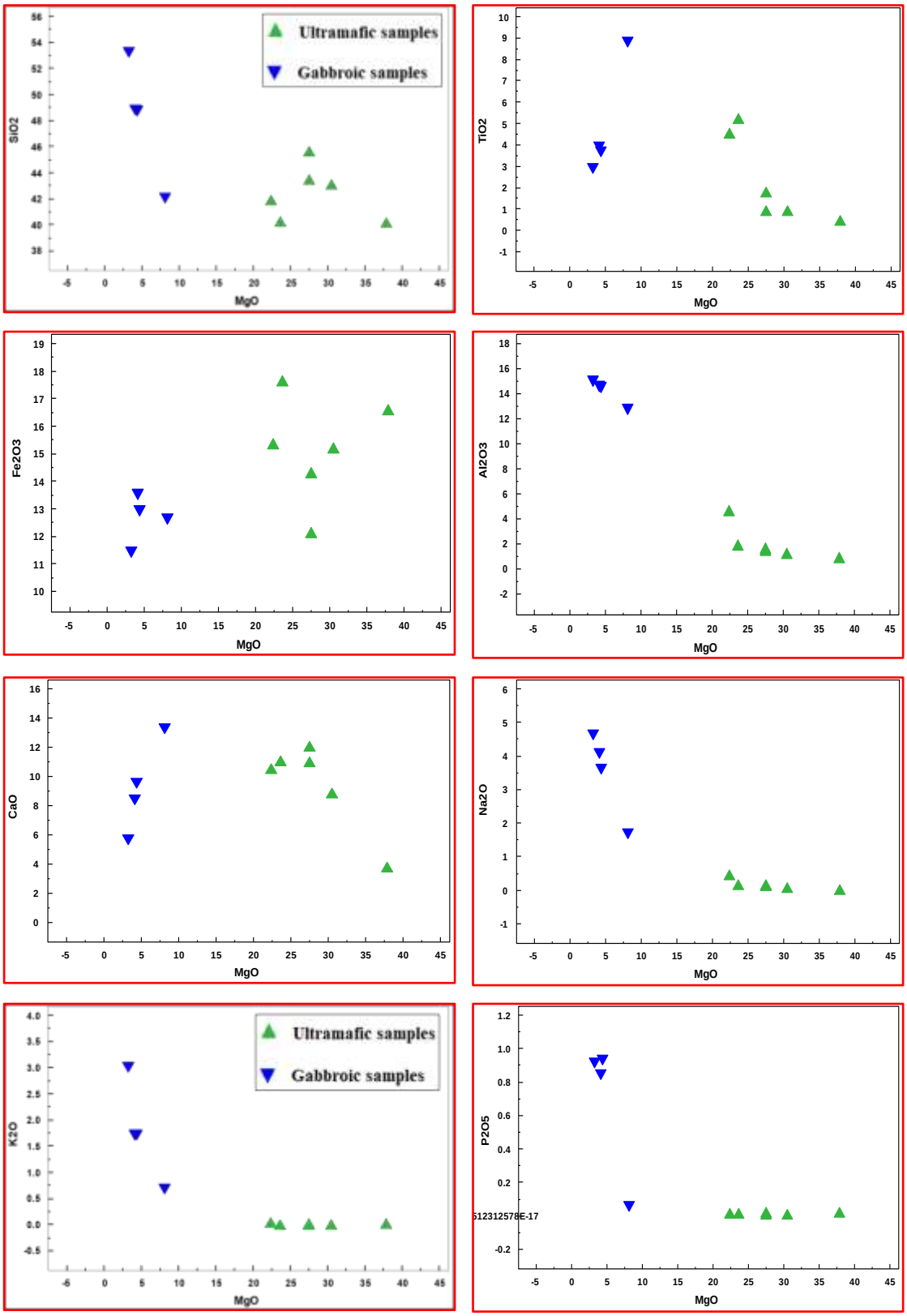

Figure 5.2: Major oxides (in wt. %) variation diagrams for Selen Wuha gabbroic and ultramafic samples. The selected major oxides are platted against to MgO. The oxides are normalized to volatile free base.

In figure 5.3, MgO is plotted against compatible (Ni, Cr and Co) and incompatible trace elements (Zr, Th and Ta) where MgO used as index of differentiation. In these diagrams, MgO correlates positively with Ni, Cr and Co for ultramafic samples and it correlates negatively with incompatible trace elements. For these samples very slight curve is shown by MgO versus Zr and Ta. For the gabbroic samples slight to strong positively increasing trend is displayed by Ni and Co while almost horizontal trend is shown in MgO versus Cr. All plots of incompatible trace elements show negative correlation. Th shows steeply decreasing negative trend in gabbroic samples but it displays horizontal trend in ultramafic samples.

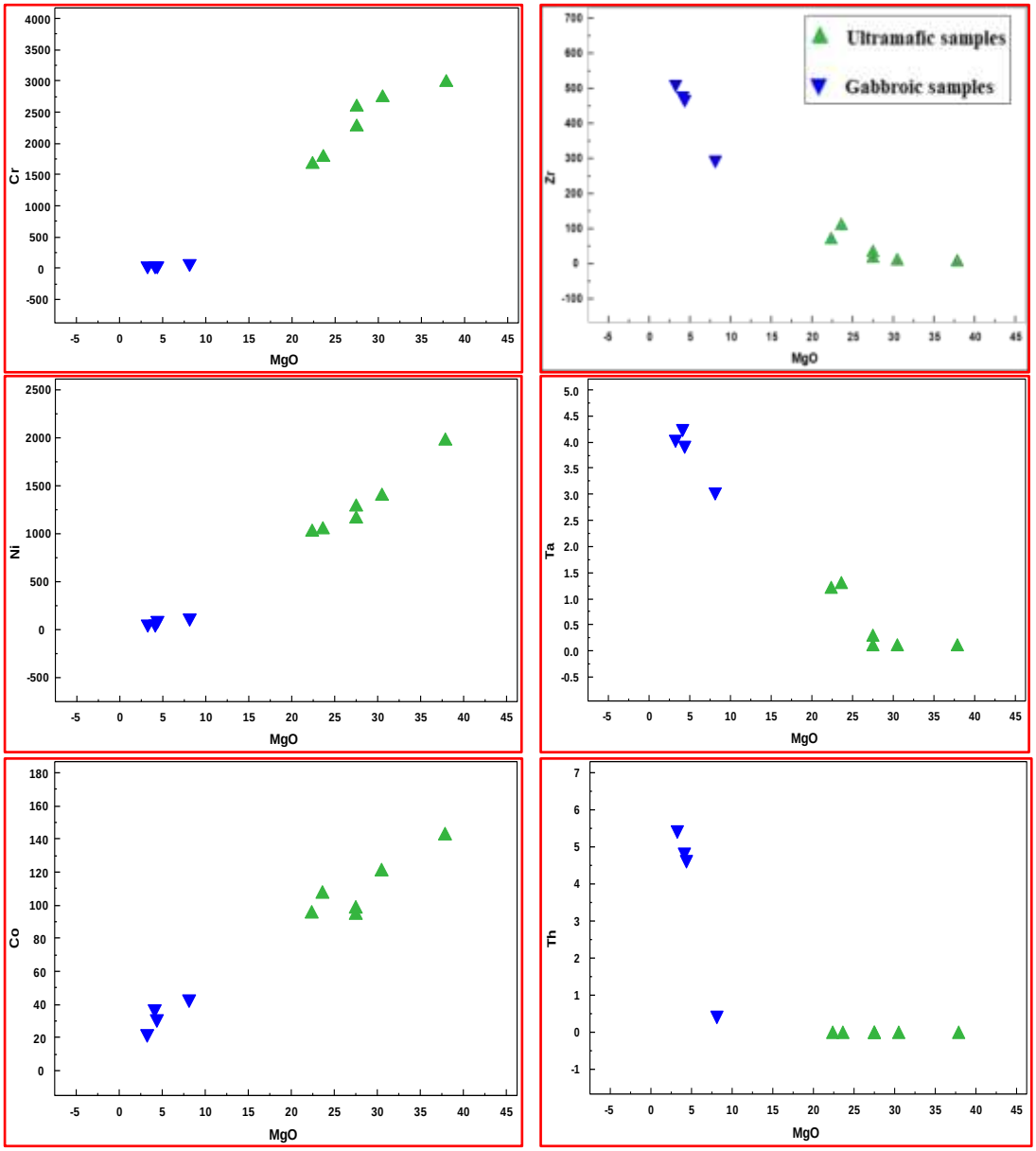

Figure 5.3: Diagrams of MgO versus compatible (Ni, Cr and Co) and incompatible trace elements (Zr, Th and Ta) for Selen Wuha gabbroic and ultramafic units.The concentration of MgO is expressed in wt. % and the concentration of trace elements is given in ppm.

In figure 5.4, Zr is plotted against Cr, Ni, V and Co and almost all the plots formed by both groups of samples exhibit defined trend. Accordingly, Cr and Ni show negative correlation in ultramafic samples and almost horizontal (constant) trend for gabbroic samples. For the ultramafic samples, V display positive correlation while Co forms decreasing to increasing inflection curve. For the gabbroic samples slightly curved negative trend is formed by V versus Zr and Co exhibits gently decreasing negative trend.

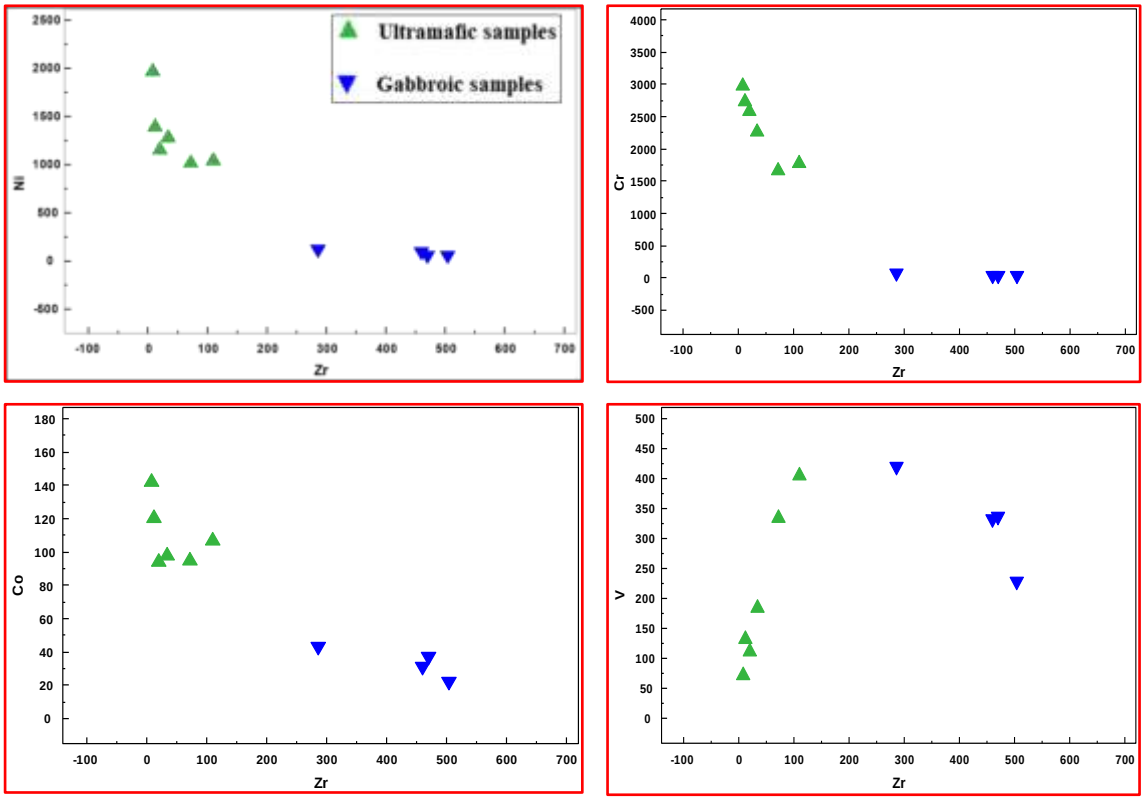

Figure 5.4: Zr versus compatible trace element variation diagrams for Selen Wuha gabbroic and ultramafic samples. The concentration of the trace elements is given in ppm.

In figure 5.5, incompatible trace elements (Th, Nb, Y, Rb, Sr and Ba) are plotted against Zr. For these ultramafic samples, Nb and Y show positive correlation whereas Th, Rb and Ba display horizontal trend. For these samples Sr shows mild clustering nature. Gabbroic samples also show almost linearly increasing positive trend in Th, Nb and Y versus Zr diagrams. In these samples Rb display upward curved trend however Ba and Sr show clustering nature. In Ba and Sr versus Zr diagram, one sample (ST4S4) is isolated and placed alone.

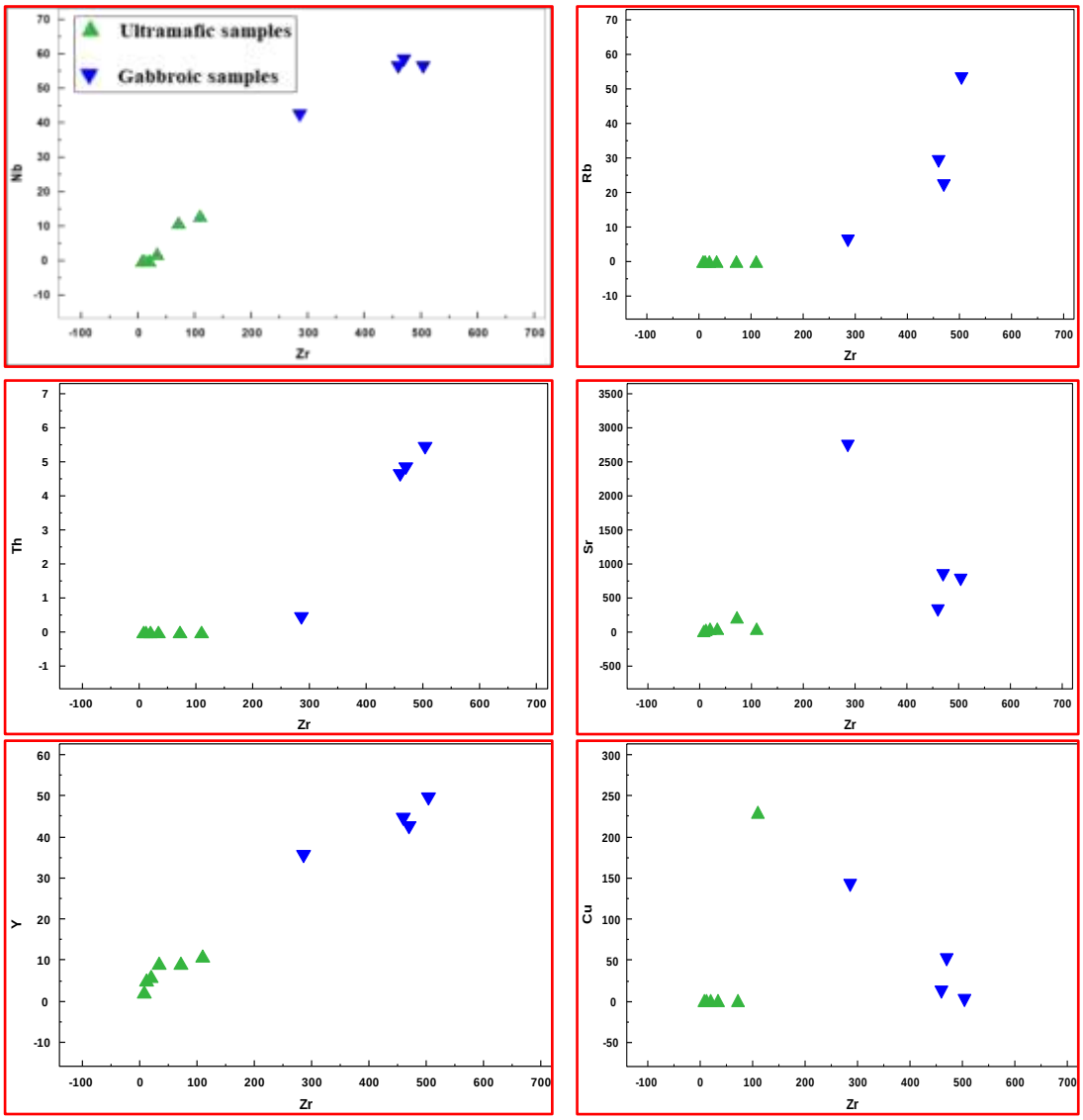

Figure 5.5: Zr versus incompatible trace element variation diagrams for Selen Wuha gabbroic and ultramafic samples. The concentration of the trace elements is given in ppm.

5.4.2. Multi-element spider diagrams

The multi-element variation diagrams of ultramafic and gabbroic samples are shown in figure 5.6 and they are normalized to primordial mantle value according to McDonough & Sun (1995). In the multi-element variation diagram produced by ultramafic samples (figure 5.6 A), most samples show steep vertical drop from Ta to K and minor increase is displayed from La to Pr. High field strength elements (HFSEs) i.e. Dy to Lu show strong decreasing trend (depletion). Strong negative anomaly is observed in Sr and K. K negative anomaly is restricted for few ultramafic samples such as ST1S7, ST5T5, ST1S11, and ST3S3. On the contrary, few ultramafic samples (ST1S11, ST3S2, ST5T5 and ST3S5) show Nd positive anomaly. Similarly, very slight positive anomaly (peak) is observed for Sm. In average, the

trend of the spider diagram produced by the ultramafic samples has horizontal (constant) trend.

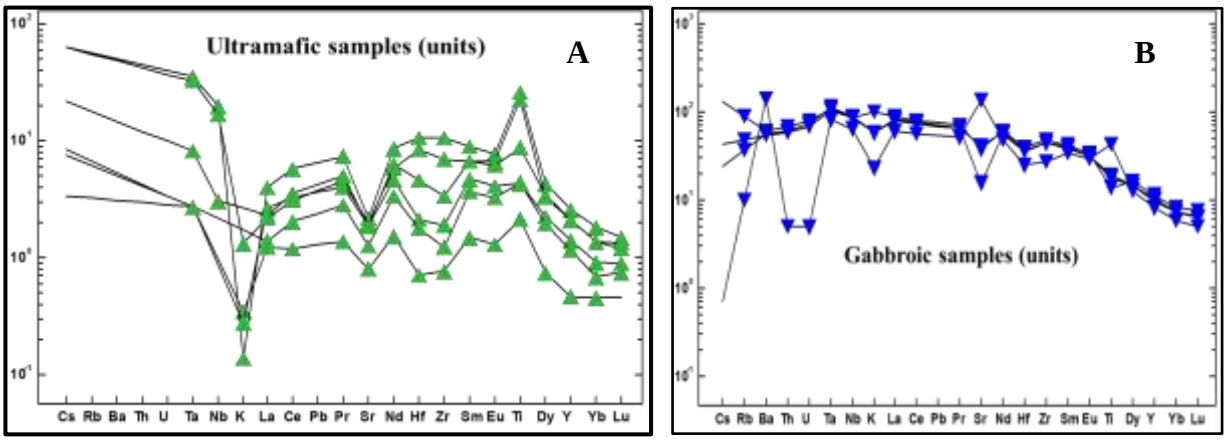

Figure 5.6: Multi-element variation diagram for Selen Wuha ultramafic and gabbroic samples. This Spider diagram illustrates the variation of the trace elements during the magmatic process. The samples are normalized to primordial mantle of value determined by McDonough & Sun (1995).

Multi-element variation diagram for gabbroic samples is shown in figure 5.6B. In that diagram one sample (ST4S4) has display positive anomaly (crest) in Ba, Sr and Ti. For this sample U and Th show pronounced negative anomaly. It shows flat trend from Ta to Pr and from Hf to Eu with minor spike in Sm. ST4S4 (gabbro) display minor decreased gentle slope from Dy to Lu. The other three gabbroic samples (ST4S8, ST5S3 and ST2S5) show slightly increasing gentle slope from Ba to Ta and slight decreasing relatively moderate slope from Zr to Lu. Small Ta positive anomaly is also shown by all the three elements. They show significant Sr negative anomaly and minor Hf negative anomaly. They display flat trend from Nb to pr. Over all, depletion of the most HFSEs (Dy, Y, Yb and Lu) is shown in the diagram.

5.4.3. Rare earth Element (REE) patterns

The concentrations of REEs are normalized to chondrite according to Sun & McDonough (1989). As shown in the diagram gabbroic samples are relatively enriched in LREEs and depleted in HREEs. This is evidenced by the ratio of MREE to HREE ($(Tb/Yb)_N$) and LREE to HREE ($(La/Yb)_N$) (Rollinson, 1993). The value of $(Tb/Yb)_N$ and $(La/Yb)_N$ ranges from 2.57 to 2.88 and from 10.01to 11.23 respectively (Table 5.1). This shows LREEs are enriched in the system than the HREEs. The value of $(La/Sm)_N$ is also less than the value of $(La/Yb)_N$. Its value ranges from 1.73 to 2.14. The Eu/Eu* value for these samples ranges from 0.98413 to1.04359 and hence pronounced Eu anomaly is not observed in the pattern. The pattern has almost uniformly deceasing trend. Comparatively, Slight gentle slope of the pattern is shown

from La to Nb and from Ho to Lu and slight steep slope is shown from Sm to Dy. In general, the overall trend of the pattern is gentle to moderately steep.

From the graph below (figure 5.7), ultramafic samples are relatively enriched in the MREEs (Nd to Gd except Pm) and LREEs (La to Pr). They are depleted in HREE (Tb to Lu). The values of (La/Yb)N and (Tb/Yb)N are range from 1.57 to 2.87 and from 1.98 to 3.31 respectively. The value (La/Sm)N ranges from 0.33 to 0.84. This supports for the above idea that MREEs are more enriched than LREEs and HREEs. Moreover, LREEs are less enriched than MREEs and better enriched than HREEs. Europium anomaly is determined by Eu/Eu* ratio. If the ratio is less than 1, it shows Eu negative anomaly and greater than 1 is to mean Eu positive anomaly (Rollinson, 1993). Therefore, the values of Eu/Eu* for Selen Wuha ultramafic samples are between 0.98093 and 1.00902. Greater than one Eu/Eu* value (i.e. 1.10829) is measured in one sample (ST3S3) and it shows slight positive anomaly than the others. It is indistinguishable unless you look it carefully. From the pattern, most samples show gentle slope from Sm to Tm. flat trend shows from Yb to Lu. Slight curved trend is observed from La to Nd.

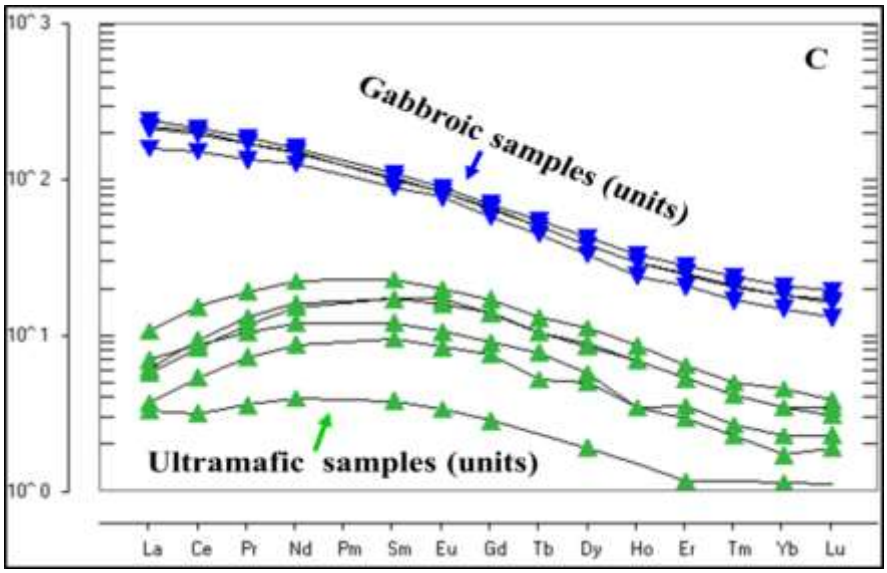

Figure 5.7: REE pattern for Selen Wuha gabbroic and ultramafic samples. The concentrations of samples are normalized to chondrite value determined by Sun & McDonough (1989).

CHAPTER SIX

DISCUSSION

6.1. Lithologic variety in the study area

According to Arkin et al. (1971), Beyth, (1972b), Merla et al. (1979) as cited in Tesfamichael Gebreyohannes (2010), Mengesha Tefera et al. (1996) and Melese Tadesse et al. (2011) the geology of the study area as part of Raya area or northwestern plateau, is belong to tertiary flood basalt of Ashange formation and Mesozoic sedimentary successions. Recently, the study area as part of Maychew area is mapped by Melese Tadesse et al. (2011) at a scale of 1:250,000. According to this regional scale, the lithologic units covered the area are only flood basalt of Ashange formation and Kemissie rhyolite (figure 2.1). However, the current study suggests that the study area is not totally covered by Ashange formation. Hence, various mappable and unmappable lithologic units are recognized in this study. Accordingly, ultramafic unit, gabbro (dyke), plagioclase olivine–phyric basalt (basalt), pyroclastic deposit and undifferentiated alluvial and lacustrine sediment deposit are the major mappable lithologic units of the area (figure 3.1). Un-mappable intrusions or dykes such as micro gabbro and micro granite are also present in the Selen Wuha area. These dykes are intruded in to ultramafic unit. As mentioned in chapter three, the areal coverage of ultramafic unit is about 53.71% (9.4km^2), plagioclase olivine–phyric basalt is about 22.57%(3.75km^2), pyroclastic material is about 10% (1.75km^2) and alluvial and lacustrine sediment is covered about 14% (2.45km^2).

The difference occurred between the two studies is perhaps due to the difference in the scale of study. In the current study, the area is mapped with the scale of 1:25,000 which is much detail than the map prepared by Melese Tadesse et al. (2011). Consequently, these listed lithologic units which are mapped in the present map scale (1: 25,000) may not be mappable units in that regional scale (i.e. 1: 250,000). That's why they have unified them in to Ashange basalt and Kemissie rhyolite. According to that regional scale, Ashange basalt and Kemissie rhyolite are covered relatively an extensive area and the above listed lithologic units are found within these two lithologic units (fig. 2.1)

6.2. Geologic structures and contact relationship between the units

Comparatively, ultramafic unit covers large area and it is in contact with all mappable lithologic units of the study area. Accordingly, this unit is in contact with basalt in the north, northeast, east and southeast direction of the mapped area. It is also contacted in the west direction with undifferentiated alluvial and lacustrine sediment deposit found in the plain of Raya valley. In the south direction of the study area, small pyroclastic deposits are found adjacent to this ultramafic unit (figure 3.1). The contacts which are found between ultramafic unit and basalt; ultramafic unit and undifferentiated alluvial and lacustrine sediment deposit are more or less controlled by tectonic structures. The tectonic structures such as lineaments and normal faults are found at the contacts of these lithologies.

Series of normal faults are found in the west of the target unit (ultramafic unit). This normal fault separates the very young undifferentiated alluvial and lacustrine sediment deposited in the plain of the valley from the relatively older ultramafic unit which occupied the escarpment and the ridges of the horst. In addition, considerable undifferentiated structural discontinuities (lineaments) are also found in the study area. The lateral extent of the studied ultramafic unit is terminated with respect to these structural discontinuities (lineaments). For instance, the contact between ultramafic unit and basalt (exposed in the north, northeast, east and southeast side of ultramafic unit) is controlled by lineaments. The gradational contact found between ultramafic unit and pyroclastic material is a lithologic contact. The unconsolidated ash (pyroclastic material) is placed on top of ultramafic unit. This unit become thicker and thicker as going away from the contact to the main exposure of this unconsolidated ash (pyroclastic material). This is from the upper most part of Melaku river toward the Tigrie Mender (village). In contrast, it becomes thinner as going from Tigrie Mender toward the upper part of Alaje river where gabbro and ultramafic units are exposed.

Even though the series of normal faults are oriented in different directions (i.e. NE- SW, NNE-SSW, NW- SE, NNW- SSE and N-S), their average orientation is looking north- south direction. This trend is similar with Afar rift or Afar depression. Similarly, the lineaments that are recognized in the study area have different orientations. Individually, they are oriented in N-S, E-W, NE-SW, NNE-SSW and NNW-SSW. In a regional view, they form two preferred orientations. These are north-south and east-west directions. The north–south oriented lineaments are probably resulted due to the effect of Raya marginal graben.

6.3. Characterizing for the main lithologies of the area

It is obvious that ultramafic rocks are constructed from dark colored mafic minerals (i.e. olivine, clinopyroxene and orthopyroxene) and more than 90% of the units are inhabited by these minerals (Styles et al., 2014). Likewise, olivine, clinopyroxene, orthopyroxene and Fe-Ti oxides (opaque) are the only mineral constituents of Selen Wuha ultramafic unit. Among them, the first three are the dominant mafic mineral constituents and they inhabit more than 90% in the unit. From these three minerals, clinopyroxenes are abundant in the seven thin sections while olivine gets dominant in the remaining three thin sections. This has been illustrated via WINROCK classification diagram shown in figure 3.6. The software is available in https://www.geologynet.com/winrock.htm.

According to that classification diagram, Selen Wuha ultramafic unit is classified in to peridotite and pyroxenite group of ultramafic units. Accordingly, the seven samples are plotted in to pyroxenite field and the three samples are plotted in to peridotite field. From the seven pyroxenite samples, four samples are plotted in olivine clinopyroxenite field, two are plotted in olivine websterite field and one sample is plotted in websterite field. Similarly, two of the three peridotite samples are plotted in wehrlite field and the remaining one peridotite sample is plotted in lherzolite field.

Gabbro and both ultramafic rocks (peridotite and pyroxenite) are characterized by porphyritic-phaneritic texture in which the grain size variation ranges from medium phaneritic (0.25mm to 2mm) to coarse phaneritc (2mm to 16mm). The entirely coarse grain size implies that almost all mineral grains are crystallized slowly at significant depth or the units are not formed at shallow depth. The grain size variation signifies two stage of mineral crystallization and the crystallization of minerals must have taken within the significant depth.

In hand spaceman, there is no significant grain size difference in both dark colored ultramafic units. The difference is only in mineral proportion and geochemistry. Peridotite samples have high concentration of olivine than pyroxenite samples and the analyzed peridotite sample (ST1S11) show high amount of MgO (37.08 wt. %), Cr (3000 ppm), Ni (1980 ppm) and Co (143ppm) as compared with pyroxenite samples. On the contrary, it shows low concentration of SiO_2 (39.22 wt. %**)** as compared with pyroxinites. They display almost similar Fe_2O_3 (16.19 wt. %) (See the detail in section 6.4).

From the geochemistry point of view, high concentration of MgO, Mg #, Cr, Ni and Co and low concentration of SiO_2, Na_2O, K_2O, Rb, Ba, Nb, Zr, Y, Hf and REEs are reported in these

ultramafic samples (table 5.1). According to that table, the concentration of MgO, Mg #, Cr, Ni and Co ranges from 22.31 wt. % to 37.08 wt. %, 72.63% to 81.94%, 1690ppm to 3000ppm, 1030ppm to 1980ppm and 96ppm to 143ppm respectively. In contrast, the concentration of SiO_2 ranges from 39.22 wt. % to 45.55 wt. %. Similarly, Na_2O and K_2O are very low in the ultramafic unit and their concentration is reported as below 1 wt. %. In addition, the concentration of Rb, Ba, Nb, Th and U is reported as below detection limit. In general, the existence of high concentration of MgO, Mg #, Cr, Ni and Co infers that the dominant minerals which establish the unit are olivine and pyroxene minerals since their abundancy is mainly related with the existence or absence of these two minerals in the system. This is also further evidenced by the presence of low concentration of SiO_2, Na_2O, K_2O, Ba, Rb, Sr and Eu/Eu*. The low concentration of SiO_2, Na_2O, K_2O, Ba, Rb, Sr and Eu/Eu* indicates that significant amount of felsic minerals (k-feldspar and calcic-feldspar) are not present in the unit. Overall, both geochemical and petrographical data are consistent and powerfully characterize the studied ultramafic unit.

The existence of high concentration of MgO (>18 wt. %), low concentration of SiO_2 (<45 wt. %) and low K_2O content in the studied unit suggests that the unit is not olivine or pyroxene phyric basalt (Ashange formation) (https://en.wikipedia.org/wiki/Ultramafic_rock). Moreover, basalts and gabbros are characterized by 28 to 38 and 26 to 79 (Mg#) respectively while ultramafic rocks are characterized by 80-88 of Mg# (Dey et al., 2017). Thus, this finding disproves the conclusion drown by for the idea of Melese Tadesse et al. (2011).

From the field observation and petrographic result, mineral segregation (layering) based on their crystallizing temperature is not observed in outcrop and in microscopic scale. This segregation is to mean that the separation of pyroxene from olivine based on their temperature of crystallization. Such kind of segregation is the characteristic of cumulate rocks or cumulate ultramafic rocks. These cumulate ultramafic rocks are crystallized (formed) at magma chamber by settling or floating of the minerals. However, the coarse grained ultramafic unit found in the study area does not show mineral layering or segregation and therefore it could not be cumulate ultramafic intrusion.

The recognized plagioclase olivine-phyric basalt is strongly fractured, moderately weathered and texturally aphanitic. In addition, swarms of basaltic and micro-gabbro dykes are intruded in this plagioclase olivine-phyric basaltic unit. From the petrographic point of view, the unit is greatly characterized by porphyritic texture with plagioclase and olivine phenocrysts. Since this characteristics is similar to the characteristics of Ashange formation (Ashange basalt), the

recognized basaltic unit is grouped in to this early Ethiopian flood basalt formation (Mengesh Tefera, 1996; Melese Tadesse et al. 2011).

6.4. The effect of alteration and metamorphism

As it has already mentioned in chapter four, abundant fractures such as normal faults, lineaments, dykes, joints and veins are present in the study area. Since fractures are open spaces, fluid materials such as hydrothermal fluid and gases can percolate easily through them and cause significant alteration on the minerals of the unit. In outcrop scale, light and dark colored secondary materials (veins) are present in both strongly weathered and relatively unaltered ultramafic units. This light colored secondary material is also present in the less welded pyroclastic materials (and 3.21). It is carbonate minerals since it reacts with diluted hydrochloric acid. The vein is also observed in microscopic scale. Fractures filling secondary materials are present in olivine mineral grains (figure 3.10 C & B). Comparatively, alteration is high in gabbro and micro-gabbro dykes.

The light and dark colored veins that are described earlier are probably resulted due to the effect of circulating hydrothermal fluid. The possible indications for the existence of hydrothermal alteration in the study area are: (1) Hot spring water is present around the study area. This is also evidenced by the existence of hot spring ponded water in Sulula river and two boreholes near the study area. One shallow borehole is located in Melaku river (i.e. above Gubana mender) and another borehole, which yields very hot water, is found to the north of Gubana mender near the escarpment. Currently, it has sealed. (2) The light colored sheeted secondary materials (veins) are reacted with diluted hydrochloric acid. In addition, these light colored sheeted secondary materials (veins) are also placed on top of hills and ridges. (3) Abundant veins are found in the study area and these veins (secondary materials) have filled the fractures of the rocks.

Dereje Ayalew et al. (2002) have not used rock samples having greater than 4.5wt % LOI content. According to this study, samples having > 4.5wt % of LOI are too altered and insignificant to interpreted the petrogenetic characteristics of the system. Therefore, they are not representative samples. In contrast, Dey et al. (2017) have obtained LOI content between 1.72wt% and 5.98wt%. They suggested that this range of LOI content is an indicative of low degree of alteration. Accordingly, the geochemically analyzed Selen Wuha gabbroic and ultramafic samples show very low content of LOI. This value ranges from 0.58 wt. % to 2.76

wt. % and from -0.14 wt. % to 2.95 wt. % respectively and this suggests the effect of alteration on both units is very low. As shown in figure 5.5, selected mobile and immobile trace elements are plotted against Zr. Mobile trace elements such as Sr and Rb are easily affected when the host rock is subjected to hydrothermal alteration, weathering, diagenesis and low grade metamorphism process. Cu is mobile element at high temperature and at high grade of metamorphism even though it is stable at low temperature (Rollinson, 1993). Whereas immobile trace elements such as Th, Nb, Y are not easily affected by hydrothermal alteration and low grade metamorphism processes. In contrast, they are unstable at high temperature and high grade metamorphism processes. When suffered for such conditions, their abundancy is disturbed and cannot show good correlation or specific array (Rollinson, 1993; Scoates et al. (2007; Wang et al., 2008).

All immobile trace elements including Rb show strong positive correlation for both ultramafic and gabbroic samples. Cu has good correlation in both groups of samples (ultramafic and gabbroic samples). Negative correlation is shown in the gabbroic samples while constant or clustering nature is shown in ultramafic samples. Negative trend is shown by gabbroic samples in Zr versus Sr diagram and almost constant trend is shown in ultramafic samples. This indicates insignificant or very limited effect of alteration or metamorphism is occurred on the studied units. On the other hand, the effect of post-crystallization alteration (hydrothermal alteration) in both units (gabbroic and ultramafic units) is very low (Wang et al., 2008).

As it has been mentioned repeatedly, the recognized mineral constituents of ultramafic unit are olivine, orthopyroxene, clinopyroxene and Fe-Ti oxides. Similarly, plagioclase, clinopyroxene, orthopyroxene and Fe-Ti oxides are the only mineral constituents of gabbroic units. Both units have porphyritic phaneritic texture and mineral grains of the units are interlocked on each other and form triple junctions. This kind of random arrangement and mineral interlocking is the common characteristics of igneous rocks since they are formed via mineral crystallization processes from hot molten magma. On the other hand, igneous rocks are resulted when hot molten magma comes to the low temperature and relatively very low deferential stress environment. Accordingly, minerals grains of the rocks are start to crystallizing freely and they are arranged randomly. These randomly arranged mineral grains are interlocked on each other and eventually form interlocked texture. Triple junction is formed at grain to grain boundary of three or more interlocked mineral grains (Thompson & Turk, 1998; Winter, 2001). Therefore, metamorphic texture or mineral alignment is not observed in all thin sections of both units. Moreover, new development of metamorphic

mineral assemblage is not observed. Consequently, Selen Wuha ultramafic unit and gabbro are not metamorphosed to low or high grade of metamorphic rocks.

Generally, the result of the present study is not consistent with the idea of Tenalem Ayenew et al. (2013), WWDSE (2011) and Merhawi GebreEgziabher (2011) concerning the age and nature (condition of metamorphism) of the units. However, it has conformed to some extent with the idea of Gezahegn Yirgu (2010) which states that Selen Wuha ultramafic unit (pyroxenite) and gabbro are not metamorphosed to meta-pyroxenite and meta-gabbro and probably it is Oligocene in age. Gezahegn Yirgu (2010) has obtained only four minerals in Selen Wuha ultramafic unit and his estimated modal proportion was ~37% (Ol), ~35% (Opx), ~20% (Cpx) and ~8% (Fe-Ti oxide). The unit is characterized by its coarse grained inequigranular texture. Based on this data the unit is named as olivine Websterite. Similarly, these four previously identified minerals are also obtained in all the ten ultramafic samples prepared in the present study and they are the only mineral constituents of the unit. Although these four common minerals are present in all thin sections, there is a variation in minerals proportions among the ten thin sections. Accordingly, all the ten samples have plotted in various fields of IUGS ultramafic rock classification and nomenclature diagram shown in figure 3.6 (Le Bas and Streckeisen, 1991). According to that diagram, the samples are plotted in both peridotite and pyroxenite fields and therefore, the studied Selen Wuha ultramafic unit is not restricted only to the mantle derived pyroxenite group of ultramafic unit. However, peridotite unit in form of werlite and lherzolite is coexisting with the pyroxenite unit. This idea is also consistent with the geochemical data provided in table 5.1. Accordingly, The presence of 37.08 wt. % (MgO), 81.94% (Mg#), 39.22 wt. % (SiO_2), 3000ppm (Cr), 1980 ppm (Ni) and 143ppm (Co) in ST1S11 indicates that ST1S11 is the most ultramafic sample and it is a representation of mantle derived peridotite unit (Reverdatto et al., 2008; Daczko et al., 2012). Reverdatto et al. (2008) have made geochemical distinction between the two ultramafic groups (i.e. mantle derived peridotite group and mantle derived pyroxenite group). On the other hand, the concentrations of MgO, Cr, Ni and other trace elements are different in both groups of mantle derived ultramafic units. Consequently, the concentrations of MgO, Cr and TiO_2 in pyroxenite group range from 27wt% to 35wt%, 2300ppm to 3300ppm and 0.02ppm to 0.08ppm respectively. However, the concentrations of MgO, Cr, TiO_2 and Ni in peridotite group range from 35 wt. % to 46 wt. %, 1750ppm to 12770ppm, 0.01ppm to 0.3ppm and 900ppm to 2500ppm respectively. In addition, the concentration of FeO, Yb, Zr,

Nb total REE etc in mantle derived peridotite group is different from their concentration in mantle derived pyroxenite group (table 5.1).

6.5. The relative ages of ultramafic and gabbroic units

Dykes of micro-gabbro, basalt and micro- granite are found as intrusions by intruding in the ultramafic unit. Hence, they are younger than the ultramafic unit. Stratigraphically, pyroclastic material is placed on top of ultramafic unit and therefore it is younger than the younger intrusions. The cross sectional map shown in figure 3.1 B, shows the relationship of the major lithology of the study area. Accordingly, gabbro is intruded in ultramafic unit and ultramafic intrusion in turn intruded in Ashange formation (basalt). This relationship implies that Ashange basalt is older than the ultramafic intrusion, which intern older than gabbro.

This idea is supported by some previous works such as Merhawi GebreEgziabher (2011) and WWDSE (2011). They have independently prepared geological map and cross-sectional map of Raya valley using borehole data. In both studies, the profile line that they have used is crossing from the western plateau of the valley to Selen Wuha river. According to these studies, Ashange basalt is found beneath the undifferentiated alluvial and lacustrine sediment of the valley plain (figure 1.5). The existence of Ashange basalt beneath the undifferentiated alluvial and lacustrine sediment of the valley plain is also reported by Dessie Nedaw (2003) from the lithological log section of Mehoni well No 1 (BH52). Moreover, the presence of Mesozoic sedimentary rocks such as Amaba Aradom sand stone (upper sand stone) are also indicated by the cross-sectional map of Merhawi GebreEgziabher (2011) and WWDSE (2011). The studied ultramafic unit is intruded in all these units (figure 1.5). Melese Tadesse et al. (2011) supports for the existence of Ashange basalt beneath the Quaternary sediment deposited in Raya valley. In his geological cross section, Kobo granites (tertiary aged granites) are intruded in this Ashange basalt (figure 2.1). According to the cross section produced by Merhawi GebreEgziabher (2011) and WWDSE (2011), the Mesozoic sedimentary rocks such as Amaba Aradom formation (upper sand stone) and Ashange basalt are moved dawn following the fault forming a graben while the ultramafic unit is pushed up with the Chercher horst.

In general, field observation, petrographic study and previous works all collectively suggests that the ultramafic unit outcropped in Selen Wuha area is not Neoproterozoic metamorphic unit. However, it is young igneous intrusion and younger than the early tertiary aged flood basalt (Ashange formation) and the Mesozoic sedimentary successions. Since almost all

Ethiopian Neoproterozoic rocks are basement metamorphic rocks, they all are changed at least to low grade metamorphic rocks (Kazmin, 1971 and 1975 as cited in Asefawossen Asrat, 2001; Vail, 1985; Stern, 1994; Kusky et al., 2003 as cited in Bosworth et al., 2005; Kzmin, 1978; Teklay Mengist et al., 1998; Gerra, 2000 as cited in Bheemalingeswara and Nata Tadesse, 2009).

According to the RVDP (1996) as cited in Mohammedsultan Abdella (2010) and in Dessie Nedaw, (2003); Melese Tadess et al. (2011), Merhawi GebreEgziabher (2011) and WWDSE (2011) Precambrian basement units, Mesozoic sedimentary successions such as Adigrate sandstone, Antalo limestone, Amba-Aradom formation and young Cenozoic volcanic units (from old to young) are outcropped in Chercher mountain belt (horst) near Moheni sub-basin of Raya marginal graben. However, the Mesozoic sedimentary successions even their remnants are not found in the study area and close to it. Their absence and outcropped of an extensive ultramafic intrusion is probably related with the uplifting following to intrusion and subsequent erosional impacts. This may be evidenced by the existence of Mesozoic sedimentary successions and Ashange formation beneath the undifferentiated alluvial and lacustrine sediment deposited in Raya graben (figure 1.5).

6.6. Petrogenetic characteristics

6.6.1. Source rock

In figure 5.2 eight major oxides are plotted against MgO for both Selen Wuha ultramafic and gabbroic samples. Seven of the eight oxides show strong correlation for both groups of samples. This strong correlation shown in both group of samples demonstrates co-genetic of the units and they are derived from homogeneous source. Furthermore, the samples are related by some common magmatic processes. If the samples show scatter nature instead of forming specific array, they are probably an indicator of source heterogeneity or background noise (Wilson, 1989; Rollinson, 1993; Ronald Frost and Carol Frost, 2014). Similarly, plots with good correlation are shown in figure 5.5 where mobile (Rb, Sr and Cu) and immobile (Th, Y and Nb) trace elements are plotted against Zr. Such diagrams can illustrate whether the studied units are derived from homogeneous source or heterogeneous source. In these diagrams, both mobile and immobile trace elements show strong correlation for both gabbroic and ultramafic samples. These diagrams signify that both gabbroic and ultramafic samples are derived from the same source and perhaps related fractional crystallization.

Mg # is more widely appropriate test whither a rock is sourced from primary magma or not. The value of Mg # for those igneous rocks derived from primary magma (mantle source) is greater than 68% (Gill, 2010). Best (2003) has specified the value of Mg# for those igneous rocks derived from primary magma. According to his idea, the value of Mg# is range from 68% to 75%. A rock resulted from mantle peridotite source is also tested by the concentration of MgO, Ni, Co and Cr. The accepted concentration of Ni and Cr in primary magma ranges from 250 -300 ppm and from 500- 600 ppm respectively (Frey et al., 1978; Hess, 1992 as cited in Dereje Ayalew et al., 2016; Wilson, 1989; Best, 2003;). Additionally, 8 wt. % MgO, 400 ppm Ni and 1000 ppm Cr are the frequently used lower limit elemental concentration of melt resulted from mantle peridotite or primary magma (Best, 2003). The concentrations of the major oxides, trace elements and REEs of studied SelenWuha ultramafic samples are given in table 5.1. In this table, the values of Mg #, MgO, Cr, Co and Ni in ultramafic samples range from 72.63 to 81.94, 22.31 wt. % to 37.08 wt. %, 1690 ppm to 3000 ppm, 96 ppm to 143 ppm and 1030 ppm to 1980 ppm respectively. These concentrations are much higher than the expected concentration of Mg #, MgO, Cr, Co and Ni in peridotite mantle source rocks documented in Gill (2010), Best (2003) and Wilson (1989). This demonstrates that the studied ultramafic unit is derived from primitive magma (melt sourced from mantle peridotite). In contrast, low concentration of Mg # (36.3 % to 56.31%), MgO (3.16 wt. % to 8.14 wt. %), Cr (<20 ppm to 30 ppm), Co (21 ppm to 42 ppm) and Ni (30 ppm to 90 ppm) are found in gabbroic samples. These concentrations are much lower than the expected concentration of Mg no, Ni and Cr in primary magma sourced igneous rocks. This implies that the gabbroic units are not derived from the primary magma however they are resulted from the evolved magma. Accordingly, these gabbroic samples have evolved or fractionated from the melt system forming ultramafic unit. This idea is evidenced via the major oxide and trace element variation diagrams shown from fig. 5.2 to 5.5 and REE pattern shown in figure 5.7. All these diagrams elaborate both group of samples (gabbroic and ultramafic samples) are derived from single parental magma and therefore, gabbroic samples have fractionated from the system forming ultramafic unit.

6.6.2. Fractional crystallization

The analyzed ultramafic samples show negative correlation of TiO_2, Al_2O_3 and CaO against MgO (figure 5.2). On the other hand, as the concentration of MgO decreases, the concentration of TiO_2, Al_2O_3, and CaO increases. This shows minerals such as magnetite, calcic plagioclase, ilmenite and titanomagnetite are not fractionating from the residual melt or

limited fractionation of these minerals is taking place in the system. The slight inflection trend shown in MgO versus CaO is an indication of changing in magma composition and thus small fractionation of clinopyroxene and olivine may occur. Constant or horizontal trend is shown in MgO versus Na_2O, K_2O and P_2O_5 suggests that they are not involved during the magmatic system. Which means their contribution on the modification of the magmatic system is very limited. Again this suggests that the involvement of crustal material or crustal contamination is null and the material is sourced from primary magma or depleted magma. The analyzed gabbroic samples show negative correlation of K_2O, Na_2O, P_2O_5, SiO_2 and Al_2O_3 against MgO and they show positive correlation in CaO, Fe_2O_3 and TiO_2. This suggests that fractionation of plagioclase, Clinopyroxene and Fe-Ti oxide bearing minerals such as magnetite, ilmenite and titanomagnetite are taking place during the magmatism processes. Conversely, Minerals such as apatite, k-feldspar ($KAlSi_3O_8$) and albite ($NaAlSi3O_8$) are not removed (fractionate) from the system (Best, 2003; Dereje Ayalew et al., 2016). This idea is consistent with the petrographic result of this study. In ultramafic thin sections, limited or small amount of opaque minerals are observed during the petrographic analysis (table 3.2). Likewise, plagioclase and alkali feldspar minerals are not observed. However, relatively better concentrations of opaque minerals are found in gabbroic samples.

There are different possibilities that can cause scattered trend in major oxide variation diagrams. Source heterogeneity, changing in the crystallization phases, mobility of the elements and oxidation of iron during weathering and hydrothermal alteration are perhaps among the main possibilities which can result a scattered trend in major oxide variation diagram (Derej Ayalew et al., 1999; Rollinson, 1993). In the present study, analyzed ultramafic samples show mild Scattering nature in MgO versus Fe_2O_3. This scattering trend may be resulted due to the effect of changing in the crystallization phases or oxidation of iron during weathering or hydrothermal alteration. Ultramafic and gabbroic samples of the study area show strong positive correlation in MgO versus compatible trace elements (Ni, Cr and Co) demonstrates the fractionation of ferromagnesian minerals such as olivine and pyroxene. Wilson (1989), Rollinson (1993), Derej Ayalew et al. (1999) and Best (2003) states that decreasing in concentration of Ni and Co indicates fractionation of olivine and pyroxene while decreasing in concentration of Cr implies accumulation (fractionation) of spinal and pyroxene.

MgO versus incompatible trace elements (Ta and Zr) shows strong negative correlation for both ultramafic and gabbroic samples suggesting that Ta and Zr bearing minerals did not fractionate from the molten system (figure 5.3). Since they are immobile, hydrothermal

alteration does not affect them. In addition, since they are highly incompatible elements, they cannot participate in the mantle source materials. However, they are expected to concentrate in crustal materials and therefore crustal materials were not contaminate to mantle source magma resulted those gabbroic and ultramafic unit of the target area. In MgO versus Th, gabbroic samples show steep decreasing slope while ultramafic samples show constant or horizontal trend. This demonstrates that Th is not participated in the magmatic process.

Multi-element variation diagram of ultramafic samples is shown in figure 5.6. In this diagram, trough (negative anomaly) is shown in K and Sr. Similarly strongly decreasing trend is shown from Dy to Lu (i.e. HFSEs). In contrast, strong crest (peak) is shown in Ti. The presence of trough in K and Sr suggests that maybe unparticipating or removal of K and Sr bearing minerals such as alkali feldspar and plagioclase feldspars. These minerals are expected to concentrate in felsic products (rocks) such as rhyolite and mafic products such as basalt respectively. However, they concentrate insignificantly in ultramafic products. Therefore, the best reason for their depletion in these ultramafic rocks is probably due to unparticipating or limited participation during the formation of these rocks. This is consistent with the petrographic result of these rocks in which plagioclase minerals are not found in all thin sections of the unit. The enrichment of Ti is related with the accumulation of Fe-Ti oxides in the system (Dereje Ayalew et al., 1999). This is also consistent with the petrographic result of these rocks in which very fine and rare fine phaneritic opaque minerals are seen in few thin sections of ultramafic samples. Particularly, considerable very fine opaque minerals are found in the fracture as fracture filling minerals. However, the existence of these opaque minerals is not as high as their concentration in gabbroic thin sections. The depletion in Dy to Lu (i.e. HFSEs) is related with the effect of garnet and amphibole in the source material. Similarly, Multi-element variation diagram for gabbroic samples is shown in figure 5.6. In that diagram, one samples shows negative anomaly in Th, K and U implies the involvement of crustal material (crustal contamination) and positive anomaly in Ba, Ta, Sr and Ti point toward the accumulation of plagioclase feldspar and opaque mineral grains. Moreover, all gabbroic samples show slight depletion in HFSE (Dy to Lu) suggesting the presence of slight effect of garnet or amphibole.

REE pattern of Selen Wuha gabbroic and ultramafic samples is shown in figure 5.7. In this figure, ultramafic samples show relatively slight depletion in light rare earth element (LREE) and strong depletion in heavy rare earth element (HREE). They show also relatively slight enrichment in Middle rare earth elements (MREEs). The slight depletion in light rare earth

element (LREE) suggests that the examined ultramafic unit may not sourced from enriched mantle and there is no significant involvement of contaminate crustal materials which can enhance the enrichment of LREE and highly incompatible trace elements (Thompson, 1984 as cited in Derej Ayalew et al., 1999). Hence, the source rock for this unit could be depleted mantle. Furthermore, the depletion of LREE could relate with either removal of LREE accommodating minerals such as sphene, apatite, monazite and allanite from the system during magmatic processes or unparticipating of these minerals in the system. Similarly, the strong depletion of HREE relates with the effect of garnet and amphibole in the source rock. On the other hand, the enrichment of MREEs related with the accumulation of titanite in the system (Wilson, 1989; Best, 2003).

REE pattern of Gabbroic samples shows the enrichment in LREE and depletion in HREE. This strong enrichment in LREE is also evidenced by the ratio of $(Tb/Yb)_N$ and $(La/Yb)_N$ (Rollinson, 1993, Dereje Ayalew et al., 1999). The values of $(Tb/Yb)_N$ and $(La/Yb)_N$ in the analyzed gabbroic samples range from 2.57 to 2.88 and from 10.01 to 11.23 respectively (Table 5.1). The enrichment in LREE is related with the accumulation of accessary minerals such as sphene, apatite, monazite and allanite in the magmatic system. In addition, it can be related with the involvement of crustal materials (crustal contamination). However, the depletion in HREE is related with the fractionation or removal of garnet and amphibole. In the diagram, slight steepness is sensed from middle rare earth element to heavy rare earth element. This demonstrates maybe garnet is left in mantle residue. The parallel to subparallel REE pattern of ultramafic and gabbroic samples are shown in figure 5.7 and that indicates both units are derived from co-genetic source.

CHAPTER SEVEN

CONCLUSION AND RECOMMENDATION

7.1. Conclusions

A combination of field observation, petrographic study, geochemical data and reviewing of the previous regional works provide new insight to Selen Wuha area. Accordingly, the present study has been arrived on the following main conclusions:

- Ultramafic, gabbro, plagioclase olivine-phyric basalt, pyroclastic deposit (tuff and ash) and undifferentiated alluvial and lacustrine Quaternary sediment deposit are the main recognized mappable lithologic units of the area. Micro-gabbro and micro-granite are relatively small intrusions (dykes) of the area that are intruded in the ultramafic unit and basaltic unit. Individually, gabbro is intruded only in the ultramafic unit while micro gabbro and micro granite are hosted in both units (ultramafic unit and basaltic unit). Swarm of micro-gabbro dykes are found in the basalt and ultramafic exposures. All these dykes have different orientations. Few micro-granitic dykes are also intruded in both ultramafic and basaltic areas. They are also oriented in different directions.
- Normal faults, lineaments, dykes, veins and joints are the recognized geologic structures in the study area. These structures have different orientations. In a regional view, normal faults are aligned in north-south direction while lineaments are aligned in north-south and east-west directions. Different orientation is observed in joint, vein and dykes. Tectonic controlled contacts are found between ultramafic unit, alluvial deposit and plagioclase-olivine phyric basalt. Particularly, series of normal faults and lineaments are controlled the contacts of the major units. Accordingly, normal faults are found at the contact of ultramafic unit and alluvial deposit while lineaments are found between plagioclase-olivine phyric basalt and ultramafic unit.
- During the field observation and petrographic study, new development of metamorphic minerals, metamorphic structures (fabric) and metamorphic texture is not recognized. However, the units are built from igneous minerals and they exhibit igneous texture and structure (massive structure). Minerals in the ultramafic unit are olivine, clinopyroxene, orthopyroxene and Fe-Ti oxides while minerals in gabbroic unit are clinpyroxene, orthopyroxene, olivine, plagioclase and Fe-Ti oxides. Grains of the minerals are arranged randomly and they form triple junction at grain to grain boundary of the adjacent mineral

grains. Since the grains of the minerals are inequigranular, the texture formed in both units is porphyritic-phaneritic texture in which the size of the grains is range from medium phaneritic to coarse phaneritic. Thus, the ultramafic unit and gabbroic units are not metamorphosed to their equivalent low or high grade metamorphic rocks. Since obducted ophiolitic ultramafic rocks are old body of oceanic crusts, they are characterized by metamorphic minerals, textures and structures. Therefore, Selen Wuha ultramafic units are not part of obducted ophiolitic ultramafic rocks.

- Few thin sections of the studied ultramafic show high amount of olivine and modal proportion of olivine in these thin sections is greater than 40%. Accordingly, peridotite ultramafic unit (werlite and lherzolite) is coexisting with pyroxenite ultramafic unit (olivine clinopyroxenite, olivine webstrerite and websterite). Since both units do not show mineral layering or segregation in outcrop and thin section scales, they are not mantle derived cumulate ultramafic rocks.
- Since gabbro, micro-gabbro and micro-granite are intruded in the ultramafic unit, they are younger in age than the studied ultramafic unit. Based on the previous studies, field observation and petrographic analysis, the studied ultramafic unit seems Cenozoic in age. According to the previous works, the studied ultramafic unit has cut (crossed) the successions of Mesozoic sedimentary rocks and early Cenozoic volcanic rocks at depth. The current field observation and petrographic study do not indicate any metamorphic signature in the Selen Wuha ultramafic and gabbroic units. Different researchers have been indicated that almost all Ethiopian Neoproterozoic basement rocks are transformed to low grade metamorphic rocks and their age is range from upper Proterozoic to lower Paleozoic era. Thus, the studied Selen Wuha ultramafic unit has not been metamorphosed to its equivalent metamorphic rock and it has cut across the successions of Mesozoic sedimentary rocks and early Cenozoic volcanic rocks at depth. Therefore, it is not Neoproterozoic in age however it is probably Cenozoic aged intrusion.
- Selen Wuha ultramafic samples show high concentration of Mg # (72.63% to 81.94%), MgO (22.31 wt. % to 37.08 wt. %), Cr (1690 ppm to 3000 ppm), Co (96 ppm to 143 ppm) and Ni (1030 ppm to 1980 ppm). This concentration is much higher than the expected concentration of Mg #, MgO, Cr, Co and Ni in peridotite mantle derived rocks and this suggests that Selen Wuha ultramafic unit is resulted from primitive magma (melt sourced mantle peridotite). Relatively low concentration of Mg # (36.3 % to 56.31%), MgO (3.16 wt. % to 8.14 wt. %), Cr (<20 ppm to 30 ppm), Co (21 ppm to 42 ppm) and Ni (30 ppm to 90 ppm) is found in gabbroic samples. This is much lower than the expected concentration

of Mg no, Ni and Cr in primary magma sourced igneous rocks. This implies that gabbroic units are not derived from the primary magma however they are resulted from the evolved magma.

- The Parallel to subparallel REE patterns of ultramafic and gabbroic samples are the indication of co-genetic. In addition, plots of MgO against selected major oxides such as TiO_2, Al_2O_3, CaO, Na_2O, K_2O, P_2O_5 shows strong correlation for both groups of samples. This strong correlation demonstrates that the samples are co-genetic and they are related by common magmatic process. The common magmatic process that relates the two groups of samples is probably fractional crystallization. In addition, in REE pattern of ultramafic samples, slight depletion of LREE is shown and this helps to generalize that ultramafic unit is not derived from enriched mantle source and crustal contamination is not carryout. However, it is derived from depleted mantle source. In contrast, an enrichment of LREE is shown in gabbroic samples and this is an indicator of crustal contamination or crystalized from evolved source.
- From the plots of incompatible versus incompatible trace elements, it is possible to conclude that both ultramafic and gabbroic samples are derived from homogeneous source since both samples show strong correlation in all plots.
- From the field observation, significant veins of ore minerals are not obtained in the studied ultramafic outcrop. Ore minerals such as chromite, hematite, magnetite and others are not also observed as a mineral form. Similarly, from the study of polished sections, significant concentration of Chromite, hematite and magnetite are not obtained. However, very few concentrations of hematite and magnetite ores are obtained. Overall, the study suggests that ore mineral deposit is not present in the studied Selen Wuha ultramafic unit.

7.2. Recommendations

On basis of field observation, petrographic study and geochemical data, the present study has arrived on the above conclusions. However, some interesting issues are still remaining open and require further detail investigation. These interesting unresolved issues are recommended here.

- The present study is used only 10 geochemical samples (i.e. 6 from ultramafic units and 4 from gabbroic samples) to characterize the geochemical characteristics and petrogenetic history of both gabbroic and ultramafic unit of the area. In addition, the study has used only 14 thin sections (10 from ultramafic and 4 from gabbroic samples) to characterize the petrographic aspect of both units. For the time being this may enough since the study is an initial study. However, it needs more geochemical samples and more thin sections to have better understanding about both units. Particularly, it needs more geochemical (i.e. major oxide, trace element and isotope geochemical data) and petrological samples to know the variety of ultramafic unit (i.e. the range from pyroxenite to peridotite). Therefore, it will be good if the area (ultramafic unit) will study with more thin section (petrological samples) and geochemical samples.
- On the basis of previous work, field observation and the petrographic study, ultramafic unit of Selen Wuha area is looking young in age. Since it has no any sign of deformation and nature of metamorphism, the current study has aged it in Cenozoic time (era). This relative age is determined based on its relationship with the surrounding rock, mineral assemblages of the unit and rock textures or the arrangement of mineral grains. Therefore, it is important if the numerical or radiometric age of Selen Wuha ultramafic unit is determined. This helps to know the actual age of the unit.
- In the study area, ultramafic unit (intrusion) has covered relatively an extensive area. It covers about 9.4km^2 or about 53.71% of the mapped area. From the previous work, field observation and petrographic study the relative age of this extensively outcropped Selen Wuha ultramafic intrusion is young and it is grouped in Cenozoic aged units. Exposing of such large Cenozoic ultramafic intrusions is uncommon. The cause for its exposing on the surface is probably uplifting and erosion. However, this reasoning is not supported with geodynamic and detail structural analysis results. Consequently, it is better if it will be determine the cause that has brought this much extensive ultramafic unit to the surface.

REFERENCE

1. Abdella Abdu (2011). Sustainable groundwater development and management for irrigation in Raya and Kobo valleys, Northern Ethiopia. Retrieved from (http://etd.aau.edu.et/bitstream/123456789/866/3/Abdella%20Abdu.pdf) accessed on 12/10/2016.
2. Afewok Desalegn, 2011. Ground water potential evaluation and flow dynamics of Hormat- Golina river catchment, Kobo valley, north Ethiopia. Retrieved from https://www.google.com/url?sa=t&rct=j&q=&esrc=s&source=web&cd=1&cad=rja&uact=8&ved=0ahUKEwjVq4HF9dXTAhXHvRQKHfkzA4AQFggmMAA&url=http%3A%2F%2Fetd.aau.edu.et%2Fbitstream%2F123456789%2F854%2F3%2FAfework%2520Desalegn.pdf&usg=AFQjCNG2LZFAsJZUwIVpBSBqD91Lt6lRQ&sig2=dvxBz_OROlxM66LlBBrFRw on 21/02/2017.
3. Arkin Y., Beyth M., Dow D.B., Levitte B., Haile T. and Hailu T. (1971). The Geological map of Mekele area. Min. Mines, Addis Ababa.
4. Asfawossen Asrat (2006). *Introduction to Physical Geology*. Addis Ababa University, Department of Earth Sciences. Addis Ababa University press, Ethiopia.
5. Asfawossen Asrat, Barbey, P & Gleizes, G. (2001). The Precambrian geology of Ethiopia: a review. *Africa Geoscince Review*, **8:** 271-288.
6. Asmelash Abay (2003). Engineering geological characterization of Oda Dam site and its catchment area (northern Ethiopia). Retrieved from (http://etd.aau.edu.et/bitstream/123456789/6677/1/10..ASMELASH%20ABAY.pdf) on 29/10/2016.
7. Ayele Almaw, Addis Kifle, Tesfamichael Gebreyohannes and Gebrerufael Hailu (2015). Spatial analysis of groundwater potential using remote sensing and GIS-based multi-criteria evaluation in Raya Valley, northern Ethiopia. *Hydrogeology Journal*. **23**: 195–206.
8. Best, M. G. (2003). *Igneous and Metamorphic Petrology*. 2nd Edition, Blackwell.
9. Beyth M. (1972b). Palaeozoic-Mesozoic sedimentary basin of Mekele Outlier, Northern Ethiopia. *AAPG Bull*. **56**: 2426-2439.
10. Bheemalingeswara, K. and Nata Tadesse (2009). Petrographic and Geochemical Study of Low Grade Metamorphic Rocks around Negash with Reference to Base Metal

Mineralization and Groundwater Quality, Tigray, Northern Ethiopia. *MEJS*, **1:**106-132.

11. Bosworth, W., Huchon, P., and McClay, K. (2005). The Red Sea and Gulf of Aden Basins. *Journal of African Earth Sciences*, **43:** 334–378.
12. Boynton W.V. (1984). Geochemistry of rare earth elements: meteorite studies, In: Henderson P. (ed.), *rare earth element geochemistry*, *Elsevier*, 63-114.
13. Co-SAERAR (1997). Feasibility study of Report for the Kobo-Girana Valley Development Study Project. Volume III: Annex B: Regional geology.
14. Daczko, N. R., Emami, S., Allibone, A. H., and Turnbull, I. M. (2012). Petrogenesis and geochemical characterisation of ultramafic cumulate rocks from Hawes Head, Fiordland, New Zealand. *New Zealand Journal of Geology and Geophysics*, ***55*:** 361-374.
15. Dereje Ayalew, Barbey, P., Marty, B., Reisberg, L., Gezahegn Yirgu and Pik R. (2002). Source, genesis, and timing of giant ignimbrite deposits associated with Ethiopian continental flood basalts. *Geochimica et Cosmochimica Acta*, **66 (8):**1429-1448.
16. Dereje Ayalew, Gezahegn Yirgu and Pik, R. (1999). Geochemical and isotopic (Sr, Nd and Pb) characteristics of volcanic rocks from southwestern Ethiopia. *Journal of African Earth Sciences*, **29 (2):** 381-391.
17. Dereje Ayalew, Jung, S., Romer, R. L., Kersten, F., Pfänder, J. A., and Garbe-Schönberg, D. (2016). Petrogenesis and origin of modern Ethiopian rift basalts: Constraints from isotope and trace element geochemistry. *Lithos*, ***258*:** 1-14.
18. Dessie Nedaw (2003). Aquifer characterization and hydro-chemical investigation in the Raya valley, Northern Ethiopia, (unpublished PhD thesis).
19. Dey, A., Hussain, M. F., and Barman, M. N. (2017). Geochemical characteristics of mafic and ultramafic rocks from the Naga Hills Ophiolite, India: Implications for petrogenesis. *Geoscience Frontiers*, **9:** 517-529.
20. Frey, F., Green, D., Roy, S., (1978). Integrated models of basalt petrogenesis: a study of quartz tholeiites to olivine melilites from South Eastern Australia utilizing geochemical and experimental petrological data. *Journal of Petrology*, **19:** 463–513.
21. Frost, B. R., & Frost, C. D. (2013). *Essentials of igneous and metamorphic petrology*. Cambridge University Press.
22. Gass, I. G. (1970). The evolution of volcanism in the junction area of the Red sea, Gulf of Aden and Ethiopian rifts. *Philosophical Transactions Royal Society of London*, **267:** 369–382.

23. Gerra, S. (2000). A short introduction to the geology of Ethiopia. *Chron. Rech. Min.,* **540:** 3-10.

24. Gezaegn Yirgu (2010).Teru Groundwater Potential Assessment Project: Geology of the Project Area. Unpublished report, WWDSE, Addis Ababa, Ethiopia.

25. Gidey Yirga (2010). Ethnobotanical Study of Medicinal Plants in and Around Alamata, Southern Tigray, Northern Ethiopia. *Maxwell Scientific Organization.* **2(5):** 338-344

26. Gill, R. (2010). *Igneous rocks and processes: a practical guide*. John Wiley & Sons.

27. Gillespie, M.R.and Styles, M.T. (1999). *British Geological Survey (BGS) rock classification scheme*, 2nd ed., NERC, Nottingham, UK.

28. Hess, P., (1992). Phase equilibria constraints on the origin of ocean floor basalts. *Geophysical Monograph*, **71:** 67–102.

29. http://www.levoyageur.net/weather-city-ALAMATA.html accessed on 08/04/2017

30. https://en.climate-data.org/location/512432/ accessed on 26/03/2017

31. https://en.wikipedia.org/wiki/Alamata accessed on 02/05/2017

32. https://en.wikipedia.org/wiki/Ultramafic_rock accessed on 21/03/2018

33. Kazmin, V. (1971). Precambrian of Ethiopia and some aspect of the geology of the Mozambique belt. Bulletin geopys. Obs., Addis Ababa *university*, **15:** 27-43.

34. Kazmin, V., Shifferaw Alemu, Balcha Tilahun, (1978). The Ethiopian basement: stratigraphy and possible manner of evolution. *Geologische Rundschau*, **67:** 531–546.

35. Kurkura K., Aynalem Zenebe, Bheemalingeswara K., Kinfe Atshbeha, Solomon Gebresilassie and Kassa Amare (2012). Mineralogical and Geochemical Characterization of Clay and Lacustrine Deposits of Lake Ashenge Basin, Northern Ethiopia: Implication for Industrial Applications. *Momona Ethiopian Journal of Science* (*MEJS)*. **4:**111-129.

36. Kusky, T. M., Mohamed Abdelsalam, Stern, R. J., Tucker, R. D. (2003). Evolution of the East African and related orogens and the assembly of Gondwana (Preface). *Precambrian Research,* **123:** 81–85.

37. Le Bas, M. J., and Streckeisen, A. L. (1991). The IUGS systematics of igneous rocks. *Journal of the Geological Society, **148*:** 825-833.

38. McDonough, W. F. and Sun, S. S. (1995). The composition of the earth. *Chem. Geol.* **120:** 223–253.

39. Melese Tadesse, Henok Bekele, Bezayit Mitiku, Meskerem Teshome, Asamenew Besufekade, Muhammed Edris, Getachew Burussa, Ezra Yehualaeshet, Shimeles

Ashenafi and Tadesse Alemu (2011). Geology, geochemistry and gravity survey of the Maychew area. Unpublished report. Geological survey of Ethiopia (GSE), Addis Ababa,Ethiopia.

40. Mengesha Tefera, Tadiwos Chernet, Workineh Haro (1996). *Explanation of the geological map of Ethiopia*, 2nd ed. EIGS Technical publication, Addis Ababa, Ethiopia.
41. Merhawi GebreEgziabher (2011). An Integrated Hydrogeological study to understand the groundwater flow dynamics of Raya Valley Basin, Northern Ethiopia. Hydrochemistry, Isotope Hydrology, and Flow Modeling Approaches. Unpublished MSc thesis, Addis Ababa University, Addis Ababa, Ethiopia.
42. Merla G., Abbate E., Azzaroli A., Bruni P., Canuti P., Fazzuoli M., Sagri M. and Tacconi, P. (1979). Comments to the geological map of Ethiopia and Somalia. Consiglio Nazionale delle Ricerche , Firenze, 95 pp.
43. Miruts Hagos (2010). Geochemical and petrographic studies of the volcano-tectonic evolution of northern Afar: implications for the structural setup of the actively expanding erta'ale depression. (Doctoral dissertation, uniwien). Retrieved from https://www.google.com/url?sa=t&rct=j&q=&esrc=s&source=web&cd=1&cad=rja&uact=8&ved=0ahUKEwio35btyqHbAhULLI8KHb1LBowQFgglMAA&url=http%3A%2F%2Fothes.univie.ac.at%2F12719%2F1%2F2010-11-26_0748564.pdf&usg=AOvVaw1AQdOCeowYrYnmaJqADX19 on 26/10/2017
44. Miruts Hagos, Bheemalingeswara K. and Jemal Ahmed (20016). A preliminary Geological and Generalized Stratigraphy of Western Margin of Northern Afar Depression, Dallol Area, Northern Ethiopia. *Momona Ethiopian Journal of Science (MEJS),* ***8(1)*****:** 1-22.
45. Mohammedsultan Abdella (2010). Ground water flow modelling assisted by GIS and RS techniques (Raya valley- Ethiopia). Retrieved from (http://www.itc.nl/library/papers_2010/msc/wrem/mohammedsultan.pdf) accessed on 20/11/2016.
46. Mohr, P. (1983a). The Morton–Black hypothesis for the thinning of continental crust-revisited in western Afar. *Tectonophysics,* **94:** 509–528.
47. Mohr, P. A. (1962). The Geology of Ethiopia. University. Coll. of Addis Ababa Press. (Reprinted in 1971 at the Haile Selassie I University Press), Asmara, Ethiopia.
48. Nigus Gebremedhn Abay, 2011. The impacts of climate change on rural livelihood and their adaptation methods: the case of Alamata woreda, southern Tigray. Retrieved

from EwjPgKiZNXTAhVLVhQKHRiXDHIQFghVMAE&url=http%3A%2F%2Fetd.aau.edu.et%2Fbitstream%2F123456789%2F3507%2F2%2FNigus%2520G.medhn.pdf&usg=AFQjCNH1Pb4gthrnE1pDZLiA8TmlE6k4uA&sig2=0313TIy8sU5mMr0Ar9CJ5A on 12/03/2017

49. Pik, R., Daniel, **C.,** Coulon, C., Gezahegn Yirgu, Hofman, C and Dereje Ayalew Ayalew (1998). The northwestern Ethiopian flood basalts: Classification and spatial distribution of magma types. *J. Volcanol. Geotherm. Res*, **81:** 91-111.
50. Pik, R., Deniel, C., Coulon, C., Gezahegn Yirgu, and Marty, B. (1999). Isotopic and trace element signatures of Ethiopian flood basalts: evidence for plume-lithosphere interactions. *Geochim. Cosmochim. Acta*, **63**:2263-2279.
51. Redfield, T.F., Wheeler, W.H & Often, M. (2003). Kinematic model for the development of the Afar Depression and its paleogeographic implications. *Earth and Planetary Science Letter*s, **216:** 383–398.
52. Relief Society of Tigray (REST) (1997). Feasibility Study Report for the Raya Valley Agricultural Development Project (Unpublished). Water Resources (Annex: Hydrology Hydrogeology, Geotechnics, Irrigation Development and, Dam & Weir.) Vol. II
53. Reverdatto, V. V., Selyatitskiy, A. Y., and Carswell, D. A. (2008). Geochemical distinctions between "crustal" and mantle-derived peridotites/pyroxenites in high/ultrahigh pressure metamorphic complexes. *Russian Geology and Geophysics*, **49**: 73-90.
54. Rollinson H. (1993). *Using geochemical data: evaluation, presentation, interpretation.* Pearson, prentice hall.
55. Raya valley development study project (RVDP) (1996). Raya valley hydrological study phase II feasibility draft report. Raya valley development study project Tigray National Regional Government.
56. Samson Tesfaye, David J. and Timothy M., (2003). Early continental breakup boundary and migration of the Afar triple junction, Ethiopia. *Geological Society of America*. **115:** 000–000.
57. Scoates, J. S., Weis, D., Franssens, M., Mattielli, N., Annell, H., Frey, F. A., Nicolaysen, K. and Giret, A. (2007). The Val gabbro plutonic suite: a sub-volcanic intrusion emplaced at the end of flood basalt volcanism on the Kerguelen Archipelago. *Journal of Petrology*, ***49*:** 79-105.

58. Solomon Tadesse (2009). Mineral Resources Potential of Ethiopia. Addis Ababa University Press. Addis Ababa. Ethiopia.

59. Stern, R.J. (1994). Arc assembly and continental collision in the Neoproterozoic East African orogen: implications for the consolidation of Gondwanaland. *Annual Reviews Earth Planetary Sciences*, **22:** 319–351.

60. Styles, M. T., Sanna, A., Lacinska, A. M., Naden, J., & Maroto-Valer, M. (2014). The variation in composition of ultramafic rocks and the effect on their suitability for carbon dioxide sequestration by mineralization following acid leaching. *Greenhouse Gases: Science and Technology*, ***4*(4):** 440-451.

61. Sun, S., and McDonough, W.F. (1989). Chemical and isotopic systematics of oceanic basalts: implications for mantle composition and processes: In Sunders, A.D., and Norry, M.J. (eds), Magmatism in ocean basins. *Geological Society Special*, **42:** 313-345.

62. Teklay Mengist., Kröner, A., Mezger, K & Oberhänsli, R. (1998). Geochemistry, Pb–Pb single zircon ages and Nd–Sr isotope composition of Precambrian rocks from southern and eastern Ethiopia: implications for crustal evolution in East Africa. *J. Afr. Earth Sci.* **26:** 207–227

63. Tenalem Ayenew, Merhawi GebreEgziabher, Seifu Kebede and Sileshi Mamo (2013). Integrated assessment of hydrogeology and water quality for groundwater-based irrigation development in the Raya Valley, northern Ethiopia. *Water International*, **38 (**4)**:** 480-492.

64. Tesfamichael Gebreyohannes, Florimond, D. S., Miruts Hagos, Solomon Gebresilassie, Kassa Amare, Kurkura, K., Abdulwassie Hussein, Jan N., Hans Bauer, Jan, M., Jozef, D., Mitiku Haile and Nurhussen T. (2010). Large-Scale Geological mapping of the Geba basin, northern Ethiopia. Retrieved from http://www.ethiopianreview.com/pdf/001/TLP_9_Geological%20Map.pdf. It is accessed on 06/11/2016.

65. Thompson, G. R., & Turk, J. (1998). *Introduction to physical geology*. Brooks/Cole Publishing Company.

66. Thompson, R.N., Morrison, M.A., Hendry, G.L., Parry, S.J. (1984). An assessment of the relative roles of a crustal and mantle in magma genesis: an elemental approach. *Phil Trans Royal Society London*, **310:** 549-590.

67. Ukstins, I. A., Renne, P.R., Wolfenden, E., Baker, J., Dereje Ayanew and Menzies, M. (2002). matching conjugate volcanic rifted margins: 40Ar/39Ar chronostratigraphy of

pre- and syn-rift bimodal flood volcanism in Ethiopia and Yemen. *Earth Planet Sci. Lett.* **198**: 289-306.

68. Vail, J. R. (1985). Pan African (Late Precambrian) tectonic terrains and the reconstruction of the Arabian Nubian shield. *Geology*, **13:** 839–842.
69. Wang, X. L., Zhou, J. C., Qiu, J. S., Jiang, S. Y., & Shi, Y. R. (2008). Geochronology and geochemistry of Neoproterozoic mafic rocks from western Hunan, South China: implications for petrogenesis and post-orogenic extension. *Geological Magazine*, ***145*:** 215-233.
70. Water works design and supervision enterprise (WWDSE) (2008). Geological investigation report on Raya valley basin, Northern Ethiopia. Unpublished report, WWDSE, Addis Ababa, Ethiopia.
71. Water works design and supervision enterprise (WWDSE) (2011). Raya valley plain pressurized irrigation project. Unpublished report, WWDSE, Addis Ababa, Ethiopia.
72. Wilson, M. (1989). *Igneous Petrogenesis a global tectonic approach*. Unwin Hyman, London.
73. Winter, J. D. (2001). *An Introduction to Igneous and Metamorphic Petrology*. Prentice-Hall Inc.
74. Zanettin, B., (1993). On the evolution of the Ethiopian volcanic province. In: Abbate, E., Sagri, M., Sassi, F.P. (Eds.), Geology and Mineral Resources of Somalia and Surrounding Regions, Istituto Agronomico per LOltremare, Firenze, Relazioni e Monografie Agrarie Subtropicalie *Tropicali Nuova Serie***, 113:** 279–310.
75. Zanettin, B., Gregnanin, A., Justin Visentin, E., Morbidelli, M. and Piccirillo, E.M. (1974). Geological and petrological researches on the volcanics of central Ethiopia. Padova, Italy

Appendix I

Petrographic data for ultramafic samples

	Recalculated modal value (%)									
Minerals	ST5T5	ST3S4	ST3S5	ST2 S3	ST3S2	ST1 S11	ST1S7	ST3 S6	TPAH	AAUM
Cpx	65.63	56	74.74	16.33	88.78	15.5	78.95	53.76	18.28	81
Opx	2.08	19	3.16	7.14	8.16	2	5.26	8.6	3.23	5
Ol	32.29	25	22.11	76.53	3.6	82.5	15.79	37.63	78.5	14
Opa.	0	0	0	0	0	0	0	0	0	0

Petrographic data for basalt samples

Minerals	Modal proportions (%)		Dominant shape		
	BAAD	BAAB	BASB	BAHB	
Plagioclase	50	63	55	45	Subhedral to euhedral
Olivine	20	15	15	25	Anhedral
Pyroxene	10	8	13	15	Anhedral
Fe-Ti oxides	20	14	17	15	Anhedral

Petrographic data for Microgranite samples

Minerals	Modal proportions (%)		Dominant shape
	ST_5S_2	ST_5S_1	
Alkali feldspar	60	55	Subhedral to anhedral
Quartz	8	5	Anhedral
Fe-Ti oxides	12	16	Anhedral
Plagioclase	20	24	Subhedral to anhedral

Appendix II

Orientation data for various measured Structural elements

Structural element	Strike directions	Dip directions	Easting	Northing
Normal fault	NNE-SSW	45 WNW	577518	1360104
	NW-SE	50 SW	577192	1360963
	N-S	45 W	576823	1362431
	NE-SW	55 NW	577057	1363799
	NNW-SSE	60 WSW	577237	1364742

Structural element	Lineament No	Strike directions
Lineaments	1	ENE
	2	NE
	3	NNE
	4	NNW
	5	NNW
	6	NNW
	7	NNW
	8	N-E
	9	NW
	10	WNW
	11	NW
	12	N-E
	13	NNW
	14	NE
	15	E-W
	16	E-W
	17	NNE
	18	ENE
	19	NE
	20	NE
	21	NE
	22	ENE
	23	EN
	24	NNE

Structural element	Strike direction	Dip direction	Easting	Northing	Dyke type
Dykes	NW	15SW	577375	1362206	Basaltic
	E-W	30S	578463	1363069	Basaltic
	WNW	10SSW	579089	1364090	Basaltic
	NE	20NW	580177	1362525	Basaltic
	ENE	25SSE	580221	1362574	Basaltic
	NE	20SE	580347	1362437	Basaltic
	WNW	10NNE	577952	1360261	Basaltic
	SW	13NW	577985	1359959	Basaltic
	E-W	24S	578276	1364019	Basaltic
	E-W	50S	578463	1362970	Gabbro
	NW	40NE	577463	1362887	Gabbro
	NW	35NE	577414	1362442	Gabbro
	NE	25NW	577864	1359998	Micro- gabbro
	WNW	30SSW	577463	1362843	Micro-gabbro
	NW	15SW	589133	1363783	Micro-gabbro
	SSW	30WNW	579908	1362909	Micro-gabbro
	NW	15NE	578913	1364458	Micro-granite
	WSW	27SSE	580051	1362777	Micro-granite
	ENE	35NNE	579891	1362931	Micro-granite
	SW	13SE	578084	1360822	Micro-granite
	N-S	17W	578221	1363783	Porphyritic basalt

Structural element	Strike direction	Dip direction	Easting	Northing
Joint	E-W	65N	577584	1360977
	E-W	80N	577698	1360960
	E-W	70S	577698	1360960
	E-W	75S	577584	1360977
	NE	70NW	578859	1360897
	NW	75SW	578840	1361175
	SE	80SW	578985	1361289
	N-S	87W	578677	1360759
	N-S	78W	578677	1360759
	NE	75NW	578680	1360758
	NE	85NW	578680	1360753
	NW	80NE	578663	1360902

Joint	E-W	87N	577989	1360982
	NNE	70WNW	577859	1362352
	NNE	60WNW	578798	1360595
	ENE	75SSE	577989	1360982
	ENE	85SSW	578561	1361716
	N-S	77W	577888	1359444
	NW	65SW	577450	1362210
	SSE	70WSW	577986	1359647
	SSE	65ENE	579029	1361275
	WNW	75NNE	577864	1359322
	WNW	85NNE	578054	1359412
	NNW	75WSW	578814	1360564
	NNW	60ENE	577496	1362352
	NE	80NW	578659	1360912
	SSW	70ESE	578854	1361184
	SSW	60WNW	577847	1362512
	SE	55SW	577962	1360210
	E-W	80S	578215	1359634
	NW	87NE	578758	1360613
	NE	85NW	578761	1360364
	E-W	85S	577989	1360982
	E-W	76N	577989	1360982
	E-W	80S	577989	1360982
	NNE	80WSW	578275	1361985
	E-W	65N	578381	1361821
	N-E	60W	578300	1361671
	SW	40NW	578405	1361473
	SW	40NW	579852	1362886
	NW	30SW	580134	1362617
	WSW	55NNE	580343	1362046
	NW	70NE	580173	1362189
	NNW	65WSW	580268	1362122
	WNW	25SW	578198	1363784
	SE	30SSW	578162	1363705
	SSW	45WNW	578375	1364054
	ESE	25SSW	578375	1364121
	NW	75SW	578328	1361496
	NW	80NE	578479	1361140
	NW	85NE	578681	1361080
	NE	70NW	578661	1361144
	E-W	70S	579959	1361381
	E-W	75N	579948	1361306

Joint	E-W	70N	580094	1361362
	E-W	70 N	577414	1360728
	WSW	50NNW	577513	1360736
	E-W	60N	577671	1360752
	WNW	65NNW	577770	1360756
	WNW	50SSE	577719	1360811
	WNW	30SSE	578285	1360807
	E-W	60N	578423	1360772
	NNW	55WSW	578447	1360823
	WSW	50SSE	578483	1360803
	NE	60NW	578724	1360407
	ENE	80SSE	578653	1360459
	SSE	50WSW	578685	1360364

Structural element	**Strike direction**	**Dip direction**	**X**	**Y**	**Vein type**
Veins	SE	35NE	577714	1360613	LIGHT
	SW	15NW	578489	1361185	DARK
	NW	25SW	577426	1360751	DARK
	NE	40NW	577842	1360807	DARK
	NE	15SE	577761	1361275	LIGHT
	SSE	20WSW	578116	1362253	LIGHT
	E-W	60N	577842	1360651	LIGHT
	E-W	45S	578187	1360840	DARK
	SSW	30ESE	577803	1362492	LIGHT
	N-S	55W	577269	1362275	LIGHT
	N-S	10E	578947	1362887	DARK
	WNW	20SSE	578583	1362906	DARK
	NW	45NE	578267	1361620	DARK
	NE	20NW	577353	1362661	LIGHT
	NNE	15ESE	578763	1360656	DARK
	NE	35NW	578390	1361984	LIGHT
	NNW	70ENE	577610	1362778	DARK
	NW	50SW	578021	1362353	LIGHT
	SW	60NW	578569	1360528	DARK
	SE	30SW	577459	1361119	LIGHT

Appendix III

Normalized major oxide data

Sample	SiO_2	TiO_2	Al_2O_3	Fe_2O_3	MnO	MgO	CaO	Na_2O	K_2O	P_2O_5	Total
ST1S11	40.14	0.44	0.89	16.57	0.22	37.95	3.78	-	0.01	0.02	100
ST1S7	40.25	5.22	1.85	17.64	0.20	23.63	11.05	0.15	0.004	0.014	100
ST5T5	45.60	0.88	1.47	12.13	0.15	27.55	12.02	0.16	0.008	0.017	100
ST3S2	43.04	0.89	1.20	15.20	0.19	30.57	8.83	0.07	-	0.008	100
ST3S3	41.90	4.53	4.62	15.36	0.18	22.42	10.49	0.45	0.038	0.012	100
ST3S5	43.43	1.76	1.65	14.30	0.18	27.56	10.99	0.13	-	0.010	100
ST4S4	41.98	8.78	12.69	12.61	0.12	8.21	13.23	1.66	0.67	0.053	100
ST4S8	48.75	3.89	14.57	13.49	0.19	4.15	8.36	4.07	1.70	0.840	100
ST5S3	53.15	2.88	14.94	11.39	0.18	3.28	5.64	4.63	3.00	0.910	100
ST2S5	48.69	3.66	14.42	12.921	0.18	4.42	9.48	3.61	1.70	0.931	100